applied sciences

MDPI

Article

Stochastic Vulnerability Assessment of Masonry Structures: Concepts, Modeling and Restoration Aspects

Panagiotis G. Asteris [1,*], Antonia Moropoulou [2], Athanasia D. Skentou [1], Maria Apostolopoulou [2], Amin Mohebkhah [3], Liborio Cavaleri [4], Hugo Rodrigues [5] and Humberto Varum [6]

[1] Computational Mechanics Laboratory, School of Pedagogical and Technological Education, Heraklion, 14121 Athens, Greece; athanasiaskentou@hotmail.gr
[2] Laboratory of Materials Science and Engineering, School of Chemical Engineering, National Technical University of Athens, 15780 Athens, Greece; amoropul@central.ntua.gr (A.M.); mairi_apostol@central.ntua.gr (M.A.)
[3] Department of Structural Engineering, Malayer University, 65719-95863 Malayer, Iran; amoheb@malayeru.ac.ir
[4] Department of Civil, Environmental, Aerospace and Materials Engineering (DICAM), University of Palermo, Viale delle Scienze, 90128 Palermo, Italy; liborio.cavaleri@unipa.it
[5] RISCO, Department of Civil Engineering, Polytechnic Institute of Leiria, 2411-901 Leiria, Portugal; hugo.f.rodrigues@ipleiria.pt
[6] Faculdade de Engenharia, Universidade do Porto, Departamento de Engenharia Civil, 4200-465 Porto, Portugal; hvarum@fe.up.pt
* Correspondence: panagiotisasteris@gmail.com; Tel.: +30-210-2896-922

Received: 27 October 2018; Accepted: 30 December 2018; Published: 10 January 2019

Abstract: A methodology aiming to predict the vulnerability of masonry structures under seismic action is presented herein. Masonry structures, among which many are cultural heritage assets, present high vulnerability under earthquake. Reliable simulations of their response to seismic stresses are exceedingly difficult because of the complexity of the structural system and the anisotropic and brittle behavior of the masonry materials. Furthermore, the majority of the parameters involved in the problem such as the masonry material mechanical characteristics and earthquake loading characteristics have a stochastic-probabilistic nature. Within this framework, a detailed analytical methodological approach for assessing the seismic vulnerability of masonry historical and monumental structures is presented, taking into account the probabilistic nature of the input parameters by means of analytically determining fragility curves. The emerged methodology is presented in detail through application on theoretical and built cultural heritage real masonry structures.

Keywords: Artificial Neural Networks; damage index; failure criteria; fragility analysis; masonry structures; monuments; restoration mortars; seismic assessment; stochastic modeling

1. Introduction

Masonry corresponds to one of the most ancient building structure types. This explains the fact that the majority of monuments are masonry structures, meaning main building elements are joined together through the use of mortars. The main building elements could refer to stones or bricks or a combination of both and can have different geometries, ranging from orthogonal shaped elements of standardized dimensions to random shaped elements of different dimensions (rubble masonry). The inhomogeneous and anisotropic nature of this particular structure type, as well as that of the

materials comprising it, define to a great extent the seismic response of monumental buildings. In particular, a common characteristic of these structures is their high seismic vulnerability when subjected to earthquake stresses, which is attributed to the highly brittle behavior and relatively low tensile strength of the individual building materials comprising masonries. Historical masonry monumental buildings, for instance ancient masonry churches, are unique and cannot be reduced to any standard structural scheme: this makes the evaluation of their seismic reliability a very challenging task, because—in addition to the many uncertainties that are common to all existing structures—no statistics on their behavior are available [1–4]. The cultural, social and architectural values of historical buildings demand respect of their uniqueness and individual identity. Thus, any measures taken for their protection, aiming to decrease their vulnerability, must comply with the principles of reversibility and compatibility; reversibility of an intervention means that any conservation action implemented can be "undone" without any damaging alteration to the authentic structure and materials, while compatibility of the intervention means that the intervention and materials applied will not harm the authentic materials and structure in any way, i.e., provoke or intensify damaging chemical reactions, introduce soluble salts, prevent homogenous behavior regarding water transfer phenomena, cause aesthetic alteration, etc. Of course, it is difficult for an intervention, and especially a reinforcement intervention, to truly and fully abide with these two principles, however it is necessary to undertake all possible strain and measures in this direction in order to ensure that cultural heritage assets of the past are passed along to future generations with a promise of longevity for centuries to come. Thus, this obligation to protect cultural heritage assets creates the demand for the strict compliance of protection measures within the regulatory frameworks which govern these structures, on both national and international levels.

Already from the beginning of the previous century [5,6], regulatory frameworks regarding the protection of historical buildings were formulated and accepted, such as the guidelines given by the International Scientific Committee of the Analysis and Restoration of Structures of Architectural Heritage of ICOMOS in 2001, and in particular the ICOMOS Charter regarding the Principles for the Analysis, Conservation and Structural Restoration of Architectural Heritage (ISCARSAH Principle). This particular regulatory framework is based on the principles of research and documentation, authenticity and integrity, aesthetic harmony, least invasive interventions and reversibility, principles which are in accordance with the demands of the Athens and the Venice Charters, as well as with the principles established by Morton and Hume [7]. An additional prerequisite for the successful protection of these structures is related to the interdisciplinary approach, which should be adopted during the investigation and assessment of any repair scenario.

A prerequisite for the formulation of a reliable methodology to predict the seismic vulnerability of historical/monumental masonry structures is the successful simulation of the structural system, as well as of the materials comprising the masonry, through the formulation of appropriate analytical statutory laws. In this direction, however, the complex mechanical behavior of masonries, which is a multiphase material, is a serious obstacle. Furthermore, an additional and at the same time basic difficulty regarding the formulation of such a methodology is related to the probabilistic nature of the parameters influencing the behavior of masonry structures. Among these parameters are the values of the mechanical properties of the materials (due to the wide dispersion of these values regarding the whole of the structure or due to limitation regarding the accuracy of the measurements, related to the lack of sufficient accuracy of methods and instruments used, in addition to limitations imposed by monuments protection legislation regarding sampling). Additionally, the probabilistic nature of earthquakes, directly connected and influenced by a large number of parameters, must be taken into account. Due to the high uncertainty of the parameters influencing the behavior of masonry structures, the assessment of their vulnerability cannot be conducted in terms of a deterministic approach [8–23]. To the contrary, a probabilistic approach would be more appropriate, in order to be applied in cases where the response of the structure is evaluated and compared with limit states, such as specific limit values of response directly interlinked with structural damages.

In the framework of the above limitations and issues of specific consideration, this study presents an analytical methodology for the evaluation of seismic vulnerability of masonry structures, taking into account the probabilistic nature of the parameters involved through the development of analytical fragility curves.

2. Need for Research

Despite the plethora of research work conducted and published in the last two decades (Figure 1), modeling and assessment of the seismic vulnerability of masonry structures remains an open issue and, at the same time, a challenge for the practicing civil engineer.

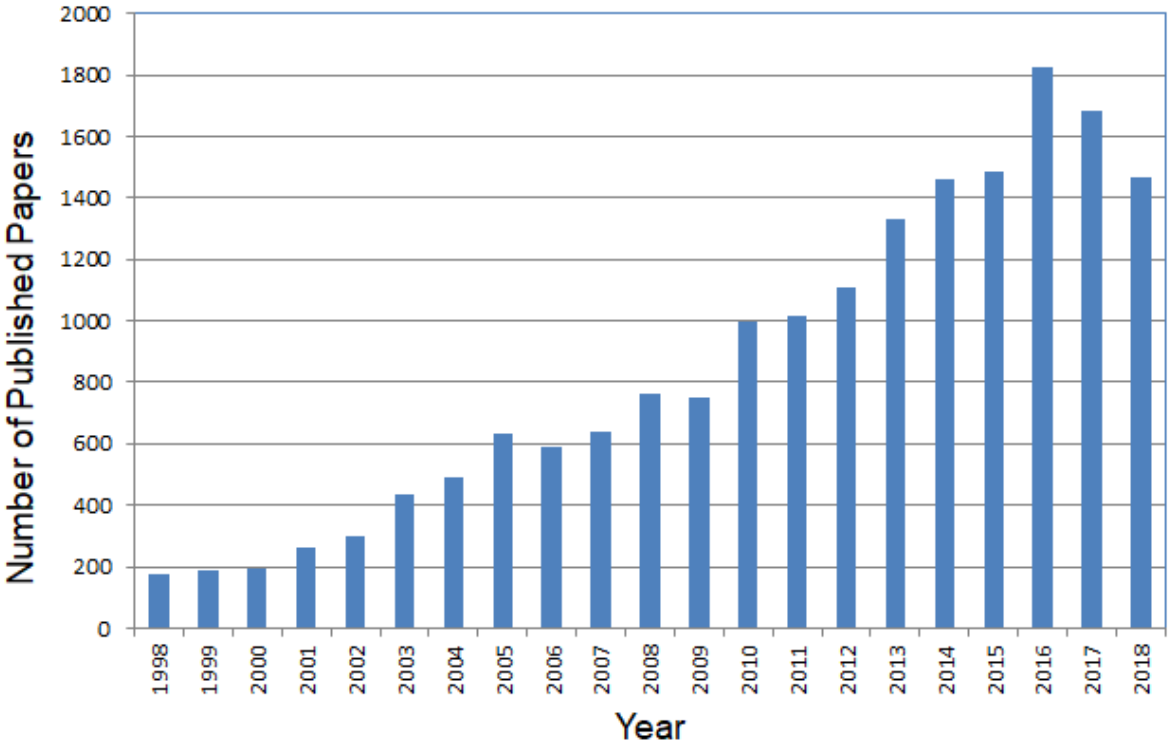

Figure 1. Evolution of number of publications concerning the masonry materials and structures based on Scopus bibliographic database (28 December 2018).

Masonry structures are an important part of today's built environment, as it is one of the oldest building systems known to humanity. It is believed to have been in use for over 6000 years and is still in use today in several regions globally. Specifically, in addition to the plethora of important historical structures and monuments which are masonry structures and must be preserved for future generations due to their historical importance, masonry is the most widely used construction type, not only in poverty-stricken countries, due to its low cost compared to the other modern materials, but also in developed countries, due to the aesthetic value that it provides when used in modern constructions. However, it should be highlighted that a common characteristic of all masonry structures is their high seismic vulnerability when subjected to seismic stresses. This is due to the fact that masonry structures are of a brittle and anisotropic nature and, subsequently, each one depicts a distinct brittle and anisotropic behavior. Indeed, masonry is a composite "material" that exhibits distinct directional properties, mainly because the mortar joints act as planes of weakness.

The modeling of the structural behavior, as well as the mechanical characteristics of masonry structures, and the materials comprising it, is still an open issue to this day. The importance of the issue, in addition to the historical values of many masonry structures and of course the safety issues involved, is also linked with economic factors, as approximately 80% of the structural cost from earthquakes is attributable to damage of masonry walls and to the consequent damage of doors, windows, and electrical and hydraulic installations [24]. The intense computational complexity

which accompanies such a complex building system is a main problem that must be overcome to successfully accomplish their modeling and assessment in relation to seismic vulnerability and thus successfully protect them by implementing various reinforcement action. For the special case of monumental masonry structures, additional necessary restrictions based on legislations for monument protection, aiming to preserve cultural, artistic, and historical values of the structure, as stated in a series of scientific Charters (e.g., the Athens Charter (1931) [5], the Venice Charter (1964) [6], etc.), make the process of modeling and restoration even more complex.

In addition to the above difficulties, one must also consider the probabilistic nature of earthquakes, which is directly connected and influenced by a significant number of parameters. Thus, due to the high uncertainty of the parameters influencing the behavior of masonry structures, the assessment of their vulnerability cannot be conducted in terms of a deterministic approach. To the contrary, as presented and validated in the following sections, it is suggested to follow a probabilistic approach, which should be applied in cases where the response of the structure is evaluated and compared with limit states, such as specific limit values of response directly interlinked with structural damages.

Taking into account the intensely anisotropic nature and behavior of masonry, it would not be an exaggeration to state that masonry material is the mother of all materials (indeed, the word material derives from μήτηρ in ancient Greek (méeteer), mater in Latin and matar in ancient Hindu, which are all words for "mother"). In fact, the authors believe that it would be extremely valuable for lectures in mechanics and material strength, aiming to educate young engineers, to be orientated to masonry materials instead of only concrete and steel, as is usual practice today. Although reinforced concrete is the choice material of today, masonry still comprises a great percentage of existing buildings and incorporates a complexity in its analysis which can be of high educational value.

3. Proposed Methodology

Taking into account the principles and guidelines of ICOMOS, as well as the results of relative research projects [25–46], a specific methodology has been developed in relation to the restoration of historical masonry structures. The flow chart of the proposed methodology is presented in Figure 2.

The proposed methodology is formulated by discrete steps. In particular, it includes the evaluation and/or determination of the mechanical properties of the materials, the simulation of the structural system and of the forces, the analysis of the structure regarding specific stresses, the determination of the failure areas of the structure and the respective damage indices, regarding both the model of the structure in its current condition, as well as for the models of the structure in relation to different repair scenarios. Finally, based on the damage indices, fragility curves are developed, which, as illustrated in the following section, contribute to the quantified assessment of the structure's vulnerability in its current condition, and to the assessment of the effectiveness of different repair scenarios.

In the framework of the proposed methodology, the following eight distinct steps that also define the structure of the present work are included.

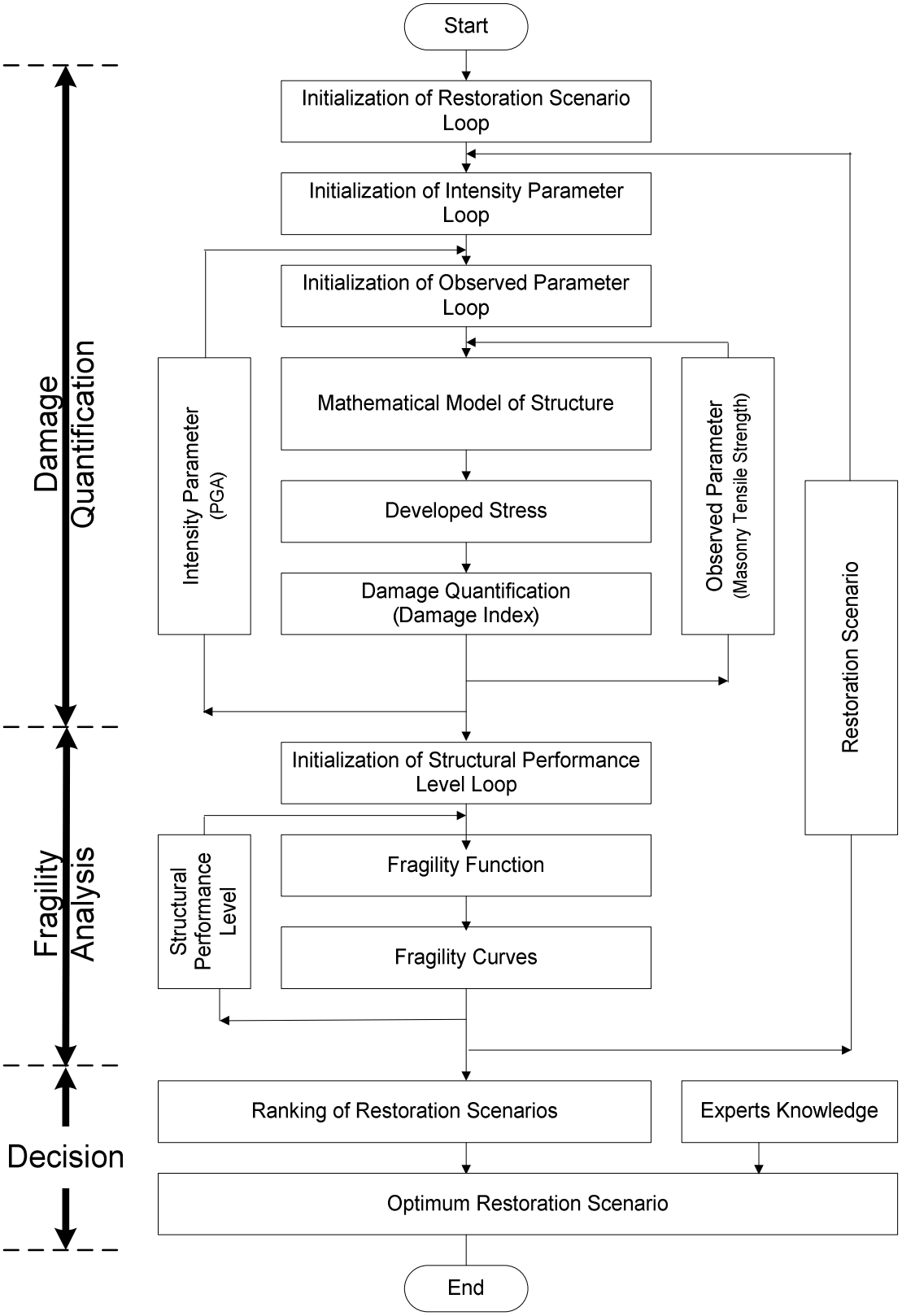

Figure 2. Flow chart of the proposed methodology.

3.1. Step 1: Reliable Reconstruction of Structure

The successful modeling of an existing masonry structure is a prerequisite for the reliable seismic vulnerability assessment and for the correct decision-making during a restoration process. To achieve that, detailed data able to represent not only the whole geometry of the structure but also the geometry and the mechanical characteristics of the constitutive materials are necessary.

Furthermore, the mathematical reconstruction is crucial to include the interconnections of materials. Connections of perpendicular walls or of walls and floors should be thoroughly investigated.

The need for detailed reconstruction of an existing structure through reliable numerical models is greater in the case of a historical masonry building. The great difference between a numerical model for the design of a new building and a numerical model of a monumental masonry structure is that in the first case the numerical model represents the reality to which the new structure (still virtual) will have to resemble, whereas in the analysis of a historical building, the reality is represented by the building itself, and the virtual model must be able to describe this singular reality. For this reason, the accurate identification of reality in all its aspects (geometry, history, traumas, deformations, materials, deteriorations, etc.) constitutes the preliminary and fundamental phase of structural analysis: only the complete knowledge of reality and the agreement between the model results and the reality itself will be able to validate the structural analysis.

In light of the above the interdisciplinary approach, a basic requirement according to ICOMOS [5,6] as mentioned in the Introduction, becomes imperative and should be adopted during all main phases comprising the proposed methodology about the stochastic vulnerability assessment of masonry historical structures. Such an interdisciplinary approach needs a close cooperation of different experts such as architects, civil engineers, chemical engineers, historians, archeologists and specialists in digital reconstruction. The participation of historians and archeologists in the research team is essential for conservation and restoration of historic buildings and their role is to detect and preserve the values of the monument, highlighting its importance. Furthermore, its participation is crucial for the documentation of the structure including aspects such as the history of the building, its chronology and the history of constructive techniques. Information concerning historical constructive issues could be obtained from documentary sources, such as ancient drawings and descriptions or historical studies [47,48] and can be supported by scientific data, as produced by the other disciplines involved [49]. In addition, the participation of specialists in the digital reconstruction is of great interest for a reliable reconstruction of such structures. In the last two decades, image-based techniques and terrestrial laser scanning have proved to be suitable tools for the digital reconstruction of such complex structures producing three dimensional models of the structure [50,51]. The production of the high-resolution 3-D model enables the extraction of the necessary conventional 2-D information.

It is common practice for researchers to focus on the detailed reconstruction of the monumental structure but at the same time give little attention to the reconstruction of the subsoil and the foundation. To this end, several data acquisition techniques such as the ground penetrating radar [52] are available for the reliable reconstruction of the subsoil and the foundation of the structure. This technique has been used with great success in the Holy Aedicule's rehabilitation of the Holy Sepulchre in Jerusalem [53]. Interpretation of the measurements revealed the position of the rock, remnants of the initial cave, which, according to tradition, is the original site of Christ's burial and resurrection, thus providing information regarding the underground features as well as details regarding the internal phases of the structure's masonry.

3.2. Step 2: Materials Characterization and Mechanical Characteristics

Among the crucial tasks for a successful modeling of masonry structures is that referring to the characterization (physical and mechanical properties) of the building materials. Furthermore, in the case of monumental masonry structures, both the characterization and the properties of materials such as stones, bricks and mortars are critical for the structural modeling of the structure. When dealing with historic masonries, the researcher must keep in mind that the structure in its current state, as well as the materials comprising it, are disturbed systems, which have been in service for centuries or even millennia under real mechanical and environmental loads [54]. Thus, the historical building materials comprising it, as well as their characteristics, are a projection of the material that was applied. Characterization of the historical materials, as well as diagnosis of their decay, is crucial to obtain input data necessary for the evaluation of the monument's response in its current state, as well as to select new compatible and performing restoration materials that will serve

adequately in relation to the mechanical stresses they are subjected to and be durable in relation to the environment factors negatively affecting them.

Analysis of the historical building stones can provide interesting information regarding historical aspects, in relation to quarries exploited during the construction of the masonry, transport routes of the era, methods of material transportation, etc. Furthermore, the study of their decay is a useful tool regarding the durability of different types of stones under environmental loads, as they have withstood natural ageing; therefore, their state of preservation is an indicator of their durability under the specific loads. New stones can be selected through a compatibility assessment of the historical stone with today's quarry stones, regarding mineralogical composition (X-ray diffraction measurements and petrographic analysis, aiming to the highest possible similarity in relation to crystalline compounds), mechanical strength (where the mechanical properties of the new stone, compressive strength, flexural strength, tensile strength, modulus of elasticity, etc.) must be as close as possible to the historical stone in order to ensure that no damage is inflicted on the weaker material), microstructural characteristics and thermohygric behavior (i.e., through mercury intrusion porosimetry, which measures the microstructural characteristics of materials, and capillary rise tests, which provide the capillary rise coefficient of the materials and reveals how water is absorbed from the underground and neighboring materials, where similar values are necessary in order to ensure homogenous moisture transfer and avoid preferential moisture accumulation). The same applies when bricks are used as main building elements or in combination with stones, however in the case of bricks, as they are artificial materials and not natural, the aim is to uncover their production technology (for example, raw materials used, firing temperature, etc.) and try and reproduce bricks of similar mechanical and physicochemical characteristics.

Mortars are a complex material, constituted of different materials. Analysis of the historical mortar can provide archaeological information regarding the materials and production technique employed [55,56], while analysis of its constituents can provide information regarding the provenance of the historical raw materials used with further archaeological implications and discoveries [49,57]. Typical investigative methods for the characterization of historical mortars—mineralogical and chemical—were analyzed to a great extent by Middendorf et al. [58,59]. Specifically, the most usual techniques applied are simultaneous thermal analysis, aiming to determine the components of the mortar and their relative proportion; X-ray diffraction to conduct mineralogical investigation and reveal the presence of crystalline compounds; and mercury intrusion porosimetry to examine the microstructural characteristics of the historical mortar [60], while correlation of the results can lead to categorization of mortar types [61]. Scanning electron microscopy coupled with microanalysis is a valuable tool, for both characterization and decay diagnosis [62], while total soluble salts are indicative of salt decay and/or accumulation [63,64]. It is obvious that all above techniques provide a different type of information, which must then be correlated and examined in total in order to achieve a correct characterization of the historical mortar, while in many cases, other techniques must be implemented in order to provide additional information.

At the same time, analysis of the historical mortars allows for the design of new restoration mortars through the reverse engineering approach, aiming to produce restoration mortars with characteristics as similar as possible to the characteristics of the historical mortars [65,66]. This is especially important in cases where the historical mortars have shown great longevity under the environmental loads and mechanical stresses they have been subjected to [67]. In many cases, to achieve the optimum synthesis, optimization can take place, aiming to enhance the restoration mortar characteristics [68]. Other considerations should also be considered, such as technical requirements, environmental loads, and worksite limitations, to design of the optimum restoration mortar [45,69,70]. Due to the significance of restoration mortars in the response of a masonry structure, while also taking into account that repointing with new restoration mortars is the most usual conservation action implemented in historical masonry restoration works, an insight into the analysis of historical mortars and a classification according to their characteristics, as well as the

philosophy behind the design and assessment of restoration mortars in relation to historical mortars, is herein included.

All the characteristics discussed are of importance to achieve a compatible, durable restoration, even though not all are necessary for modeling and structural analysis. As stressed above, the characteristics of materials composing the structure are basic input data for structural analysis. Namely, the compressive/tensile strength of the materials, the modulus of elasticity and Poisson ratio are of primary importance, at least as far as a linear/elastic analysis is concerned. For the estimation of those parameters, combinations of analytical or semi-empirical methods and experimental data have to be used. Based on the great importance and interest of the mechanical properties of masonry material for a successful and reliable modeling of masonry structures, a section about these has been included herein.

3.3. Step 3: Structural Model

The choice and the use of the most suitable mathematical model for the structural modeling of masonry structures is a difficult and challenge task for engineers. Furthermore, for the special case of complex historic structures consisting of many of materials, the structural modeling is a crucial task for the reliable modeling of the structure and of great interest for engineers. In light of the above, a state-of-the-art report on the structural modeling of masonry structures has been included in a following section. In addition, a new anisotropic finite element macro-model has been developed and presented in detail in a following section.

3.4. Step 4: Actions

Different loading cases have to be considered, including seismic actions for structures built in seismic areas. Combinations of dead loads, live loads and earthquake demands, have to be used. Earthquake has to be considered along all unfavorable directions for the building. Nevertheless, certain issues are still open, regarding, e.g., the poor hysteretic behavior of masonry or the adverse influence of the simultaneous vertical component of the seismic action.

3.5. Step 5: Analysis

Using input data of the previous steps, a finite element analysis is performed and stresses (normal-shear)—displacements at the joints of the mesh—are calculated. Due to the actual behavior of plain masonry and the high degree of uncertainty in the previous steps, elastic analysis is a first valuable tool for such structures, especially before any repair and/or strengthening.

3.6. Step 6: Failure Criterion and Assessment

A failure criterion must be established for the definition of the damaged regions of the structure (as a first insight). Taking into account the conclusions of Step 2 concerning materials' characteristics, such a criterion is proposed, and is used as an input to carry out the analysis.

These failure results are used as input data for the development of a damage index. Based on this index, the possibility of a structure to be damaged beyond a specified level (heavy, moderate, and insignificant) for various levels of ground acceleration is determined. This information is important during the analysis and redesign process for a historical structure since it gives the opportunity to investigate different scenarios with different options regarding repair/strengthening.

3.7. Step 7: Repairing and/or Strengthening Decisions and Reanalysis

According to the results of Steps 5 and 6, all the damaged regions are repaired and/or strengthened. The method to be used, the extent of the interventions, the type of the materials, etc., could be directly related to the results and are based on semi-empirical expressions for the final mechanical characteristics of masonry (see, e.g., [71]).

Last, a new structural analysis has to be performed including all the final materials, loading and structural data. Results of the analysis are subsequently used in the processes of Steps 5 and 6,

leading to a final approval (or rejection) of the decisions already taken for repair or strengthening of the existing structure.

3.8. Step 8: Explanatory Report

The last step, as a result of the proposed methodology, includes the detailed "Explanatory Report", where all the collected information, the diagnosis, including the safety evaluation, and any decision to intervene should be fully detailed. This document is essential for eventual future analyses and interventions' measures in the structure.

4. Computational and Mathematical Aspects

In this section, the most basic analytical constitutive laws and numerical models required for the successful implementation of the proposed methodology are presented in detail. In particular, the finite element model for the macro-modeling of masonry structures, the failure criteria, the damage indices, the performance levels and the mathematical background of fragility curves are presented.

4.1. Constitutive Laws of Masonry Materials

For the determination of the masonry compressive and tensile strength, several semi-empirical expressions are available in the literature. In the majority of these expressions, global effects contributing to the system resistance, such as buckling-effects or local-compression resistance are not considered. Recent studies [72,73] have shown that masonry codes underestimate the compressive strength of masonry with high coefficients of variation.

For the estimation of the masonry strengths of low-strength masonry, with a single leaf, the following formula have been proposed by Tassios and Chronopoulos [71]:

$$f_{\mathrm{wc}} = \xi\left[\left(\frac{2}{3}\sqrt{f_{\mathrm{bc}}} - \alpha\right) + \beta f_{\mathrm{mc}}\right] \quad [\text{in MPa}] \tag{1}$$

$$f_{\mathrm{wt}} = \frac{2}{3} f_{\mathrm{mt}} \tag{2}$$

where

$f_{\mathrm{wc}}, f_{\mathrm{wt}}$ are the compressive and tensile strength of masonry respectively;
$f_{\mathrm{mc}}, f_{\mathrm{mt}}$ are the compressive and tensile strength of mortar, respectively;
f_{bc} is the compressive strength of the block/stone or brick material;
α is a reduction factor due to non-orthogonality of blocks ($\alpha = 0.5$ for block stones & $\alpha = 2.5$ for rubble stones);
β is a mortar-to-block factor ($\beta = 0.5$ for rough stones and $\beta = 0.1$ for very smooth-surface stones); and
ξ is a factor expressing the adverse effect of thick mortar joints, $\xi = 1/\left[1 + 3.5\left(k - k_0\right)\right]$ (k = volume of mortar/volume of masonry and $k_0 = 0.3$).

However, for well-built and regular masonry structures, Tassios [74] proposed another expression for the estimation of the compressive strength:

$$f_{\mathrm{wc}} = \left[f_{\mathrm{mc}} + 0.4\left(f_{\mathrm{bc}} - f_{\mathrm{mc}}\right)\right]\left(1 - 0.8\sqrt[3]{\alpha}\right) \text{ for } f_{\mathrm{bc}} > f_{\mathrm{mc}} \tag{3}$$

and

$$f_{\mathrm{wc}} = f_{\mathrm{bc}}\left(1 - 0.8\sqrt[3]{\alpha}\right) \text{ for } f_{\mathrm{bc}} \le f_{\mathrm{mc}} \tag{4}$$

where

$f_{\mathrm{bc}}, f_{\mathrm{mc}}$ are the compressive strength of blocks and mortar, respectively; and

$\alpha = t_{jm}/h_{bm}$ is the ratio between average bed (horizontal) joint thickness t_{jm}, and average block height h_{bm}.

Based on a large database of compressive test results on masonry prisms from the literature and using regression analysis or soft computing techniques such as Artificial Neural Networks (ANNs) and Fuzzy Logic (FL), a plethora of mathematical models have been proposed for the estimation of masonry compressive strength. Detailed state-of-the-art reports can be found in the works of Sarhat and Sherwood [72], Thaickavil and Thomas [73], and Garzón-Roca et al. [75]. A common feature of these proposals (Table 1) is that they only consider the compressive strength of brick and mortar.

Table 1. Formulae for the estimation of masonry compressive strength.

Sl. No.	Reference	Formula
1	Engesser (1907) [76]	$f_{wc} = \frac{1}{3} f_{bc} + \frac{2}{3} f_{mc}$
2	Bröcker (1963) [77]	$f_{wc} = 0.68 f_{bc}^{1/2} f_{mc}^{1/3}$
3	Mann(1982) [78]	$f_{wc} = 0.83 f_{bc}^{0.66} f_{mc}^{0.18}$
4	Henry and Malek (1986) [79]	$f_{wc} = 0.317 f_{bc}^{0.531} f_{mc}^{0.208}$
5	Dayaratnam (1987) [80]	$f_{wc} = 0.275 f_{bc}^{0.5} f_{mc}^{0.5}$
6	Rozza (1995) [81]	$f_{wc} = (v_u f_{bc} + 0.8 v_m f_{mc})/10$
7	Bennett, Boyd and Flanagan (1997) [82]	$f_{wc} = 0.3 f_{bc}$
8	AS 3700 (2001) [83]	$f_{wc} = \mathrm{K}_h \mathrm{K}_m f_{bc}^{0.5}$
9	Dymiotis and Gutlederer (2002) [84]	$f_{wc} = 0.3266 f_{bc} \times (1 - 0.0027 f_{bc} + 0.0147 f_{mc})$
10	Eurocode 6 (2005) [85]	$f_{wc} = \mathrm{K} f_{bc}^{0.7} f_{mc}^{0.3}$
11	Kaushik, Rai and Jain (2007) [86]	$f_{wc} = 0.317 f_{bc}^{0.866} f_{mc}^{0.134}$
12	Gumaste, Rao, Reddy and Jagadish (2007) [87]	$f_{wc} = 0.63 f_{bc}^{0.49} f_{mc}^{0.32}$
13	Christy, Tensing and Shanthi (2013) [88]	$f_{wc} = 0.35 f_{bc}^{0.65} f_{mc}^{0.25}$
14	Garzón-Roca, Marco and Adam (2013) [89]	$f_{wc} = 0.53 f_{bc} + 0.93 f_{mc} - 10.32$
15	Sarhat and Sherwood (2014) [72]	$f_{wc} = 0.886 f_{bc}^{0.75} f_{mc}^{0.18}$
16	Lumantarna, Biggs and Ingham (2014) [90]	$f_{wc} = 0.75 f_{bc}^{0.75} f_{mc}^{0.31}$
17	Kumavat (2016) [91]	$f_{wc} = 0.69 f_{bc}^{0.6} f_{mc}^{0.35}$

f_{wc}, masonry compressive strength; f_{bc}, brick compressive strength; f_{mc}, mortar compressive strength; v_u, relative volume of unit; v_m, relative volume of mortar; K is a constant in Eurocode 6 formula, modified according to the National Annex for different countries. The value of this constants in the UK is 0.52 [92] while in Greece is 0.20–1.00 depending on brick/block unit properties and their arrangement; K_h is a factor in Australian AS 3700 code [83] that accounts for the ratio of unit height to mortar joint thickness (1.3 for blocks of 190 mm high blocks and mortar joints with 10 mm thickness); K_m is also a factor in Australian AS 3700 [83] code that accounts for bedding type (1.4 for full bedding and 1.6 for face-shell bedding).

Recently, Thaickavil and Thomas [73] proposed a formula taking into account the majority of parameters affecting the masonry compressive strength. Namely, the authors, based on regression analysis on many test data (232 datasets) corresponding to the masonry unit strength of 3.1–127.0 MPa, mortar strength of 0.3–52.6 MPa and *h*/*t* ratio of 1.15–5.75, have proposed the following formula:

$$f_{wc} = \frac{0.54 \times f_{bc}^{1.06} \times f_{mc}^{0.004} \times VF_b^{3.3} \times VR_{mH}^{0.6}}{\left(h/t\right)^{0.28}} \quad (5)$$

where VF_b is the volume fraction of brick and VR_{Mh} the volume ratio of bed joint to mortar defined by the following equations:

$$VF_b = \frac{V_u}{V_p} \quad (6)$$

where V_u is the volume of masonry units and V_p is the volume of prism.

$$VR_{mH} = \frac{V_{mH}}{V_{mH} + V_{mV}} \quad (7)$$

where V_{mH} is the volume fraction of mortar in horizontal joints and V_{mV} is the volume fraction of mortar in vertical joints. The volume fraction is obtained by dividing the respective volume with the corresponding total volume in the prism. The above proposed analytical formula (Equation (5)) seems to be the most reliable for the determination of masonry compressive strength [93] among a plethora of proposed equations available in the literature [76–91].

4.2. Structural Modeling Techniques for Masonry Structures

As pointed out above, masonry is in fact a heterogeneous material comprising masonry units and mortar. Due to the existence of mortar joints as planes of weakness, a masonry wall exhibits distinct directional mechanical properties. Therefore, a masonry wall can be treated as an orthotropic material. Depending on the orientation of the joints to the stress directions and the applied normal stress level, four different failure modes are feasible for unreinforced masonry walls according to FEMA 356, 2000 [94]. Namely, pier diagonal tension, toe crushing, bed joint-sliding, and rocking failure can occur. The first two failure modes are considered force-controlled (brittle failure) and hence no plastic deformation capacity is considered. The last two failure modes are considered deformation-controlled (ductile failure) and a plastic deformation capacity is taken into account.

To model the structural behavior of a masonry wall, there are some influencing factors such as material properties of masonry units and mortar, dimension of the units, mortar thickness and the brittle behavior of masonry units, which should be taken into account properly. If these factors are incorporated suitably into a structural model of a masonry wall, the four above-mentioned failure modes can be simulated.

Depending on the required level of accuracy and simplicity, there are different structural modeling strategies for masonry wall elements as follows.

4.2.1. Modeling Masonry as a Three-Phase Material (Detailed Micro-Modeling Approach)

In this approach, the masonry constituents (units, mortar and unit-mortar interfaces) are modeled as they are in masonry wall elements. In other words, units and mortar in the joints are represented by continuum elements, whereas the unit–mortar interface is represented by discontinuous elements accounting for potential slip planes as shown in Figure 3b. Even though the accuracy of this approach is high, it needs high computational costs and time. In addition, the elastic and inelastic material properties of both masonry units and mortar and the unit/mortar interface mechanical property as well, are required to be determined by some realistic masonry sample tests. Therefore, this approach is mostly preferred for the analysis of small-scale experimental specimens and structural details to determine accurately their components' stress distribution (Lourenço and Pina-Henriques, 2006 [95]; Papa, 2001 [96]; Rots, 1991 [97]; Tzamtzis and Asteris, 2003 [98]; Zucchini and Lourenço, 2006 [99]).

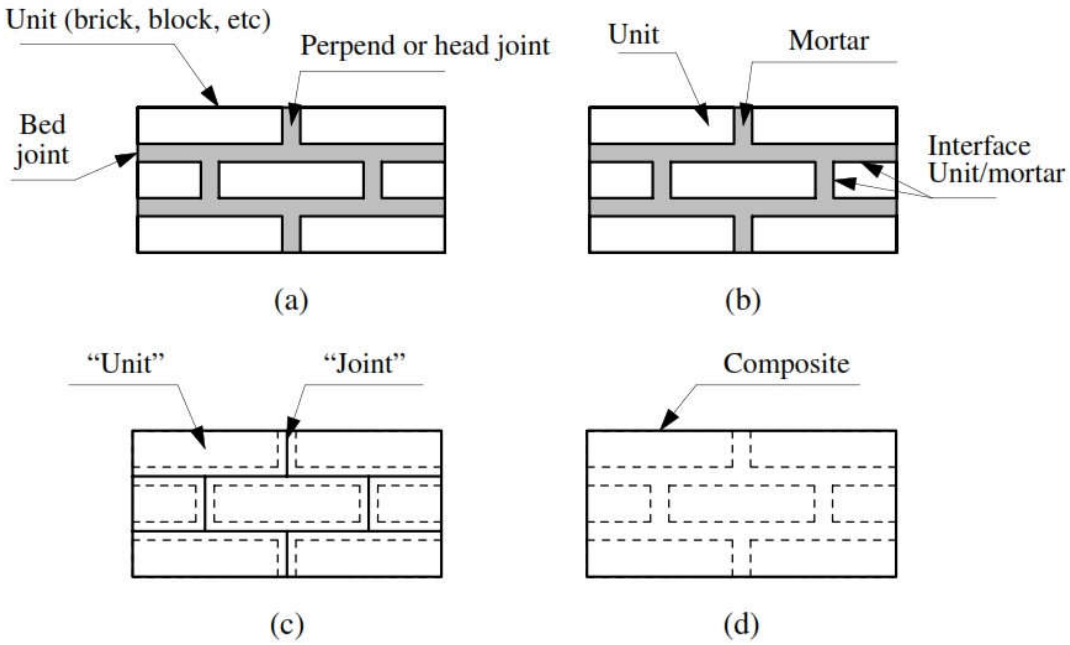

Figure 3. Modeling strategies for masonry: (**a**) typical masonry specimen; (**b**) detailed micro-modeling; (**c**) simplified micro-modeling; and (**d**) macro-modeling (Lourenço, 1996 [100]).

Recently, Sarhosis and Lemos (2018) [101] proposed a detailed micro-modeling approach for the analysis of masonry couplets and prisms. In this approach, masonry constituents are represented as an assemblage of densely packed discrete irregular deformable particles bonded together by zero thickness interface elements. The advantage of this approach is that failure can occur at the masonry units, mortar and/or brick–mortar interface in a realistic manner. In this approach, the crack initiation and propagation can be traced as well.

4.2.2. Modeling Masonry as a Two-Phase Material (Simplified Micro-Modeling Approach)

In this approach, masonry units/blocks are represented by fictitious expanded units in size (Phase I) to keep the geometry consistent, however, mortar is not modeled explicitly. The fictitious expanded unit dimensions are of the same size as the original dimensions plus the real joint thickness, as shown in Figure 3c. The interface's stiffness is represented numerically by the stiffness of the real joint. The elastic or inelastic, isotropic model is used for the behavior of the masonry units to simulate properly their possible crushing and cracking propagation patterns. The interaction between the expanded units is represented by an interface element (Phase II). To simulate the behavior of mortar joints, the properties of the mortar and the interface elements are lumped into the zero-thickness common interface elements. This approach leads to the reduction in computational intensiveness and yields a model that is applicable to a wider range of structures. In fact, the drawback of the large computational effort required by the detailed micro-modeling is partially overcome by the simplified micro-modeling strategy. Cracking in the masonry units can also be simulated by assigning potential vertical zero thickness interfaces (unit to unit) at the unit's center lines (Lourenço 1996 [100]). Another important factor influencing the accuracy of the simplified micro-modeling strategy is the masonry units' aspect ratio that should be taken into account. According to Schlegel and Rautenstrauch (2004) [102], aspect ratio of stone masonry units (stone shape or the ratio of stone unit length to height lst/hst) has an effect on the joint failure and load-carrying capacity of masonry walls. For example, as shown in Figure 4, the load-carrying capacity of a masonry wall increases as a result of the decreasing stone rotation with an increasing ratio of lst/hst. Furthermore, it can be observed in this figure that an increase in the stone unit dimensions in each direction (expanding stone units), would increase the ultimate load to some extent depending on the ratio of lst/hst. Therefore, it can be concluded that expanding masonry units in the simplified micro-modeling strategy may alter the accuracy of the analysis depending on the

mortar joint relative thickness. Finally, it should be kept in mind that, although this procedure is preferred to the abovementioned detailed micro-modeling approach, it is still time consuming as the masonry structure size increases [103]. This modeling strategy has been used successfully in the literature to investigate nonlinear static and dynamic behavior of masonry wall elements [104–109], masonry buildings [110,111], ancient structures [112–117], stone masonry arches and aqueducts [117–123] and masonry infilled frames [124].

Recently, Mohebkhah et al. (2018) [124] used this strategy to investigate the nonlinear dynamic behavior of an ancient dry-joint stone masonry tower subjected to earthquake excitations. The numerical model developed using the distinct element method software 3DEC [125], in which the stone blocks are assumed to behave as rigid elements connected by zero-thickness interfaces. The zero thickness interfaces between adjacent blocks were modeled using the Mohr–Coulomb slip model. Since the tower has been constructed with dry joints, both the cohesion and tensile strength at the interfaces are assumed to be zero. During the dynamic analysis, no viscous damping is assumed, the only dissipation being due to frictional sliding on the joints. This conservative assumption is often used in simulating stone masonry structures containing dry joints (Papantopoulos et al., 2002, [126]). This study shows that the tower sustains considerably large lateral drifts in each direction without collapse. This large lateral drift may be attributed to the governing failure mode of the tower, which is a sliding shear failure mode throughout the tower height.

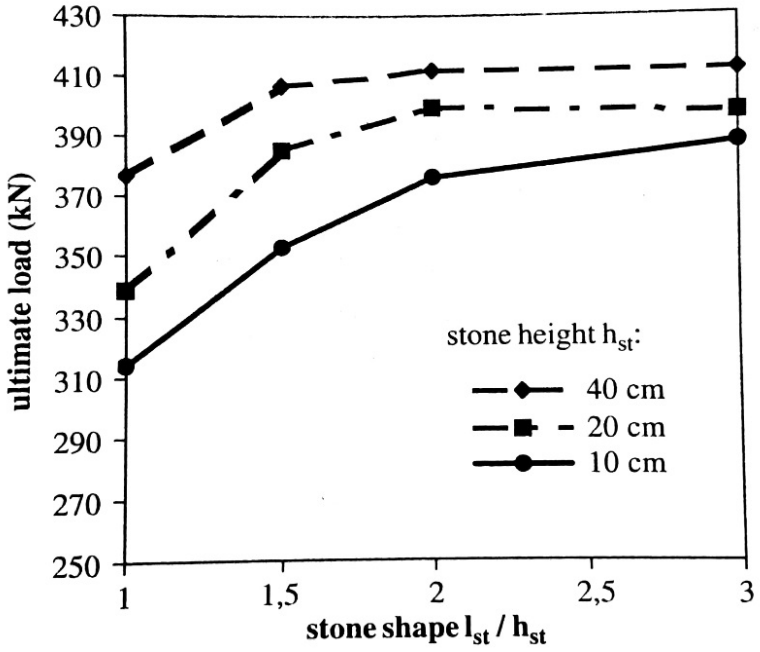

Figure 4. Ultimate loads for different variations of stone height (hst) and of stone unit length (lst) (Schlegel and Rautenstrauch, 2004 [102]).

4.2.3. Modeling Masonry as a One-Phase Material (Macro-Modeling Approach)

In this approach, there is no distinction between the masonry constituents (i.e., units and mortar) and in fact they are smeared out in a homogeneous, isotropic or anisotropic continuum (Figure 3d). For the cases in which blocky behavior is the dominant deformation mode such as small masonry walls or masonry structures with large masonry units, considering a masonry wall as a homogeneous media may lead to the difficulty of simulating the failure modes. However, this approach is preferred for the analysis of large-scale real masonry structures, because of the reduced time and memory requirements. On the basis of this approach, some computational models based on continuum plasticity (Lourenço, 1996 [100] and Lourenço et al., 1998 [127]) and continuum damage (Papa et al., 2000 [128]) have been developed and implemented successfully for in-plane

analysis of masonry shear walls. Lourenço et al. (1998 [127]) developed a homogeneous anisotropic continuum model for the analysis of masonry as a composite. In this model, the behavior of the composite media is stated, based on average stresses and strains, assuming different elastic and inelastic properties along the material axes.

Syrmakezis and Asteris [129]) proposed a general anisotropic (orthotropic) failure criterion for masonry under biaxial stress state, using a cubic tensor polynomial. This failure criterion was then used by Asteris and Tzamtzis [130] for the non-linear macro-modeling and analysis of unreinforced masonry shear walls under biaxial stress state using the finite element method. The proposed failure criterion takes into account all possible combinations of plane stress state and makes it easier to be included into existing software for the analysis of masonry walls. The detailed description of this methodology is given in Sections 3.3 and 3.4. Asteris [131] also investigated the influence of the masonry infill panel opening in the reduction of the infilled frames stiffness by means of this technique.

El-Dakhakhni et al. [132] developed a macro-model for in-plane analysis of concrete masonry walls with and without reinforcements. In this multi-laminate model, a masonry wall is simulated by an equivalent homogeneous media consisting two sets of planes of weakness along the head and bed joints. To determine the global behavior of the model, the influence of these planes of weakness is smeared. This modeling technique allows prediction of the different possible failure modes, whether the planes of failure follow the mortar joints or not (El-Dakhakhni et al., 2006, [132]). The advantage of this model is that it can predict the initiation and progress of different failure modes (i.e., head joint, bed joint or homogeneous media failure) in a separate or a combined manner.

4.2.4. Modeling Masonry Using Equivalent Frame Method

The most widely used method for the modeling of real cases masonry structures is the simplified analysis method (SAM). The SAM is based on the macro-element approach that has been first proposed and developed by Magenes and Della Fonata (1998) [133] to overcome the shortcomings of the previously proposed method of "story-mechanism" by Tomazevic and Weiss (1990) [134]. The SAM stems from the concept of framed buildings analysis using beam and beam–columns elements. In fact, in the SAM to simulate the in-plane behavior of a masonry wall panel, the constituent piers and spandrel beams are substituted by the equivalent beam–columns elements with appropriate mechanical properties. Therefore, sometimes the SAM is called the equivalent frame method (EFM) which is a familiar method and has been widely used to analyze RC coupled shear walls in the literature (Figure 5).

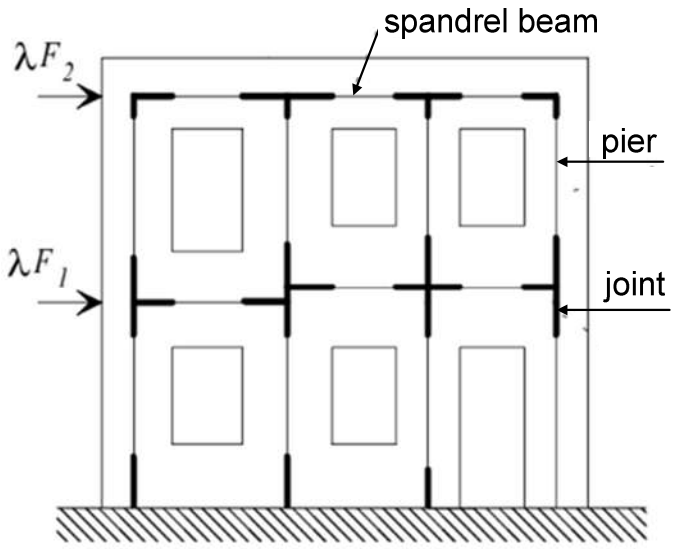

Figure 5. A schematic representation of equivalent frame model for planar walls with openings (Magenes, 2000, [134]).

The SAM has been used successfully by Magenes and Della Fontana (1998) [133] to analyze two multi-story masonry walls subjected to lateral loads. The SAM was then developed by Magenes (2000) [135] to be used for seismic assessment of practical and historic masonry buildings making use of displacement spectra and of the substitute-structure approach. Kappos et al. (2002) [136] investigated the effectiveness of the SAM or EFM for the design and/or assessment of masonry buildings. Penelis (2006) [137] based on the concept of the EFM proposed an approach for the pushover analysis of URM buildings. This approach is similar to the SAM of Magenes and Della Fontana (1998) [133], however, it uses an analytical approach and a Mohr–Coulomb failure criteria for flexural and shear strengths, respectively. Furthermore, the shear stiffness and ultimate shear deformation capacity of wall elements are estimated from experimental tests results (Penelis, 2006, [137]). Pasticier et al. (2008) [138] investigated the capability of a commercial software for pushover analysis of masonry buildings using the EFM. This study showed that the EFM can be used only for pushover analysis of masonry walls of usual and regular geometry (Pasticier et al., 2008, [138]). This is because the software does not take into account the effects of axial load variation in the piers' shear strength capacity during the analysis process.

The main advantage of the SAM is that it is based on simple strength criteria of masonry piers and spandrel beams corresponding to the well-known flexural and shear failure modes (Magenes and Della Fontana, [133]). In addition, it requires low computational effort to simulate both linear and nonlinear lateral load behavior of practical large masonry wall panels. Detailed state-of-the-art reports can be found in [139–154].

In light of the above and despite the plethora of mathematical models that have been proposed for the modeling of masonry structures, for real masonry structures, it is preferable to use simplified macro-models such as modeling the masonry as a one-phase material (macro-modeling approach) while the use of more sophisticated micro-models is suggested for the modeling of special parts of the masonry structural model. Detailed works on the advantages and disadvantages among different mathematical models about masonry structures can be found in [40,100,101,155,156].

4.3. Anisotropic Finite Element Macro-Model

The basic concepts of the finite element method are well documented and are not repeated in this paper. Only the essential features are presented. In this paper, an anisotropic (orthotropic) finite element model is proposed for the macro-modeling of masonry structures. Specifically, a four-node isoparametric rectangular finite element model with eight degrees of freedom (DOF) is used (Figure 6).

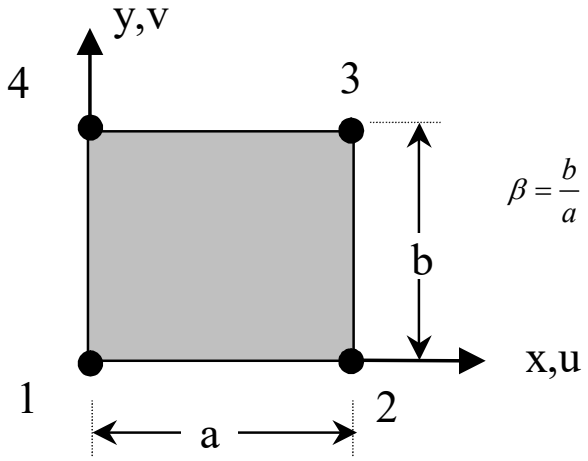

Figure 6. Finite element macro-model dimensions.

The major assumption when modeling masonry behavior under plane stress is that the material is homogeneous and anisotropic. Specifically, the material shows a different modulus of elasticity in

the x direction (E_x) (direction parallel to the bed joints of brick masonry) and the y direction (E_y) (perpendicular to the bed joints). In the case of plane stress, the elasticity matrix is defined by

$$D = \begin{bmatrix} \frac{E_x}{1-\nu_{xy}\nu_{yx}} & \frac{E_x\nu_{yx}}{1-\nu_{xy}\nu_{yx}} & 0 \\ \frac{E_y\nu_{xy}}{1-\nu_{xy}\nu_{yx}} & \frac{E_y}{1-\nu_{xy}\nu_{yx}} & 0 \\ 0 & 0 & G_{xy} \end{bmatrix} \quad (8)$$

where ν_{xy} and ν_{yx} are the Poisson's ratios in the xy and yx plane, respectively, and G_{xy} is the shear modulus in the xy plane. It is worth noticing that, in the case of plane stress in an anisotropic material, the following equation holds

$$E_x\nu_{yx} = E_y\nu_{xy} \quad (9)$$

4.3.1. Displacement Functions

Figure 6 shows the four node isoparametric rectangular finite element model, with nodes 1, 2, 3, 4 numbered in an anticlockwise order. The displacements of a node have two components, namely

$$\delta_i = \begin{bmatrix} u_i \\ v_i \end{bmatrix} \quad (10)$$

and the eight components of element displacements are listed as a vector

$$\delta^e = \begin{Bmatrix} \delta_1 \\ \delta_2 \\ \delta_3 \\ \delta_4 \end{Bmatrix} \quad (11)$$

The displacements within an element have to be uniquely defined by these eight values. The simplest representation is given by two linear polynomials, namely

$$\begin{aligned} u(x,y) &= \alpha_1 + \alpha_2 x + \alpha_3 xy + \alpha_4 y \\ v(x,y) &= \alpha_5 + \alpha_6 x + \alpha_7 xy + \alpha_8 y \end{aligned} \quad (12)$$

The eight constants α_i (where i = 1, 2, …, 8) can be evaluated easily by solving the two sets of four simultaneous equations, which will arise if the nodal coordinates are inserted and the displacements equated to the appropriate nodal displacements.

4.3.2. Strain (Total)

The total strain at any point within the element can be defined by its three components which contribute to the internal work. Thus,

$$\varepsilon = \begin{bmatrix} \varepsilon_{xx} \\ \varepsilon_{yy} \\ \gamma_{xy} \end{bmatrix} = \begin{bmatrix} \dfrac{\partial u(x,y)}{\partial x} \\ \dfrac{\partial v(x,y)}{\partial y} \\ \dfrac{\partial u(x,y)}{\partial y} + \dfrac{\partial v(x,y)}{\partial x} \end{bmatrix} \tag{13}$$

With displacements known at all points within the element, the strains at any point can be determined. These will always result in a relationship that can be defined in matrix notation according to:

$$\varepsilon = B\delta^{e} \tag{14}$$

where B is a suitable linear operator.

4.3.3. The Stiffness Matrix

The stiffness matrix of the finite element is defined by the general equation

$$K^{e} = \int_{V^{e}} B^{T} DB \; d(vol) \tag{15}$$

The analytical form of the anisotropic finite element stiffness matrix is defined by integration over the area of the element (see Appendix A). Extensive research works on the modeling of anisotropic brick masonry behavior using finite elements can be found in Samarasinghe's PhD thesis [157], Asteris's PhD thesis [158] and a work by Asteris [159] focused on the problem of the analysis of anisotropic non-linear masonry.

4.4. Failure Criteria

The key point for a reliable seismic vulnerability assessment of masonry is the failure criterion used for the determination of masonry failure. In this section, failure criteria both for isotropic and anisotropic behavior of masonry materials are presented. Namely, two semi-empirical isotropic failure criteria, the cubic tensor polynomial failure criterion, and a failure criterion based on Artificial Neural Networks (ANNs) are presented in the following three sub-sections.

4.4.1. Semi-Empirical Isotropic Failure Criteria

Despite the distinct anisotropic nature of masonry material, many researchers use for the modeling of its failure isotropic failure criteria such as the failure criterion proposed by Kupfer and Gerstle [160] for concrete material and the Von Mises modified failure criterion proposed by Syrmakezis et al. [8,25] for modeling masonry under biaxial stress state.

The first isotropic criterion was proposed by Kupfer et al. [160,161] and has been adopted by many researchers [162–164] assuming isotropic behavior for masonry material. Based on this criterion, the failure (Figure 7) can be approximated for the three-stress state under the axis of symmetry $(\sigma_1 = \sigma_2)$ by the following expressions in terms of principal stress:

For the case under biaxial compression by

$$\left(\frac{\sigma_1}{f_{wc}} + \frac{\sigma_2}{f_{wc}} \right)^2 + \frac{\sigma_2}{f_{wc}} + 3.65 \frac{\sigma_1}{f_{wc}} = 0 \tag{16}$$

for the case of heterosemous biaxial stress state (tension/compression) by

$$\frac{\sigma_1}{f_{wc}} = \frac{f_{wt}}{f_{wc}}\left(1 + 0.8\frac{\sigma_2}{f_{wc}}\right) \tag{17}$$

and for the case under biaxial tension by

$$\frac{\sigma_1}{f_{wc}} = \frac{f_{wt}}{f_{wc}} \tag{18}$$

It should be noted that a very small area of the heterosemous biaxial stress state is expressed by Equation (16), as can be noticed in Figure 7.

The second isotropic criterion (Figure 8) is the Von Mises modified isotropic failure criterion proposed by Syrmakezis et al. [8,25] for the modeling of masonry under biaxial stress state and has been adopted by many researchers [165–170] assuming isotropic behavior for masonry material.

Based on this criterion, the failure can be approximated for the three-stress state under the axis of symmetry $(\sigma_1 = \sigma_2)$ by the following expressions also in terms of principal stress:

For the case under biaxial compression by

$$\left(\frac{\sigma_1}{f_{wc}}\right)^2 + \left(\frac{\sigma_2}{f_{wc}}\right)^2 - \frac{\sigma_1}{f_{wc}}\frac{\sigma_2}{f_{wc}} - 1 = 0 \tag{19}$$

for the case of heterosemous biaxial stress state (tension/compression) by

$$\frac{\sigma_1}{f_{wc}} = \frac{f_{wt}}{f_{wc}}\left(1 + \frac{\sigma_2}{f_{wc}}\right) \tag{20}$$

and for the case under biaxial tension by

$$\frac{\sigma_1}{f_{wc}} + \frac{\sigma_2}{f_{wc}} = \frac{f_{wt}}{f_{wc}} \tag{21}$$

4.4.2. Cubic Tensor Polynomial

A key point for a successful application of the proposed methodology is the use of a reliable failure criterion for the modeling of the masonry failure. To this end, a tensor polynomial has been used for the modeling of the masonry failure. Specifically, according to this criterion, the masonry material is assumed to exhibit a distinct anisotropic nature and the failure surface can be described by the following equation:

$$f(\sigma) = F_i\sigma_i + F_{ij}\sigma_i\sigma_j + F_{ijk}\sigma_i\sigma_j\sigma_k + \cdots \begin{cases} < 1 \text{ no failure} \\ = 1 \text{ failure} \\ > 1 \text{ exceeded failure} \end{cases} \tag{22}$$

where i, j, k = 1, 2,..., 6. F_i, F_{ij} and F_{ijk} are (strength) tensors of the second, fourth and sixth rank, respectively.

Based on the above equation, restricting the analysis to a plane stress state and assuming that a cubic formulation is a reasonably accurate representation of the failure surface and by taking into consideration the symmetry and anisotropic nature of the material [129,171,172], the masonry failure surface, known as the cubic tensor failure criterion, can be expressed by Equation (23).

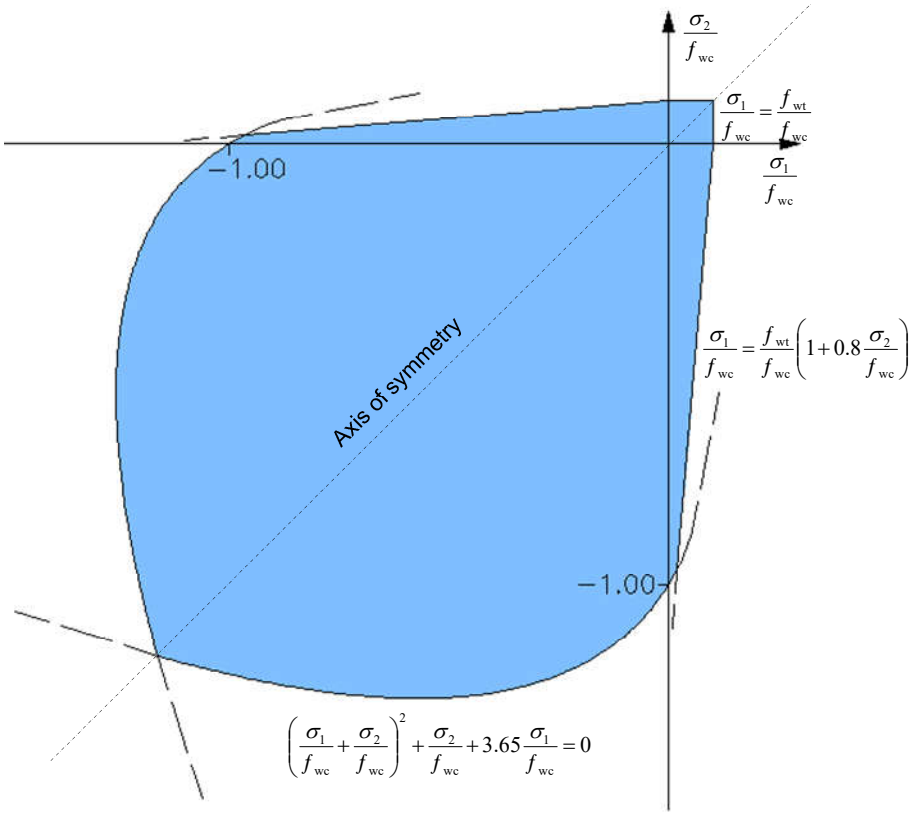

Figure 7. Kupfer and Gerstle isotropic failure criterion.

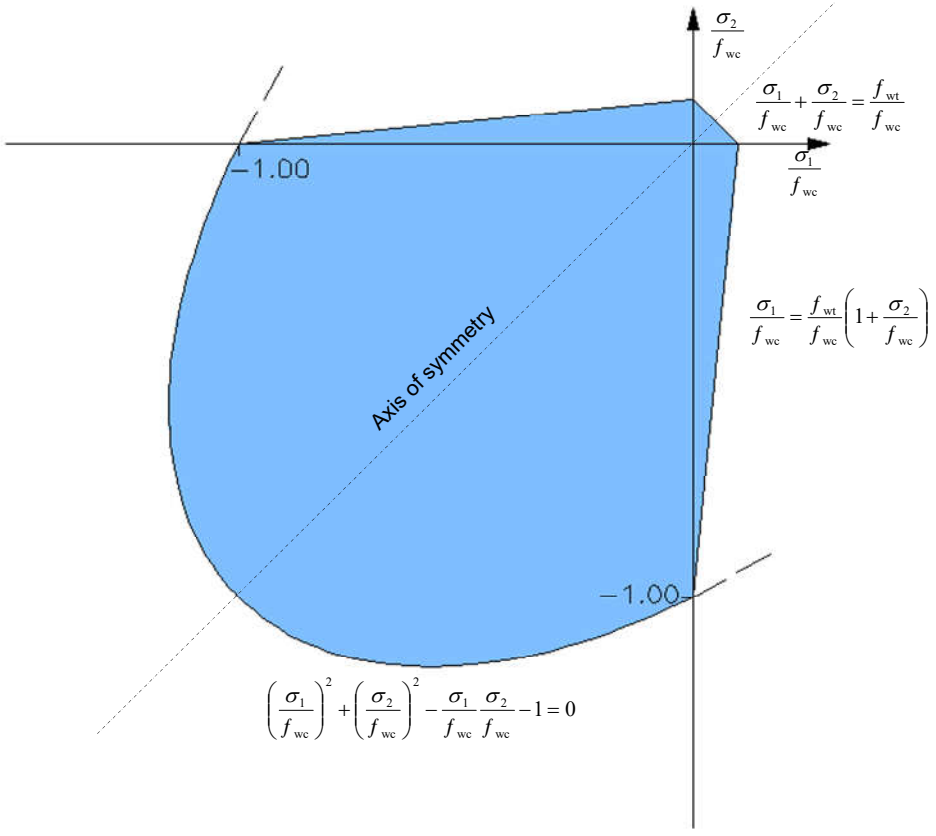

Figure 8. Von Mises modified isotropic failure criterion.

$$\left.\begin{array}{l} f\left(\sigma_x,\sigma_y,\tau\right)=2.27\sigma_x+9.87\sigma_y+0.573\sigma_x^2+1.32\sigma_y^2+6.25\tau^2-0.30\sigma_x\sigma_y+ \\ 0.009585\sigma_x^2\sigma_y+0.003135\sigma_x\sigma_y^2+0.28398\sigma_x\tau^2+0.4689\sigma_y\tau^2=1 \end{array}\right\} \quad (23)$$

By using the dimensionless terms $\left(\bar{\sigma}_x=\frac{\sigma_x}{f_{wc}^{90^\circ}},\ \bar{\sigma}_y=\frac{\sigma_y}{f_{wc}^{90^\circ}},\ \bar{\tau}=\frac{\tau}{f_{wc}^{90^\circ}}\right)$ and taking into account that $f_{wc}^{90^\circ}=7.555\ \mathrm{Mpa}$, the above equation can be written in the form of:

$$\left.\begin{array}{l} 17.15\,\bar{\sigma}_x+74.57\,\bar{\sigma}_y+32.71\,\bar{\sigma}_x^2+75.34\,\bar{\sigma}_y^2+356.74\bar{\tau}^2+ \\ -17.12\,\bar{\sigma}_x\bar{\sigma}_y+4.13\,\bar{\sigma}_x^2\,\bar{\sigma}_y+1.35\,\bar{\sigma}_x\bar{\sigma}_y^2+122.46\,\bar{\sigma}_x\bar{\tau}^2+ \\ +202.20\bar{\sigma}_y\bar{\tau}^2=1 \end{array}\right\} \quad (24)$$

Eliminating all third-order terms in Equation (24), a simplified failure criterion is derived [129,171,172]:

$$\left.\begin{array}{l} 17.15\,\bar{\sigma}_x+74.57\,\bar{\sigma}_y+32.71\,\bar{\sigma}_x^2+75.34\,\bar{\sigma}_y^2+356.74\bar{\tau}^2 \\ -25.91\,\bar{\sigma}_x\bar{\sigma}_y=1 \end{array}\right\} \quad (25)$$

This simple form of the criterion has already been used [173–176]. In Figures 9 and 10, graphical representations of cubic and simplified failure criterion in dimensionless principal and normal stress terms are depicted. Detailed description about the cubic tensor polynomial masonry failure criterion can be found in the works of Syrmakezis and Asteris [129] and Asteris [171,172].

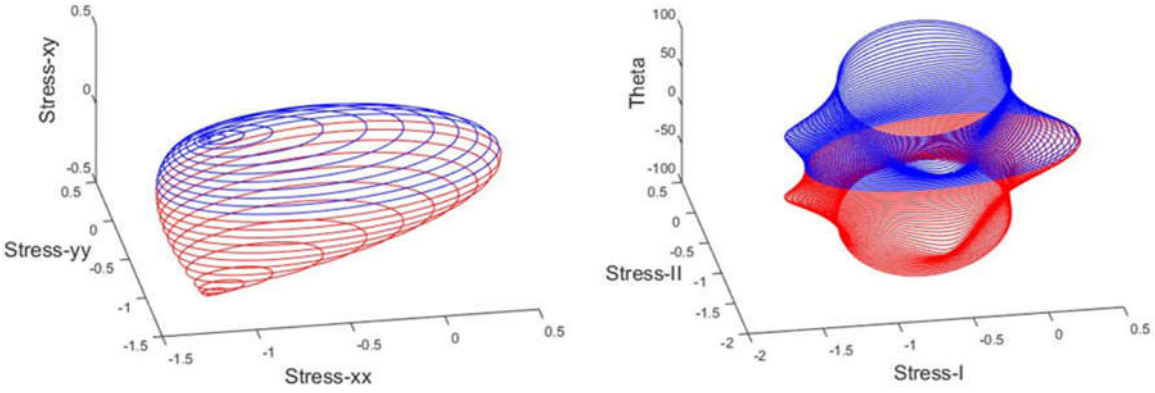

(**a**) (**b**)

Figure 9. Dimensionless failure surface of masonry material using the cubic tensor polynomial failure criterion: (**a**) non-dimensionless normal stress terms; and (**b**) non-dimensionless principal stress terms.

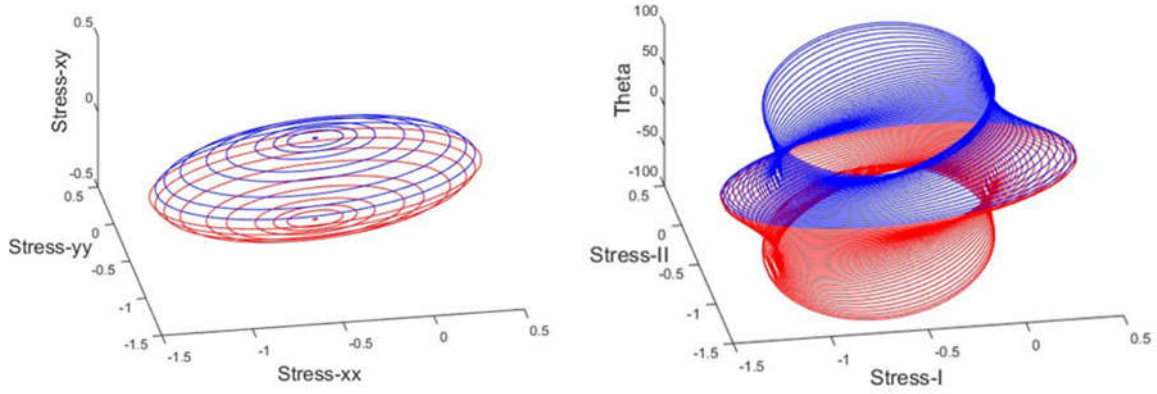

(**a**) (**b**)

Figure 10. Dimensionless failure surface of masonry material using the simplified failure criterion: (**a**) non-dimensionless normal stress terms; and (**b**) non-dimensionless Principal stress terms.

4.4.3. Failure Criterion Based on Artificial Neural Networks

This section summarizes the basic concepts of artificial neural networks (ANNs) as well as the architecture of the optimum ANN model developed for the modeling of masonry compressive strength. ANNs are information processing models configured for a specific application through a training process. A trained ANN has learned to rapidly map a given input into the desired output quantities (similar to curve fitting procedures) and thereby can be used as a meta-model enhancing the computational efficiency of a numerical analysis process. This major advantage of a trained ANN over conventional numerical analysis procedures, such as regression analysis, under the condition that the training and validation data cover the entire range of input parameters values, is that the results can be produced with much less computational effort [93,177–186].

In the present study, using the available in the literature experimental results conducted by Kupfer and Gerstle (1973) [160] concerning the failure of concrete under biaxial stresses, the Back-Propagation Neural Network (BPNN) technique was used for the development of a reliable and robust ANN that can predict the failure of concrete. To this end, for each failure point (experimental data), the polar angle was used as input parameter, while the polar radius was selected as output parameter.

In light of the above, 36,900 BPNN models (900 with one hidden layer and 36,000 with two hidden layers) were studied. The parameters used for the training of NN models are summarized in Table 2. All developed ANN models were ranked based on the Root Mean Square Error (RMSE). Based on the results, the optimum BPNN model is that of 1-3-5-1 structure. This network corresponds to the case of architecture with two hidden layers of 3 and 5 neurons, respectively (Figure 11). Using this optimum ANN model, the concrete failure criterion under biaxial stress state both in dimensional principal stresses terms (Figure 12a) and in polar coordinates (Figure 12b) was produced.

Table 2. Training Parameters of BPNN models.

Parameter	Value
Training Algorithm	Levenberg–Marquardt Algorithm
Number of Hidden Layers	1; 2
Number of Neurons per Hidden Layer	1 to 30 by step 1
Cost Function	Mean Square Error (MSE); Sum Square Error (SSE)
Transfer Functions	Hyperbolic Tangent Sigmoid transfer function (tansig); Log-sigmoid transfer function (logsig); Linear transfer function (purelin)

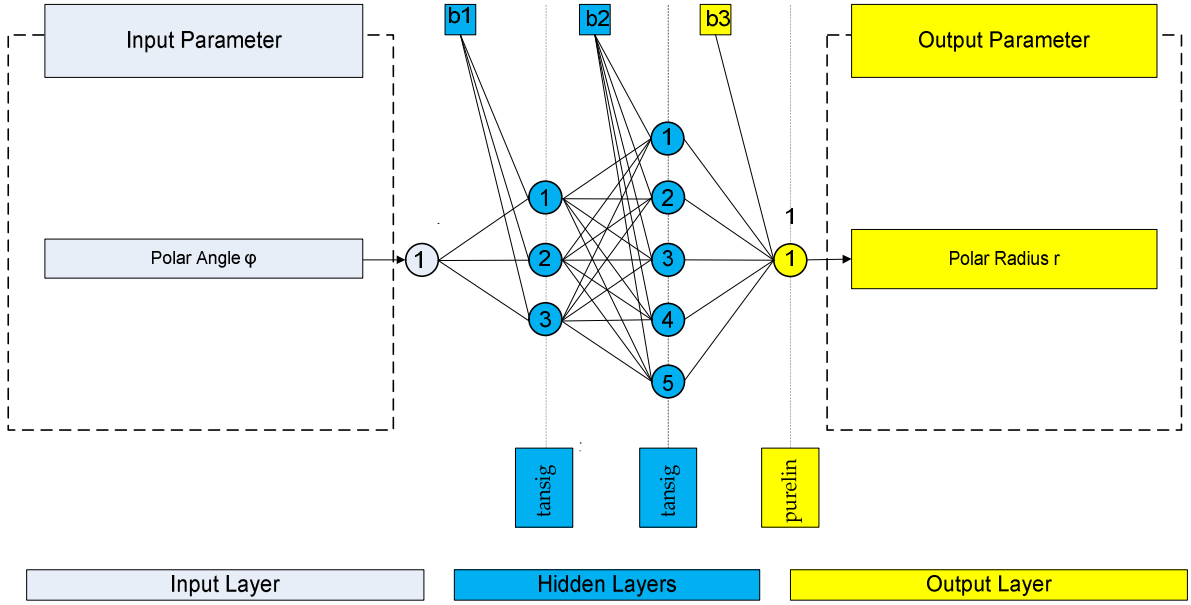

Figure 11. Architecture of the optimum 1-3-5-1 BPNN model.

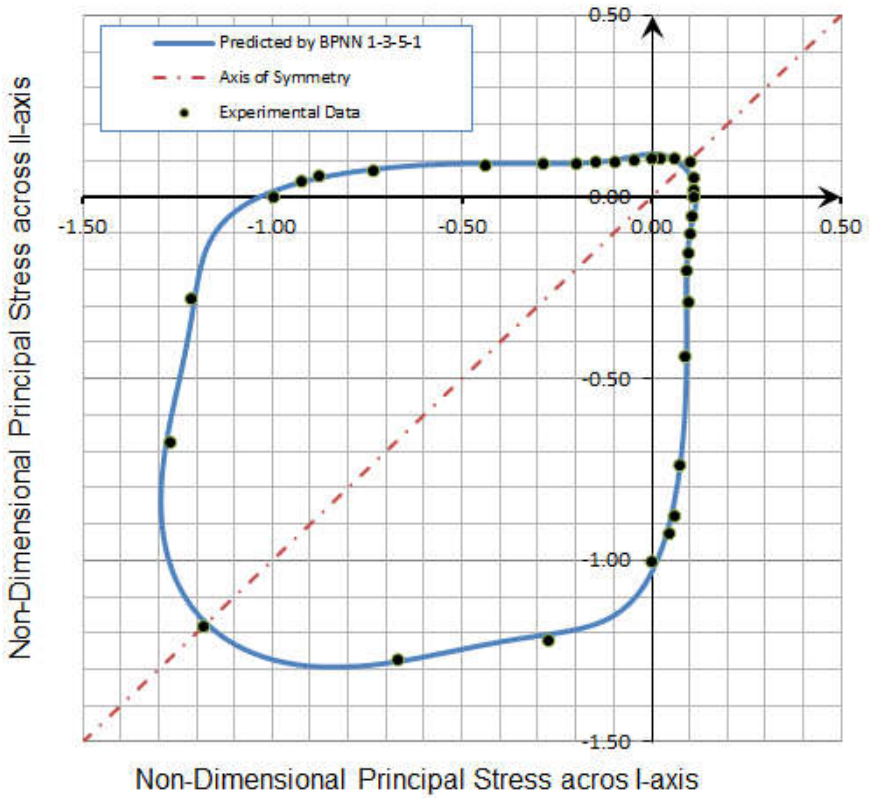

(**a**)

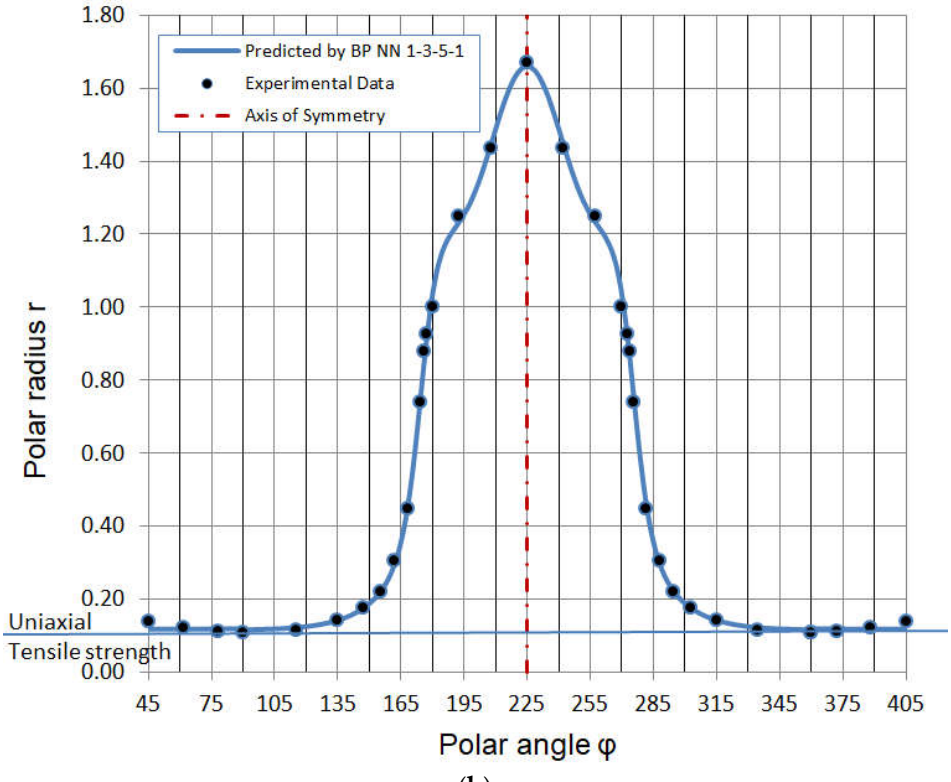

(**b**)

Figure 12. Concrete failure criterion under biaxial stress state: (**a**) in dimensional principal stresses terms; and (**b**) in polar coordinates.

It is common practice in published literature on NN models for the authors to present the architecture of the optimum NN model without providing any information regarding the final values of NN weights. Admittedly, this practice has very little value for other researchers and practicing engineers. To be useful, a proposed NN architecture should be accompanied by the (quantitative) values of weights [186]. In such a case, the NN model can be readily implemented in an MS-Excel spread sheet, thus available to anyone interested in the issue of modeling.

In this study, the final values of weights and biases of the optimum proposed BPNN 1-3-5-1 model are explicitly reported in Figure 13 and Table 3. By using the reported values of weights and biases, as well as the architecture of the NN (Figure 11), one can easily build an ANN-based estimator for the failure criterion of concrete under biaxial stress state.

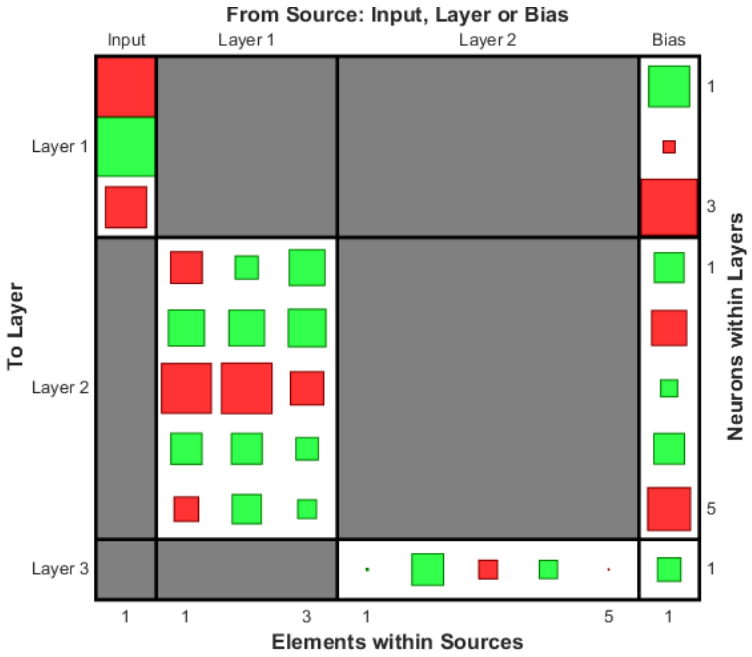

Figure 13. Final weights and bias values of the optimum BPNN model 1-3-5-1 (the values are presented in Table 3).

Table 3. Final weights and bias values of the optimum BPNN model 1-3-5-1.

iw{1,1}					**b{1,1}**
−4.200000					4.200000
4.200000					0.000000
−4.200000					−4.200000
	iw{2,1}				**b{2,1}**
−0.769482	1.643125	1.561766			2.393966
0.598218	1.776735	1.488765			−1.196983
−0.551786	−1.290814	−1.939177			0.000000
0.995858	2.075282	0.657683			1.196983
−0.754269	2.267663	−0.140916			−2.393966
		iw{3,2}			**b{3,1}**
0.264303	0.136018	0.055781	−0.495701	0.754626	0.996540

iw{1,1}, weights values for input layer; iw{2,1}, weights values for first hidden layer; iw{3,2}, weights values for second hidden layer; b{1,1}, bias values for first hidden layer; b{2,1}, bias values for second hidden layer; b{3,1}, bias values for output layer.

4.5. Damage Index

Damage control in a building is a complex task, especially under seismic action. Several response parameters can be instrumental in determining the level of damage that a particular structure suffers during a ground motion; the most important are: deformation, relative velocity, absolute acceleration, and plastic energy dissipation (viscous or hysteretic). Controlling the level of damage in a structure consists primarily in controlling its maximum response. Damage indices establish analytical relationships between the maximum and/or cumulative response of structural components and the level of damage they exhibit [38,187–191]. A performance-based numerical methodology is possible if, through the use of damage indices, limits can be established to the maximum and cumulative response of the structure, as a function of the desired performance of the building for the different levels of the design ground motion. Once the response limits have been established, it is then possible to estimate the mechanical characteristics that need to be supplied to the building so that its response is likely to remain within the limits.

For the case of masonry structures, a new damage index was proposed by Asteris et al. (2014) [38], which employs as response parameter the percentage of the damaged area of the structure relatively to the total area of the structure. The proposed damage index (DI) for a masonry structure can be estimated by

$$[DI] = \frac{A_{fail}}{A_{tot}} \times 100 \tag{26}$$

where A_{fail} is the damaged surface area of the masonry structure and A_{tot} is the total surface area of the masonry walls of the structure.

For a discussion on alternative damage indexes, the reader is referred for instance to the Ph.D. thesis by Rota [192] and to the master theses by Zamora [193], Douvika [194] and Skentou [195].

4.6. Damage States and Structural Performance Levels

As is common practice today, performance-based seismic design is initiated with an interplay between demands and appropriate performance objectives. The task of the engineer is to then develop a design capable of meeting these objectives. Performance objectives are expressed as an acceptable level of damage, typically categorized as one of several performance levels, such as immediate occupancy, life safety or collapse prevention, given that ground acceleration of specified severity is experienced.

In the past, the practice of meeting performance-based objectives was already included in design practice, but in a rather informal, simplistic and non-standardized way. Some engineers would characterize performance as life-safety or not; others would assign ratings ranging from poor to good. This qualitative approach adopted for performance prediction was appropriate given the limited capability of seismic-resistant design technology to deliver building designs capable of quantifiable performance.

In the approach presented herein, we consider three structural performance levels in a similar way to the Federal Emergency Management Agency [196]: (a) heavy damage; (b) moderate damage; and (c) insignificant damage. The performance levels and the associated damage states are defined by the values of DI, as shown in Table 4 and Figure 14. In particular, a value of DI less than 15% can be interpreted as insignificant damage; from 15% to less than 25%, as moderate damage; and greater than or equal to 25% as heavy damage. Of course, other approaches could be used, according to the recent European Codes [197], based on a more engineered (and more detailed) estimation of damage.

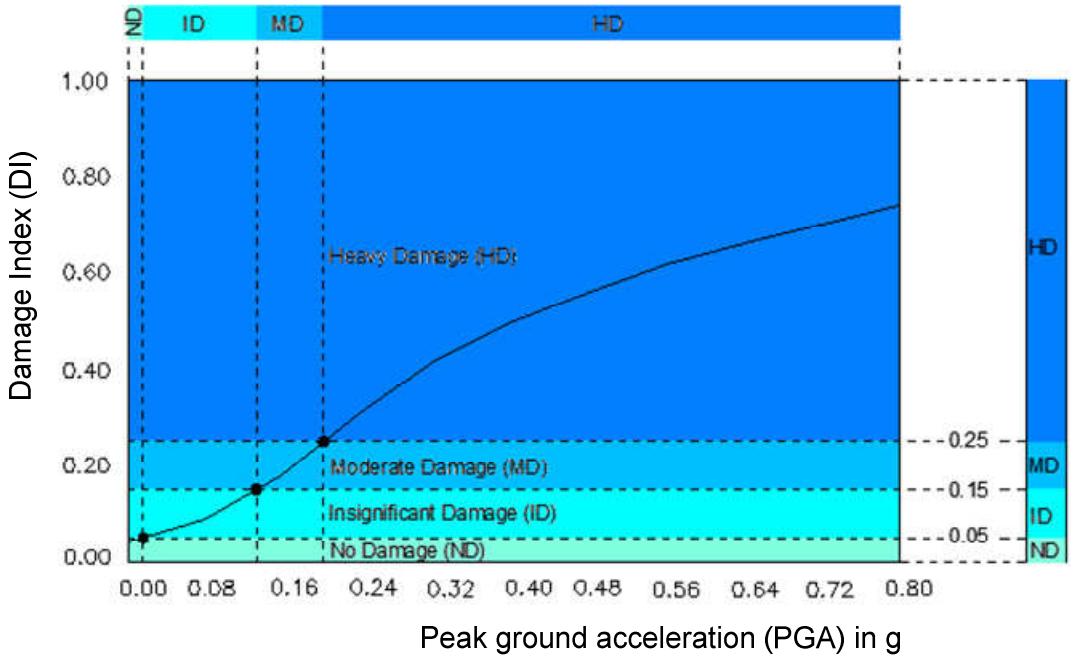

Figure 14. Definition of Limit States (LS) thresholds and Damage States (DS) ranges.

Table 4. Proposed Structural Performance Levels for un-reinforced masonry.

Damage State	Insignificant Damage	Moderate Damage	Heavy Damage
Element	Minor cracking of veneers. Minor spalling in veneers at a few corner openings. No observable out-of-plane offsets.	Extensive cracking. Noticeable in-plane offsets of masonry and minor out-of-plane offsets.	Extensive cracking. Face course and veneer may peel off. Noticeable in-plane and out-of-plane offsets.
[SL]	0.05 ≤ DI <0.15% Immediate occupancy	0.15 ≤ DI <0.25 Life safety	0.25% ≤ DI <1.00 Collapse prevention

It is worth noting that, for the definition of damage States (DS) ranges, expert opinions are needed. When no experimental data are available and analysis of the behavior is not feasible, one or more knowledgeable individuals (experts) can offer an opinion as to values of SL defining the damage states (DS) ranges, based either on experience or judgment. Furthermore, these SL must be periodically updated based on experimental and analytical data, when such data are available.

4.7. Fragility Curves

One of the problems the engineer must face and resolve at the later stages of this integrated approach involves the quantitative vulnerability assessment of the building in its current state (damaged or not), as well as its projected behavior once it has been "modified" after interventions. In other words, a method is necessary to assess the seismic vulnerability of the existing structure as well as to assess the intervention scenarios and rank them according to the reduction they induce to the seismic vulnerability, thus leading to the selection of the optimal intervention scenario. One of the most important tools is considered to be fragility analysis, which provides a measure of the safety margin of the structural system above specified structural performance/hazard levels.

Several methodologies for performing fragility analysis have been proposed in the past (used to assess the behavior of structural systems). Simplified methodologies for fragility evaluation were proposed by Kennedy et al. (1980) [198], Kircher et al. (1997) [199], Porter et al. (2007) [200,201], D'Ayala et al. (2010) [202], Cattari and Lagomarsino (2012) [203] and Kazantzi et al. (2015) [204]. A detailed state-of-the-art report can be found in HAZUS 2003 [205].

A very interesting 3D homogenized FE limit analysis software package was produced by Milani and Venturini (2011) [4] for the fragility curve evaluation of existing masonry churches. It is a two-step approach. In the first phase, homogenized masonry strength domains are obtained using a simplified kinematic procedure applied on a three-leaf unitary cell. In the second phase, homogenized domains are implemented at a structural level on a plate and cell kinematic FE software. The procedure is tested on two real scale existing churches located in Italy and compared to results provided by means of a conventional elastic approach performed by means of a standard commercial software. The global behavior at failure and the overall strength of the buildings are assessed through Monte Carlo simulations varying both masonry mechanical properties and direction of the equivalent seismic load. Recently, Azizi-Bondarabadi, Mendes, Lourenço and Sadeghi 2018 [206], based on the fact that school facilities in Iran, in particular masonry schools, have shown poor performance during past earthquakes and can be identified as one the country's most vulnerable infrastructures to earthquakes, proposed a method to perform index-based damage assessment for brick masonry schools located in the province of Yazd, the central region of Iran, using a comprehensive database of school buildings. The database occurred from field survey forms applied for each observed school, which collected the features and damages of each structure. The results of a vulnerability index method developed in Iran were employed as input data to obtain empirical fragility curves for the school inventory. The Macroseismic model [207] and GNDT II level method [208] were two empirical methods combined in this procedure. Finally, the procedure was verified using damage survey data obtained after recent earthquakes (1990 Manjil-Rudbar earthquake and 2003 Bam earthquake) that occurred in Iran.

Evaluating seismic fragility information curves for structural systems involves: (a) information on structural capacity; and (b) information on the seismic hazard. Since both aforementioned contributing factors are uncertain to a large extent, the fragility evaluation cannot be carried out in a deterministic manner. A probabilistic approach, instead, needs to be utilized in the cases in which the structural response is evaluated and compared against "limit states", that is limiting values of response quantities correlated to structural damage (see Table 4).

Fragility, as shown in Figure 15, is the probability of the structural damage to reach or exceed a certain damage threshold di (performance level) under a given earthquake level (Peak Ground Acceleration (PGA)). It generally increases as the earthquake intensity level increases. The failure domain is where a Damage Index (DI) overcomes a specified threshold (damage index or performance level).

Fragility is evaluated as the total probability of a response parameter R exceeding the allowable response value r_{lim} (limit-state), for various earthquake intensities I. In mathematical form, this is simply a conditional probability (Barron-Corverra 2000 [209] and Reinhorn et al. 2001 [210]) given by

$$Fragility = P\left[R \geq r_{\lim} \middle| I\right] = \sum_{j}^{3} P\left[R \geq r_{\lim} \middle| I, C\right] P\left(C = c_j\right) \quad (27)$$

where P(C = c_j) denotes the probability that capacity c_j occurs, R is the response parameter and I is the earthquake intensity.

In related literature, for the determination of the probability, the use of Probability Density Functions (PDF) is indicated, such as the normal distribution, the lognormal distribution, the Weibull distribution, the Gamma distribution, etc. [211]. In the current research, normal and logarithmic distributions were used. In Section 7, where case studies are presented, basic steps for the development of the fragility curves are presented in a detailed manner.

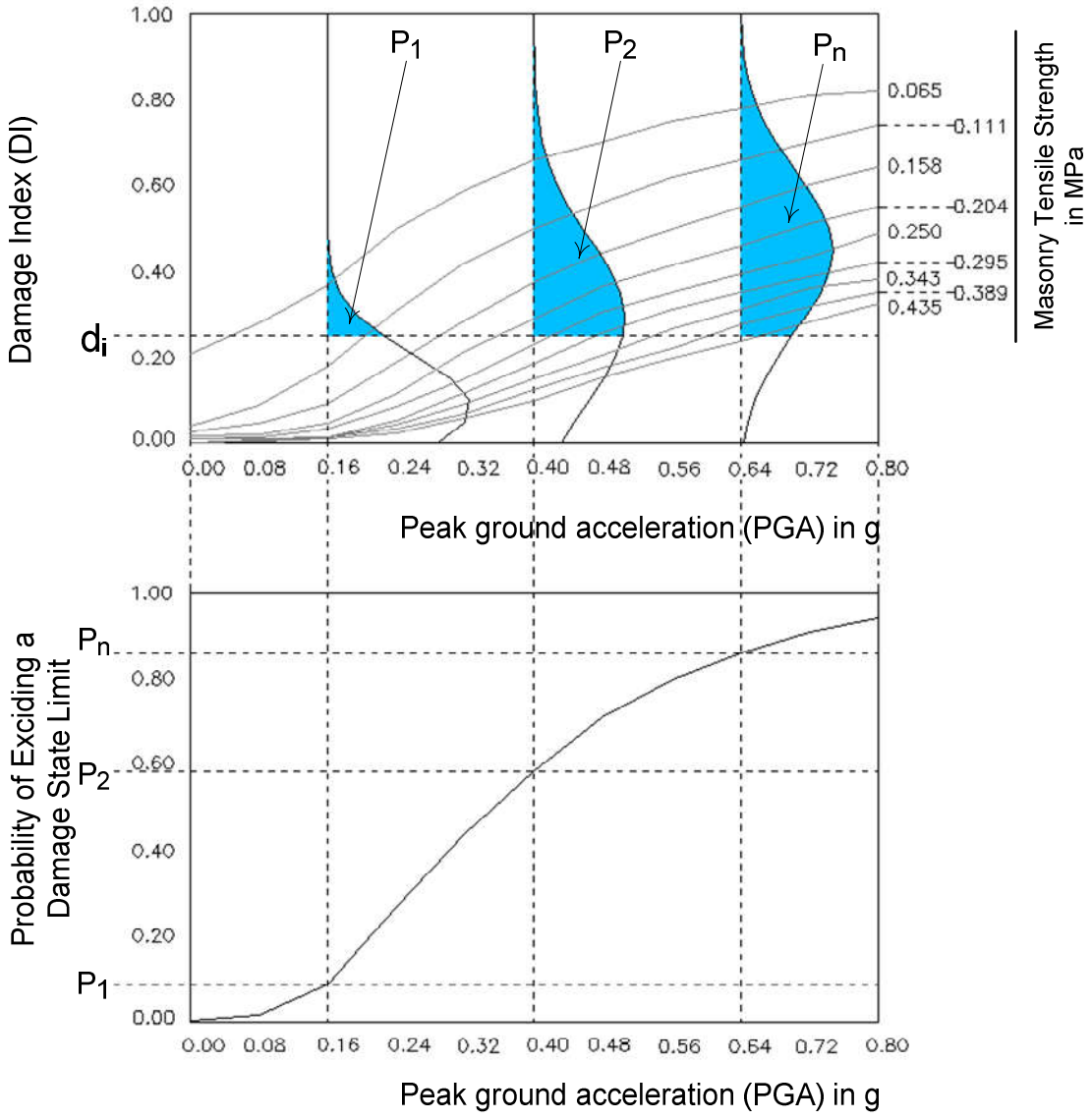

Figure 15. Development process of analytical fragility curves.

Detailed state-of-the-art reports on the fragility analysis of masonry buildings and more specifically on the derivation of fragility curves one can be found in the works by Erberik [14,15], in the Ph.D. thesis of Rota [192], in some Master theses [193,212] and in other works [213–222].

5. Finite Element Code

Based on the above proposed FE macro-model, a computer code called MAFEA (MAsonry Finite Element Analysis), in MATLAB® programming language was developed for the structural design and analysis of unreinforced masonry (URM) walls. In the following two subsections, the basic computational characteristics of the code are presented, as well as a step by step short presentation of its main advantages and novelties, illustrated through a case study: the analysis of a 2D masonry wall that is part of a set of 2D masonry walls, presented detailed in Section 7 entitled *Case Studies*.

5.1. Basic Characteristics of Finite Element Code

The code was developed in the Computational Mechanics Laboratory at the School of Pedagogical & Technological Education, Athens, Greece, under the supervision of Prof. Asteris. In particular, the code was developed during the last decade in the framework of the Master's Program in *Applied Computational Structural Engineering (ACSE)*. The code was continuously updated in the course of supporting a series of Master Thesis under the supervision of Professor Asteris [194,195].

During the development procedure, special attentionwas given to matrix processing techniques that economize storage and solution time by taking advantage of the special structure of the stiffness matrix. Specifically, based on the symmetry, sparse, and band form to the principle diagonal of the stiffness matrix, an iterative solution technique—such as the Gaussian elimination algorithm, tailored to the specific case of banded matrix (half bandwidth)—was used for the solution of finite element equilibrium equations of the structure. One of its main advantages has to do with the assembling of total Stiffness Matrix of the structure using the stiffness matrix of each one Finite Element comprising the total structure. In this way, the stiffness matrix of each one FE is expanded from 8 × 8 to n × n, where n being the number of degrees of freedom (DOF) of the entire structure. The MATLAB® code below was written to expand the FE stiffness matrix to the total stiffness matrix of the structure.

```
clc; clear;

eldof = 8; % eldof (=8)the number of dofs per element
% Form the steering vector from element's degrees of freedom
eldofs = [1; 2; 5; 6; 7; 8; 10; 11];
%{
% Assemble the global stiffness matrix putting the element stiffness matrix in
global system
%}
for i = 1:eldof
  if eldofs(i) ~= 0
    for j = 1: eldof
      if eldofs(j) ~= 0
      k_glob(eldofs(i),eldofs(j))=k_glob(eldofs(i),eldofs(j))+k_elem_glob(i,j);
      end
    end
  end
end
```

During the development procedure, special attention was given to the graphic imaging of the analysis results. The program possesses the capability of automatic crack pattern generation and associated damage indices for the set of masonry failure criteria that are presented in the previous section. For each criterion, a color image is generated depicting the failure areas of the masonry wall and highlighting in distinct ways the kind of stress underpinning the failure. Namely, the developed failure of the masonry wall is marked as failure under biaxial tension, which is the most crucial for structure, failure under biaxial compression and the most common case of failure, under heterosemous biaxial stress state (tension/compression).

5.2. Presentation of the Finite Element Code

For the presentation of the main advantages and novelties of the FE code, a 2D masonry wall aws used, which is part of four 2D masonry walls, presented detailed in Section 7 entitled *Case Studies*. Namely, the 2D masonry wall L50100 was studied using the MAFEA code. The geometrical and mechanical characteristics are presented in Section 7 (Figure 36 and Table 9.)

Using the MAFEA code, Figures 16–34 have been produced. The first eight figures present the usual, well-known diagrams (undeformed and deformed shape, and stress contours in both normal and principal stress terms) which derive from all structural analysis programs and are therefore not further explained. In Figures 24 and 25, the developed stress states in both normal and principal stress terms are presented. For each stress state, a different color is used depicting the stress state. Namely, the developed stress state of the masonry wall is marked as stress state under biaxial tension, which is the most crucial for structure, stress state under biaxial compression and the most common case of stress under heterosemous biaxial stress state (tension/compression). These figures are especially useful, as they combine the information of the usual Figures 18–23 while at the same time providing useful information regarding the developed stresses in a simple and comprehensive manner. This enables a quick preliminary assessment of the seismic vulnerability. For example, in Figure 24, it is confirmed that the most vulnerable area of the masonry is around the corners of the openings, which is to be expected, as this is the area where cracks usually are generated, leading to the consequent damages. Correspondingly, Figures 26 and 27 contribute in the same direction, where the values of the developed stresses are depicted for each joint of the FE mesh. With knowledge of the maximum values of developed stresses alone, one can design and propose repair mortars to ensure that the developed stresses are adequately addressed, thus improving the seismic response of the structure.

In addition to this preliminary evaluation of vulnerability, Figures 28–31 provide a more in-depth assessment of vulnerability on a second, more detailed level. Namely, in these figures, the failure of the masonry wall for each failure criterion presented in the previous section is presented. For each criterion, a color image is generated depicting the failure areas of the masonry wall and highlighting in distinct ways the kind of stress underpinning the failure, namely the developed failure of the masonry wall marked as failure under biaxial tension, which is the most crucial for structure; failure under biaxial compression; and the most common case of failure, under heterosemous biaxial stress state (tension/compression). Such a diagram is of great interest and extremely useful for the assessment of more complicated structures, as well. As can be easily perceived, different repair measures are demanded when failure occurs under biaxial compression, different measures are demanded in the case of biaxial tension and different measures are demanded in the case of heterosemous biaxial stress state (tension/compression).

Beyond the above advantages of the MAFEA code, it is also an educational tool of great importance, which supports lectures to both undergraduate and graduate students in relation to the seismic behavior of structures (Figures 32–34). Furthermore, the above presented basic characteristics and the advantages of the MAFEA code are presented in more detail Section 7 entitled *Case Studies*.

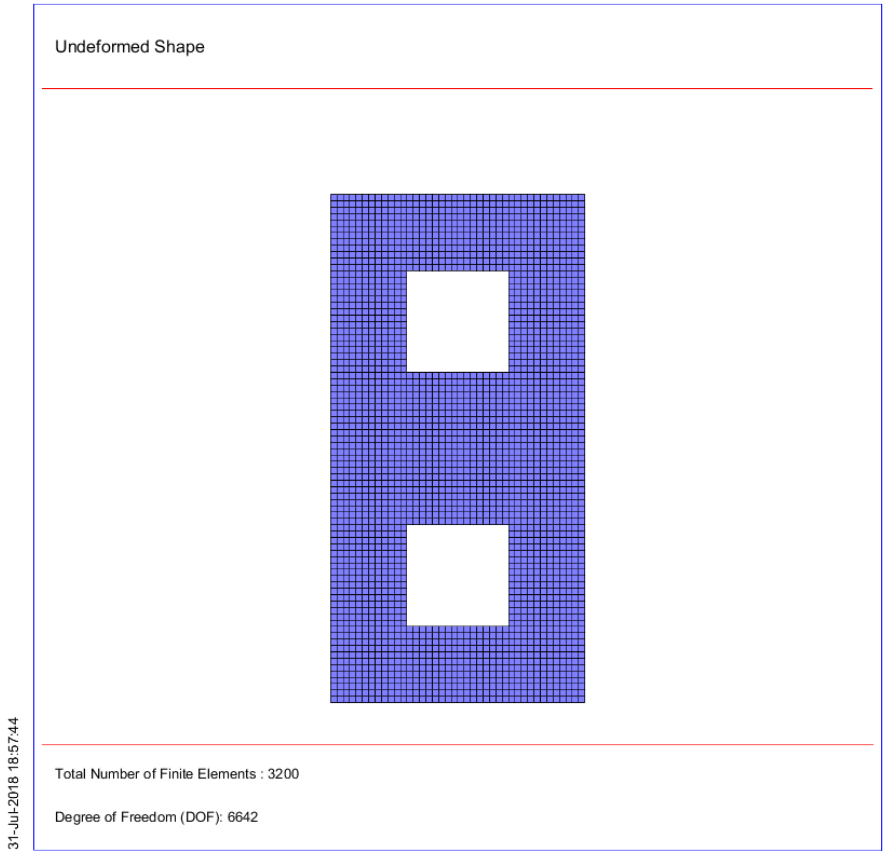

Figure 16. Undeformed shape and FE MESH of 2D masonry wall L50H100 (Figure 11a) with two openings (PGA = 0.40 g).

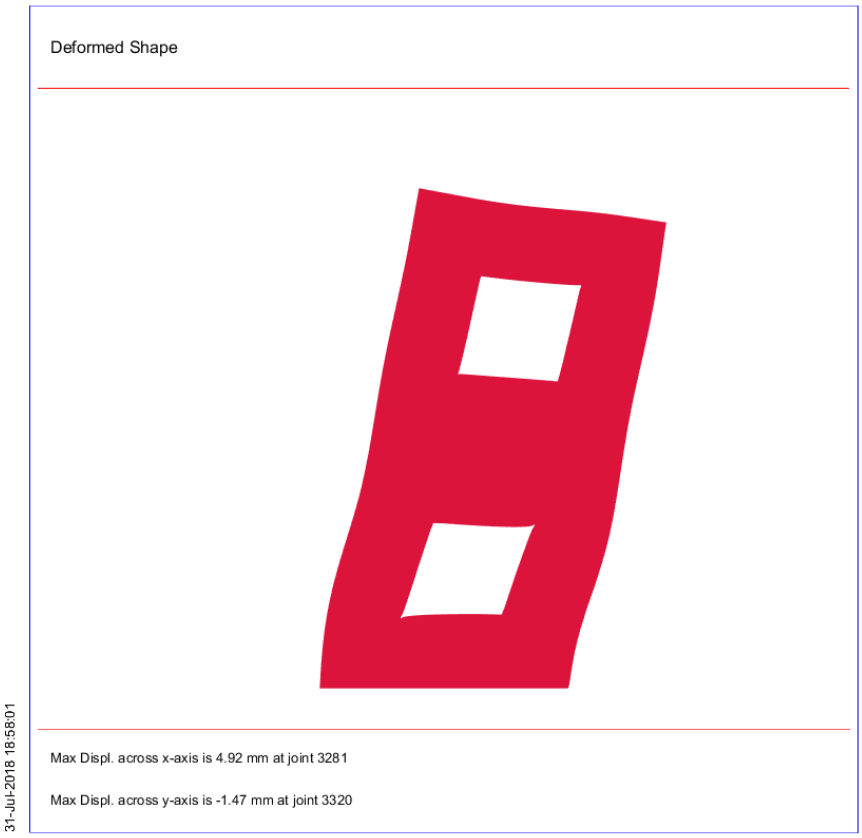

Figure 17. Deformed shape of 2D masonry wall L50H100 (Figure 11a) with two openings (PGA = 0.40 g).

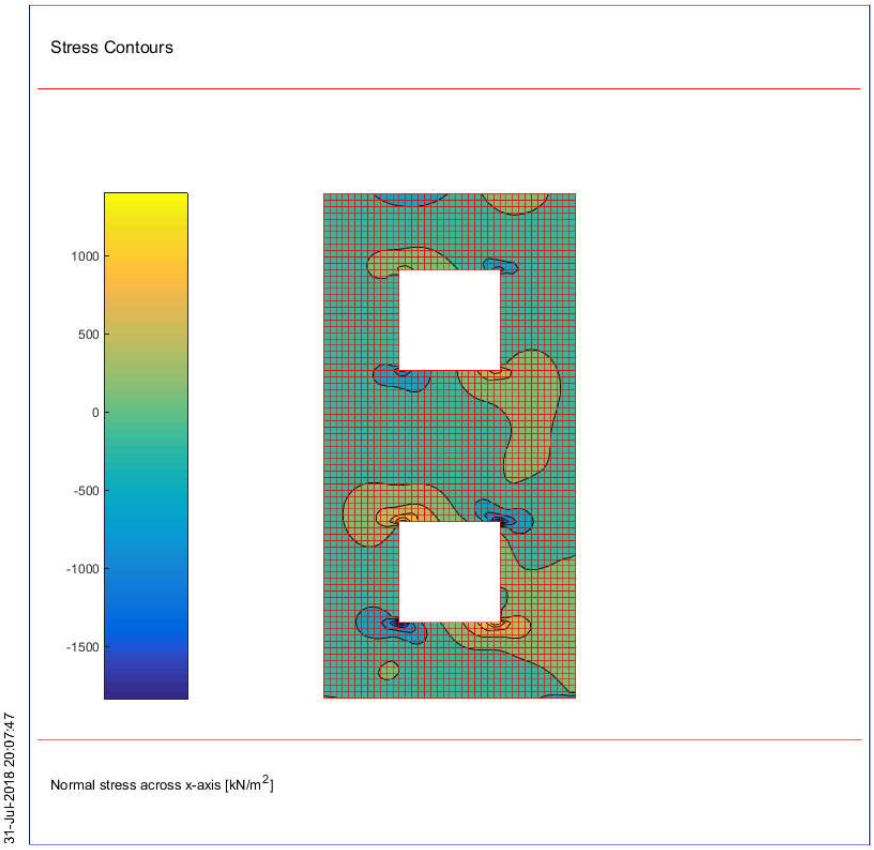

Figure 18. Stress contours of normal stress across x-axis (PGA = 0.40 g).

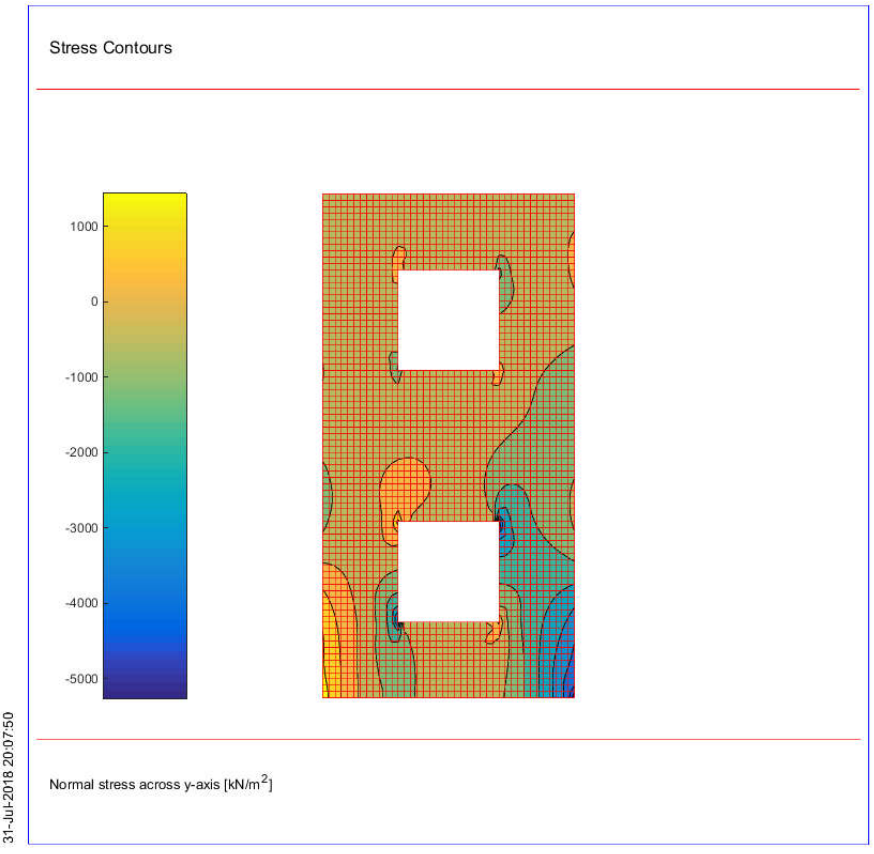

Figure 19. Stress contours of normal stress across y-axis (PGA = 0.40 g).

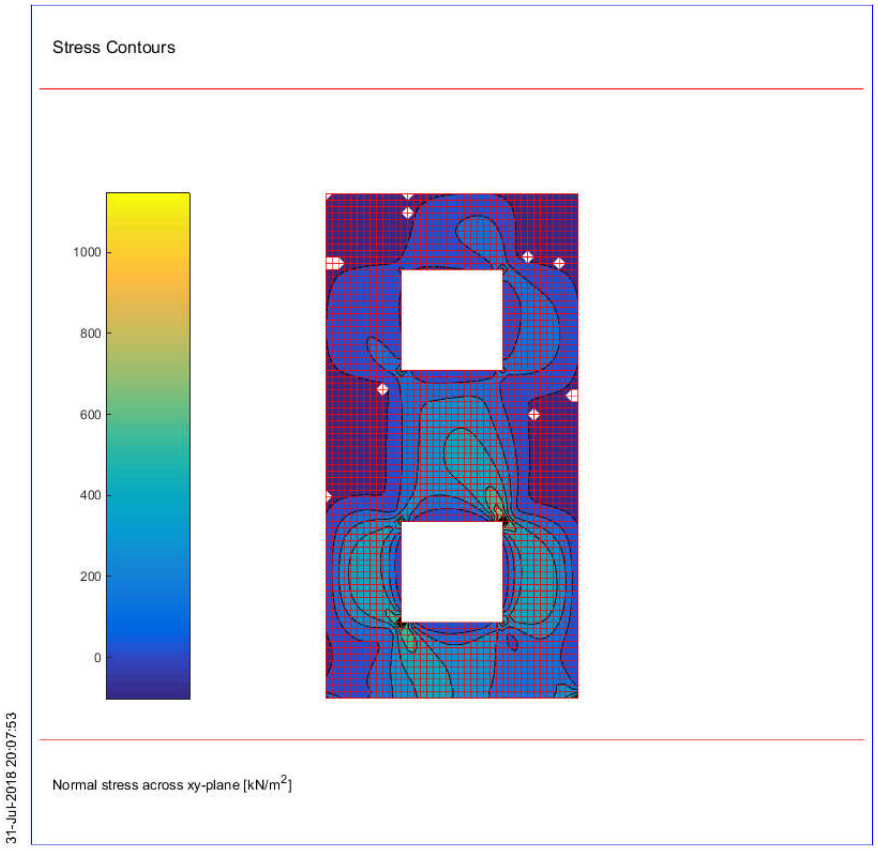

Figure 20. Stress contours of shear stress (PGA = 0.40 g).

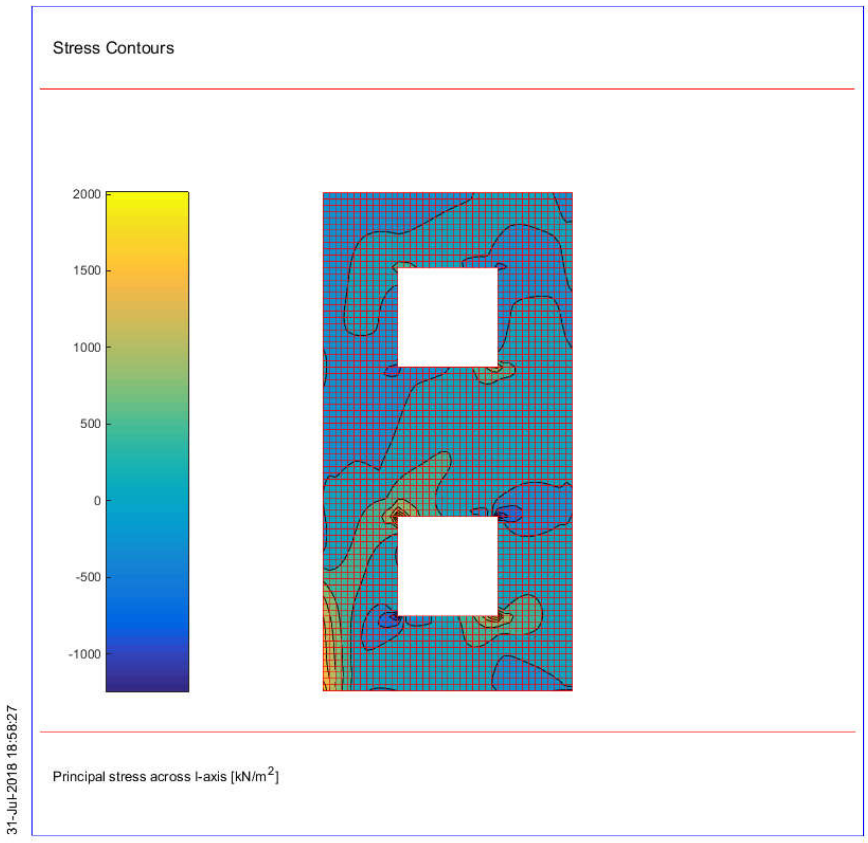

Figure 21. Stress contours of principal stress across I-axis (PGA = 0.40 g).

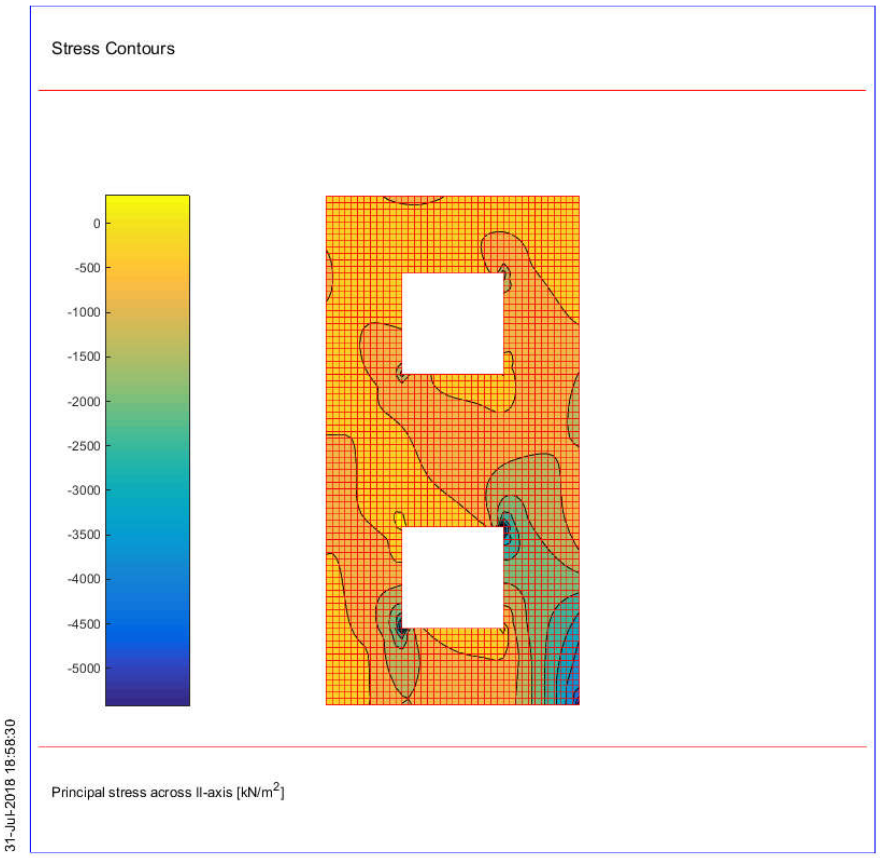

Figure 22. Stress contours of principal stress across II-axis (PGA = 0.40 g).

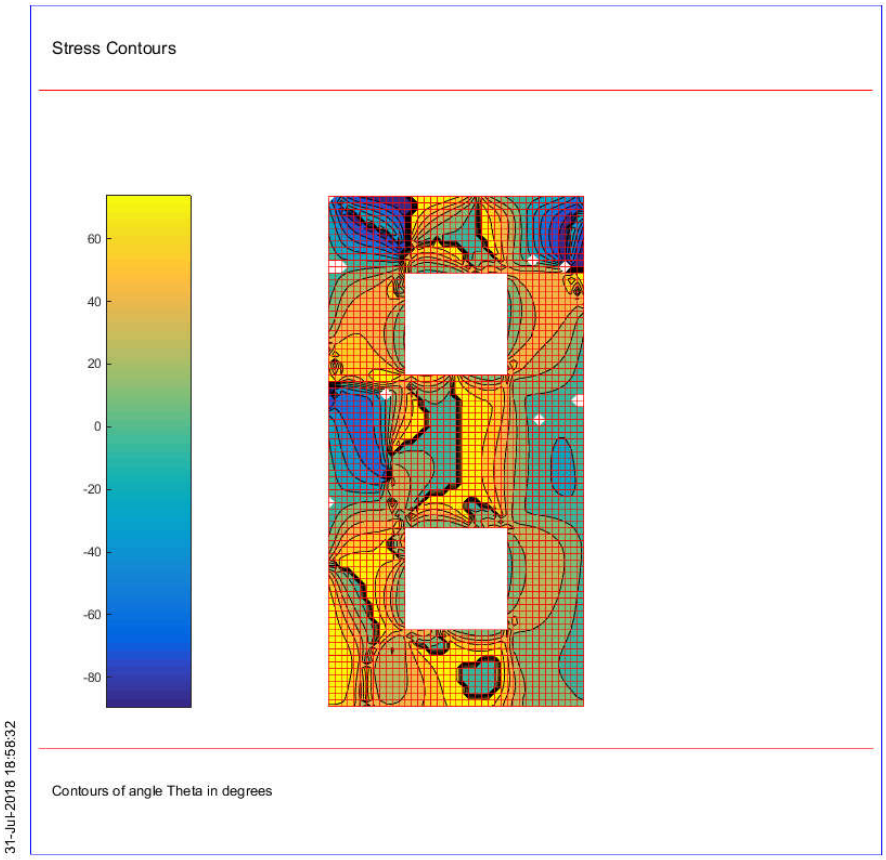

Figure 23. Contours of angle theta (PGA = 0.40 g).

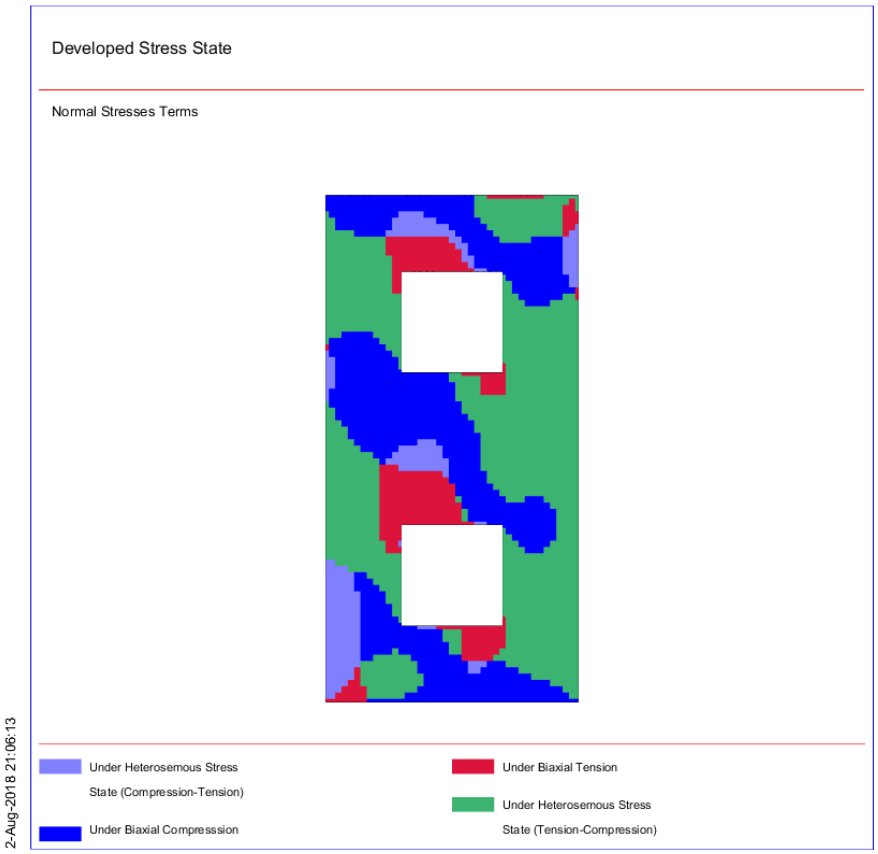

Figure 24. Developed stress state in normal stresses terms (PGA = 0.40 g).

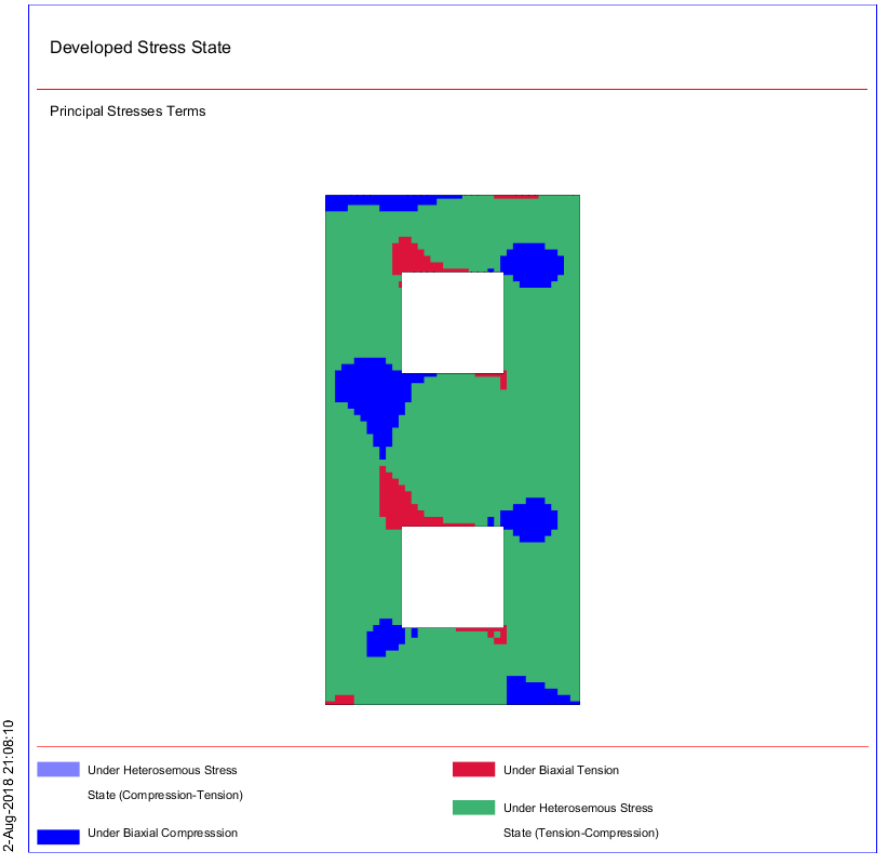

Figure 25. Developed stress state in principal stresses terms (PGA = 0.40 g).

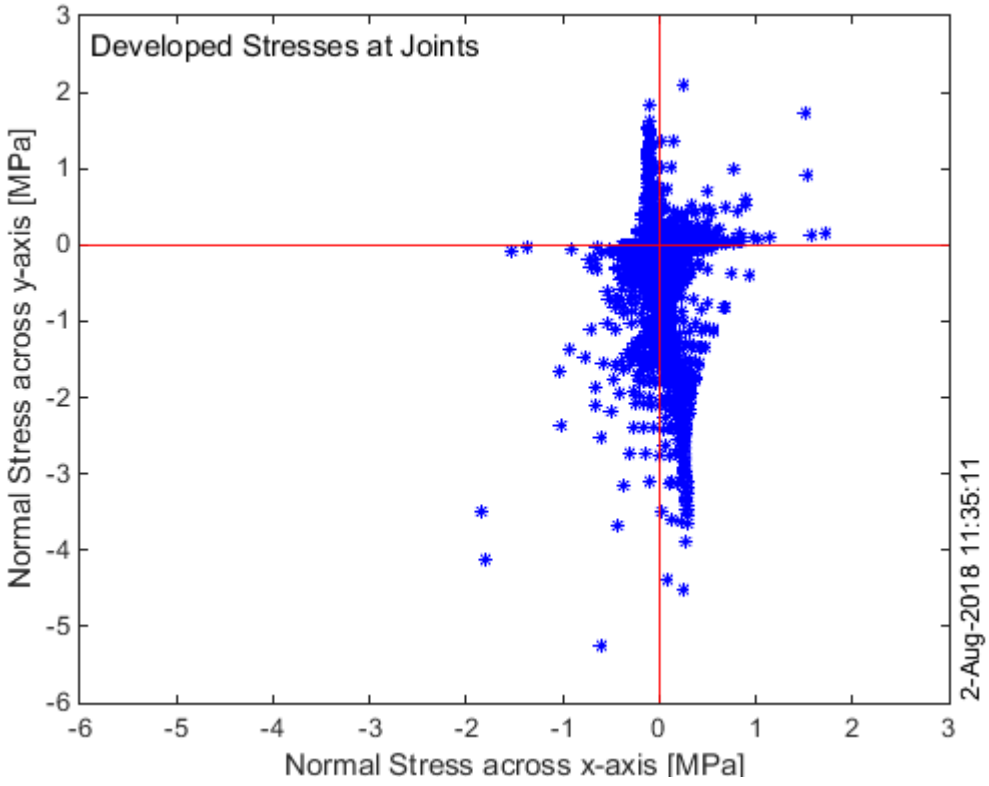

Figure 26. Developed stresses in normal stresses terms (PGA = 0.40 g).

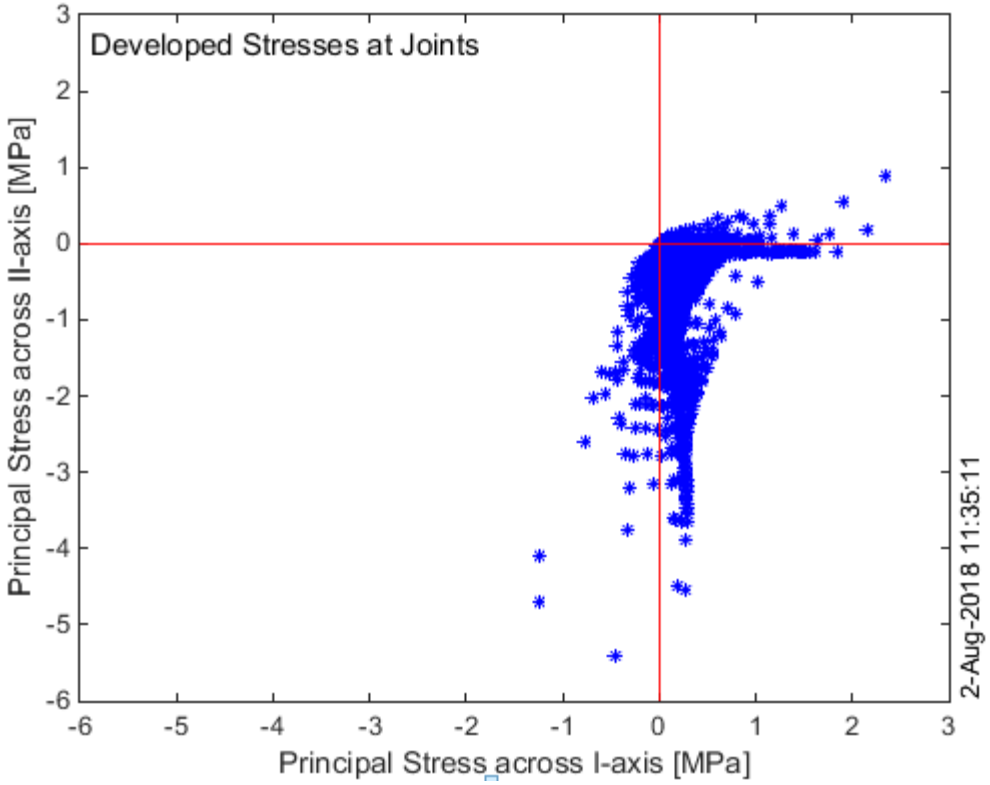

Figure 27. Developed stresses in principal stresses terms (PGA = 0.40 g).

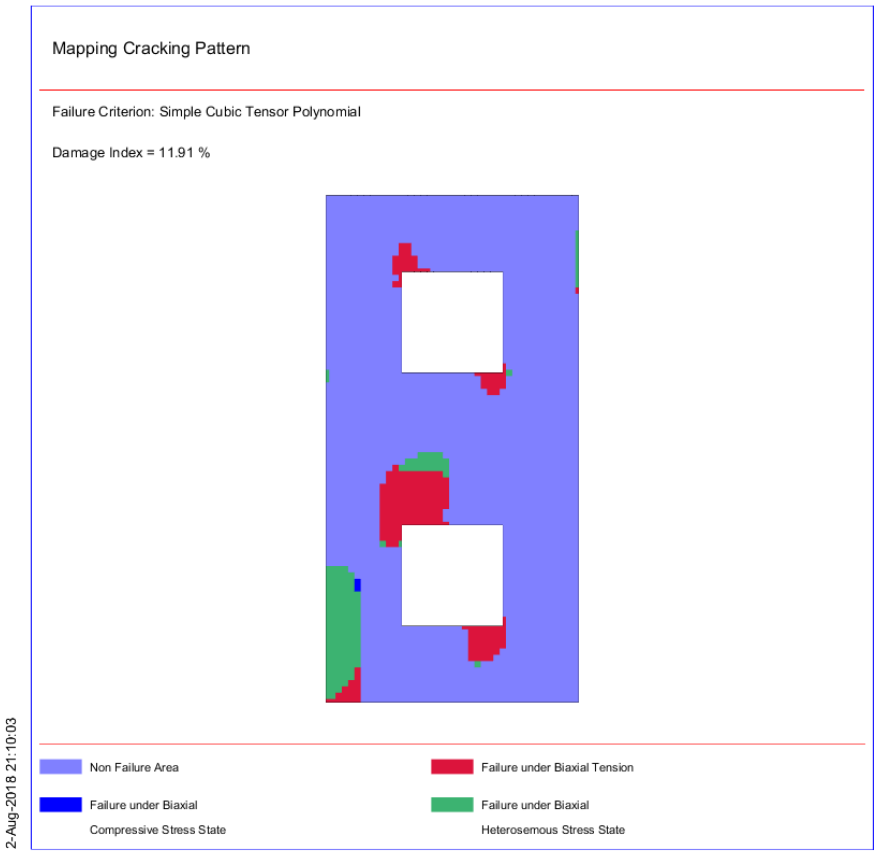

Figure 28. Mapping cracking pattern based on simple cubic tensor polynomial failure criterion.

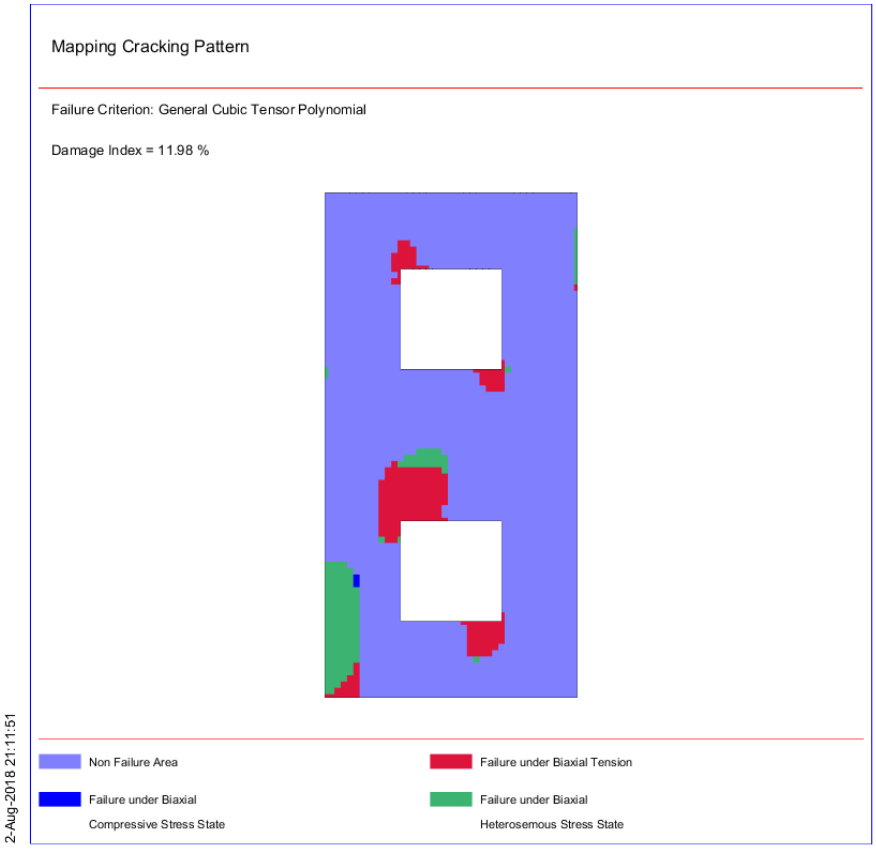

Figure 29. Mapping cracking pattern based on general cubic tensor polynomial failure criterion.

Figure 30. Mapping cracking pattern based on Syrmakezis et al.'s (1995) failure criterion.

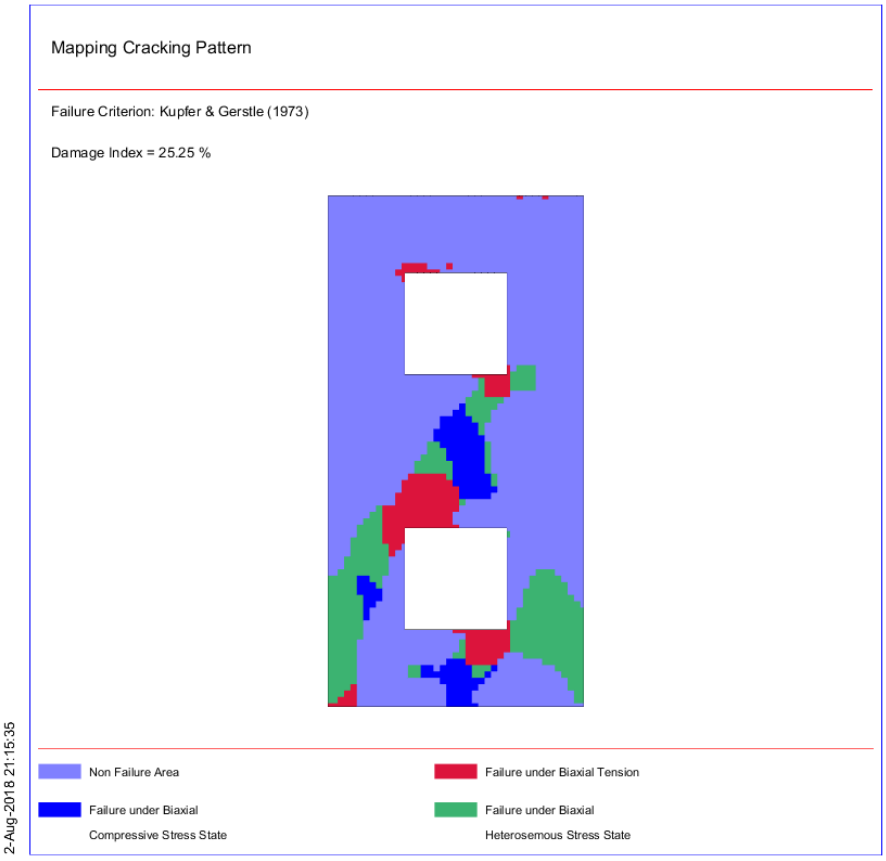

Figure 31. Mapping cracking pattern based on Kupfer and Gerstle's (1973) failure criterion.

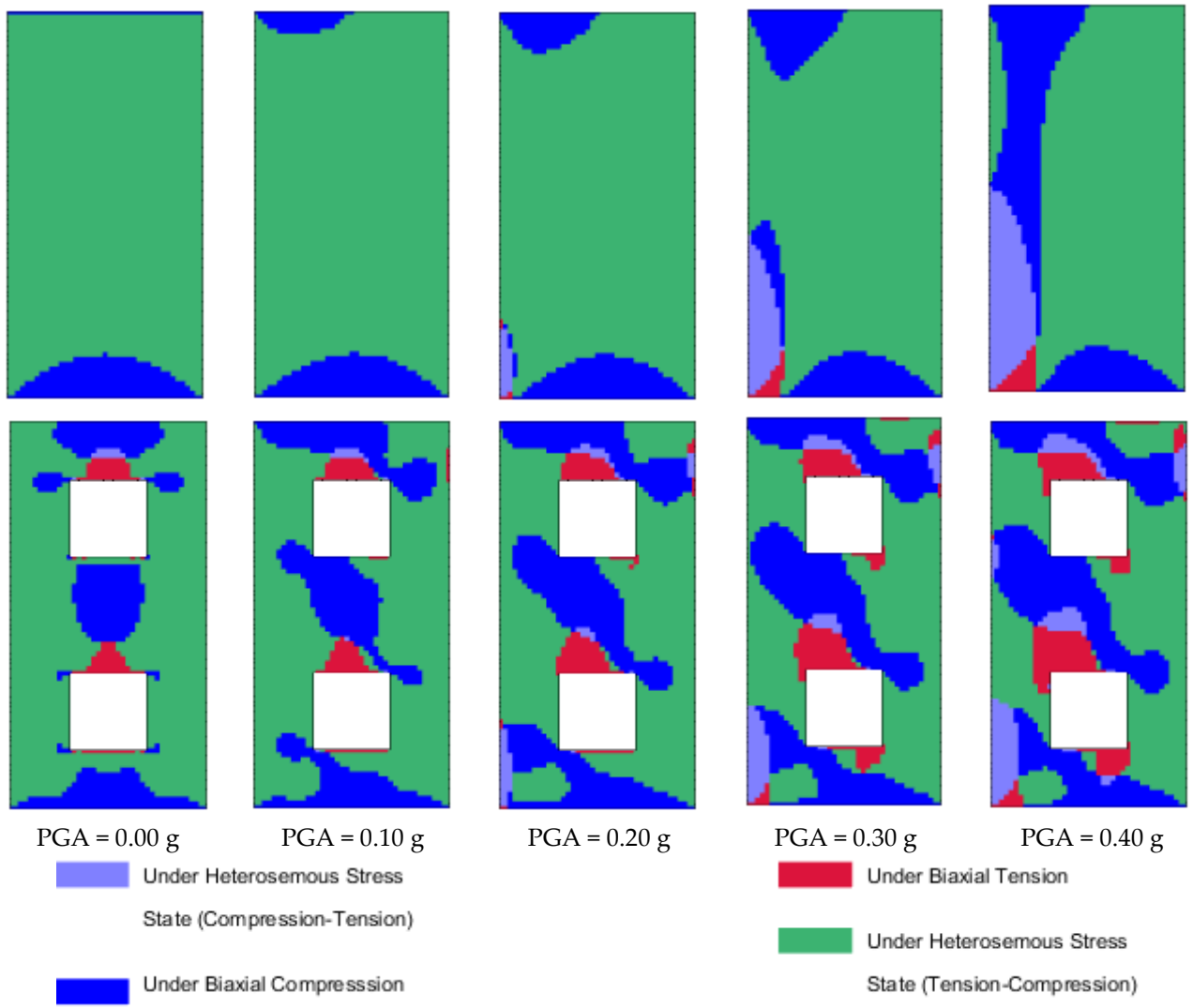

Figure 32. Evolution of the developing stress state in normal stress terms for values of PGA ranging from 0.00 to 0.40 g by step 0.10 g.

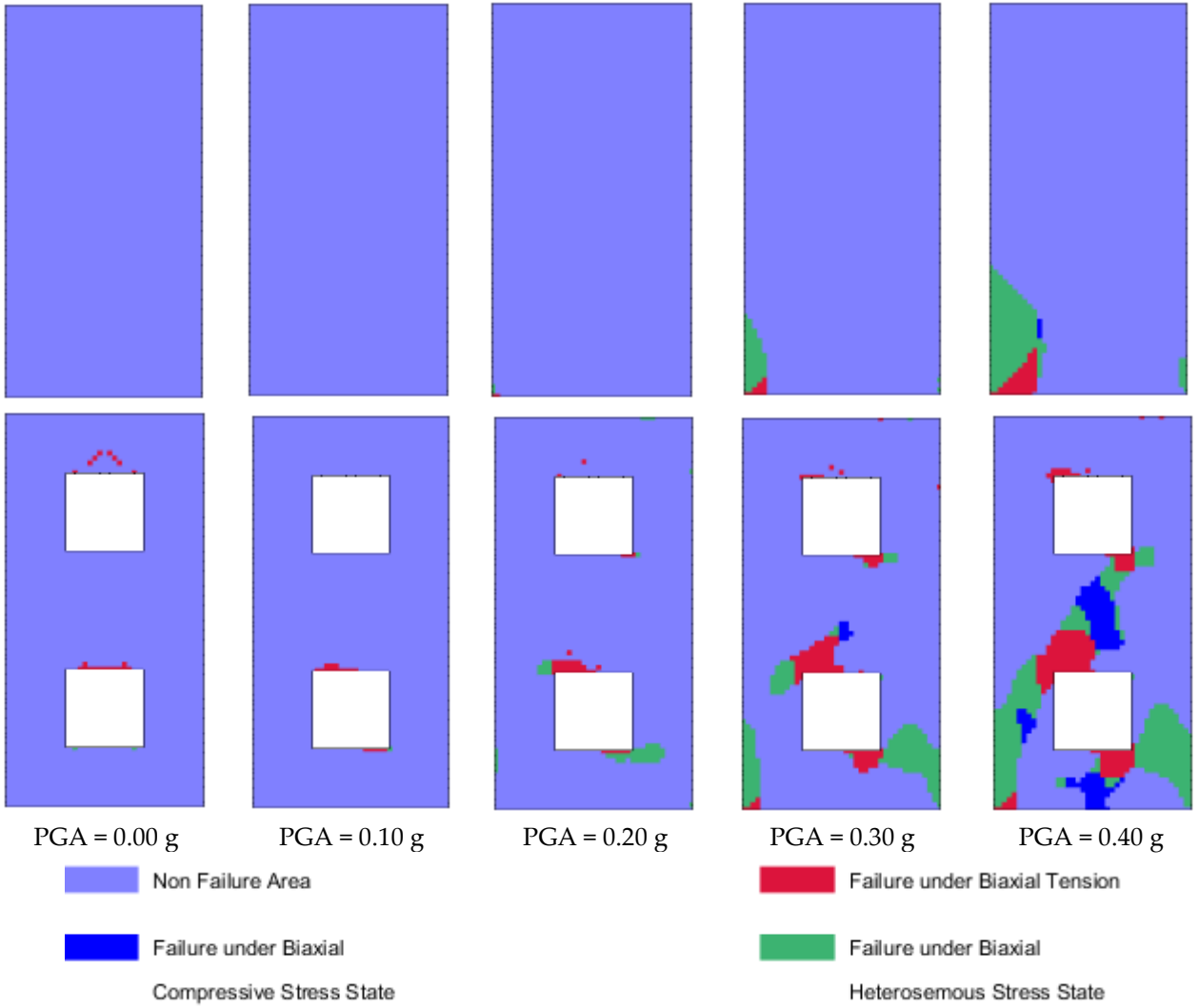

Figure 33. Evolution of the developing failure based on Kupfer and Gerstle's (1973) failure criterion for values of PGA ranging from 0.00 to 0.40 g by step 0.10 g.

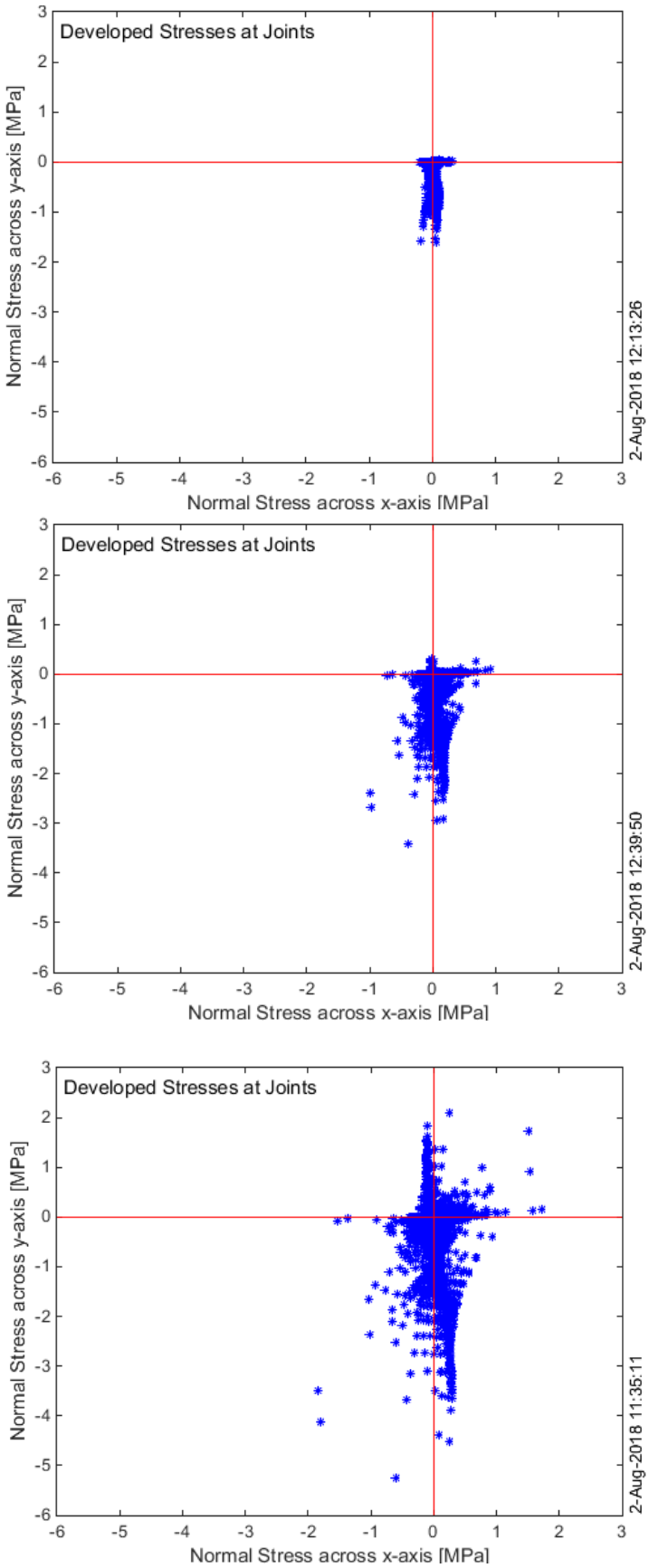

Figure 34. Evolution of the developing normal stresses for values of PGA ranging from 0.00 to 0.40 g by step 0.20 g.

6. Restoration Aspects

The notion of built heritage protection was first legislated in 1931 in the "Athens Charter for the Restoration of Historic Monuments". This charter is important as many principles still applied today are first stated. However, at this point, the concept of compatibility is absent, as they approve the judicious use of all resources at the disposal of modern technique and more especially reinforced concrete [5]. In the next decades, the detrimental effect of the use of incompatible materials is obvious on many cultural heritage assets, and thus, in the declaration of Amsterdam in 1975, it is stated that misapplied contemporary technology and ill-considered restoration may be disastrous to old structures [223], as well as that new materials and techniques should be used only after approval by independent scientific institutions [224]. This lays the foundations for a new approach, which is applied today, of preserving monuments with compatible and performing materials, aiming to preserve monuments and historical structures with structural integrity for future generations, however without compromising the values they carry [225].

This approach is not easy to follow, as various considerations must be taken into account. The values of the historical asset must be preserved, thus any restoration material and technique must be compatible with the values of the monument (aesthetic, historical, etc.). The monument must be adequately strengthened to avoid collapse and ensure its preservation for future generations. However, this must be done with the application of compatible restoration materials, which do not jeopardize the longevity of the historical materials of the asset and do not harm them in any way [69]. It is obvious that the above considerations are often in conflict, as some compatible materials may not present the demanded mechanical strength to achieve the required structural reinforcement. For this reason, it is important for researchers today to develop the appropriate tools that can assist in decision making to enable the selection of the optimum restoration material, which can provide adequate strengthening, without jeopardizing compatibility [45].

6.1. Historical Mortars as a Basis for the Design of Restoration Mortars

In the restoration of masonry cultural heritage assets, restoration mortars play an important role, as they are not only the most vulnerable material of masonry, but they also carry the memory of the civilization that produced them, whether it was a small society in some village of the Mediterranean using local materials, or the Roman empire, with its vast resources and technological advances. Thus, the analysis of historical materials is three-fold: one can learn about the history of the people that designed and produced the historical mortar, as this is a value, the value of memory; one can design new restoration mortars through the reverse engineering approach, ensuring compatibility and continuity; one can reveal the secrets of the great craftsmen of the past, in order to produce not only compatible, but enhanced restoration mortars.

6.2. Historical Mortars

Mortars have been used since antiquity and the raw materials as well as the technology of their production varies according to the use of the mortar in the structure, the raw materials available and the technological state of the era and region. Historical mortars can be separated into categories, the main ones being: (i) typical lime mortars, which is the oldest type of mortar along with gypsum mortars [226]; (ii) gypsum mortars; (iii) hydraulic lime mortars; (iv) pozzolanic mortars, where lime is mixed with pozzolanic additives; and (v) crushed brick–lime mortars [63,64]. The study of a great number of historical mortars has allowed researchers to establish ranges for the values of their characteristics, assisting in their categorization, as can be seen in [61] where value ranges of the chemical and physico-mechanical characteristics of historical mortars belonging to different types are stated, while PCA has assisted in the correlation of these properties and the categorization of historical mortars [227].

Lime mortar has been used since the third millennium BC, as evidenced in historical structures of that era, and is widely used until today. Gypsum mortar, which is produced using calcinated gypsum as binder material in the mortar, is also one of the oldest types of mortar. This is greatly

attributed to the low firing temperature required to burn the gypsum rock and transform it into the correct form that can be used, after grinding, as binder of the mortar. Gypsum mortars were used in ancient Egypt for the construction of the pyramids in 3000 BC [228]. In Portugal, gypsum mortars have been widely used for plastering of walls and ceilings since the time of the Roman empire, with an intense presence during the 18th–20th centuries [229]. Gypsum was also used in many medieval structures in Germany, while recently scientists discovered gypsum mortars in the Holy Aedicule in Jerusalem, dating from the construction of Constantine the Great [49]. Although the use of gypsum was extensive in the past, today it is not used for the restoration of monuments, mainly due to the materials inadequate durability in high moisture conditions, although recent research is concerned with the production of durable gypsum mortars. Hydraulic lime mortars are acquired through the calcination of impure limestone containing aluminosilicates. Hydraulic lime mortars have been found in ancient mortars in Crete, in monuments of the Roman era, etc. [226]. Crushed brick–lime mortars were already in use in Cyprus and Greece in the Late Bronze Age, with their main use in floors and areas of high moisture (such as water channels). This is an indication that, as early as the Late Bronze Age, craftsmen acknowledged the high durability that this combination presented in high moisture environments, while in the Levant this technological advance seems to have occurred already from the Early Bronze Age [63]. Another interesting fact about this type of mortar is that it was extensively used in byzantine monuments, contributing to their earthquake resistance [67]. A timeline of mortar types used in different areas and monuments can be found in [61,228]. In Table 5, the most important instances in mortar production throughout the ages are summarized.

Table 5. Summarized timeline of mortar technology.

3000 BC	Bitumen was used as binding material by Babylonians and Assyrians
3000 BC	Mud mortars mixed with straw were used as joint mortars to join bricks, while gypsum was preferred to join carved stone blocks in Egypt
2450 BC	In Khafaje in Mesopotamia the ruins of a furnace, used for lime production, were found, proving the technology of lime calcination
500 BC	Studies of the cistern of Kameiros–Rhodes (500 BC), where pozzolanic concrete is covering the walls of the cisterns, confirm the knowledge of concrete production to the pre-roman era
300 BC	Pozzolan from Pozzuoli mixed with lime is used to build several structures. In Greece Santirine earth was used as a pozzolanic additive. The technology of adding pozzolan to lime was spread to the entire roman empire. During this era, crushed bricks were also used as pozzolanic additives and hydraulic lime was used extensively, deriving from the calcinations of appropriate limestones.
1793	Hydraulic lime is rediscovered by John Smeaton
1860	The era of modern cement initiates

Another issue that must be considered is the fact that, due to the many centuries that historical masonry structures have been in use, past restoration materials are present in the structure. This could create confusion if they are not documented interventions and they are not easily discernible. Furthermore, these restorations are not always compatible, and thus, deterioration products may be present, attributed to these materials. For example, in one study, researchers have analyzed two types of hydraulic brick–lime mortars from an Ottoman bath wall and have found that, although being exposed to the same environment, the historic repair plaster is structurally unsound in comparison to the authentic historical mortar, which was found in an excellent state of preservation. Furthermore, it was found that the historical repair mortar contained ettringite crystals, which expanded and detached the mortar; the presence of ettringite was attributed to the use of a small amount of gypsum to the lime–brick mix during the past repair and the consequent formation of ettringite due to the high moisture environment [230]. This is an excellent example of the care that must be taken when adding additives, as one property may be enhanced, however other properties could be detrimentally altered.

6.3. Restoration Mortars

Reverse engineering emerges as the ideal methodological approach for the design and production of compatible and performing restoration materials [66]. The main steps (Figure 35) of this methodological approach are: (i) characterization of historical materials in order to select similar raw materials for the production of the restoration mortars and design the mortar mixture directives, always taking into account that the historical mortar is a disturbed system and is not the system that was initially produced and applied; (ii) preparation of restoration mortars, i.e. the production of designed mortar mixes; (iii) evaluation of the restoration mortar properties, in terms of fresh mortar characteristics, such as workability, bulk density, retained water, air content, etc., as well as in terms of the mortar characteristics during setting and hardening, i.e. the evolution and final state of chemical phases, microstructural characteristics and acquired mechanical strengths; (iv) optimization of the mortar mixes, which allows for modifications of the mortar mix in order to obtain the best possible characteristics; and (v) pilot application on the cultural heritage asset in order to assess the restoration mortar on masonry scale [231]. This methodology has been enhanced and NDTs can assist the evaluation, especially in the final step of pilot application [70]. Restoration mortars based on traditional materials and techniques can be separated into categories [231], as shown in Table 6, while the use of cement in any quantity should be avoided [69] due to the incompatibility it presents and the subsequent deterioration of the historical materials [56].

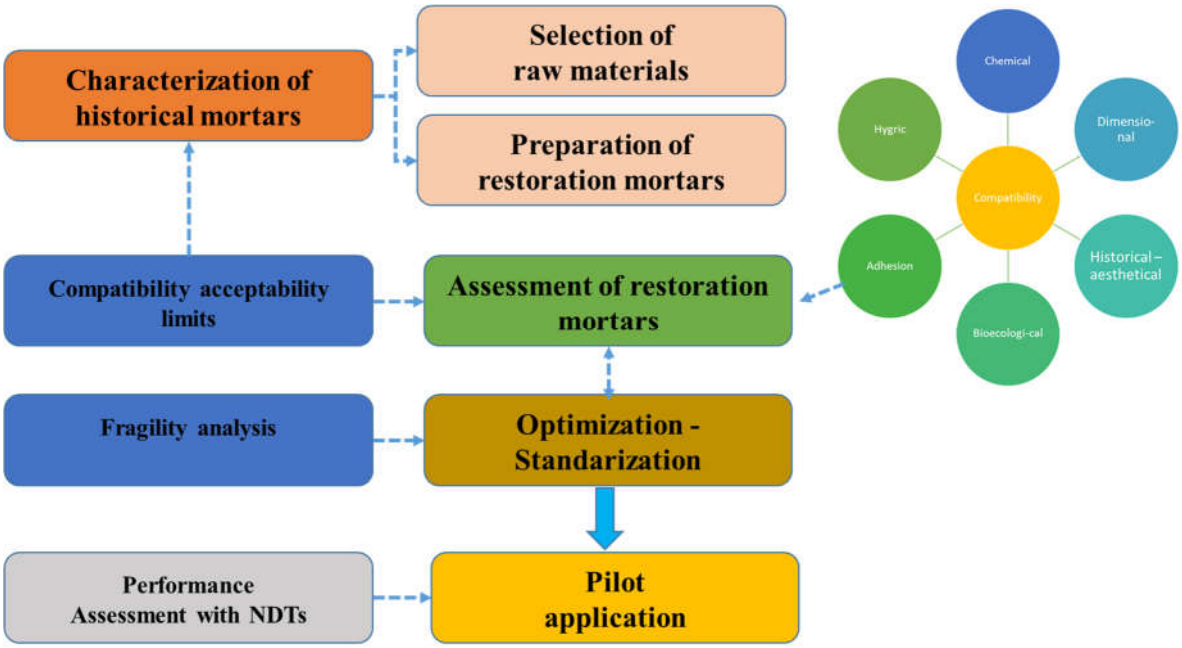

Figure 35. Basic methodological framework for restoration mortar design and assessment.

Table 6. Mechanical properties of restoration mortars after nine months of hardening according to Moropoulou et al. [231] and of historical mortars of each type [66].

Mortar Type	Restoration Mortar			Historical Mortar Tensile Strength (MPa)
	Compressive Strength (MPa)	Flexural Strength (MPa)	Tensile Strength (MPa)	
Typical lime mortars	1.1–1.2	0.3–0.4	0.2–0.3	<0.35
Hydraulic lime mortars	2.9–4.9	0.5–0.7	0.4–0.5	0.35–0.55
Lime–pozzolan mortars	0.9–1.6	0.4–0.4	0.3–0.3	>0.60
Lime–crushed brick mortars	1.1–2.0	0.3–0.4	0.2–0.3	>0.60
Hydraulic lime–crushed brick mortars	3.4–5.2	0.7–1.8	0.5–1.2	>0.55

The analysis of many historical mortars has allowed researchers to establish requirements that the raw materials used to produce restoration mortars for historical structures must comply with [231]. An interesting example of the lessons we can learn from the craftsmen of the past is related to the firing temperature of the bricks which will be crushed and used as raw materials in lime–crushed brick mortars, where scientists have discovered that the pozzolanic reaction and the best mortar characteristics are acquired when the brick has been fired at low temperatures, lower than firing temperatures today. In recent years, researchers have studied the use of metakaolin, an extremely active artificial pozzolan, which contributes to the production of mortars with excellent characteristics [232].

Compatibility is a quite complex term, as it is assessed chemical, dimensional, hygric, aesthetical, adhesion, mechanical and bioecological terms [69]. Moropoulou et al. established a range of acceptability limits of physical, chemical and mechanical characteristics that should be fulfilled by the restoration mortars, deriving from the evaluation of historical mortars, for different mortar types (Tables 7 and 8) [233]. The use of acceptability limits to assess restoration mortars can be found in [69], while it should be noted that mechanical strength compatibility is linked with the requirement that the restoration mortar is not stronger than the historical building units, in order to avoid failure of the historical materials.

Aesthetic compatibility is achieved when the restoration mortar has the same appearance as the authentic mortar. The color, texture, symbolisms, and aesthetic must create an overall appearance similar to the original [6]. The shape and design, materials used, and workmanship are often addressed as key heritage values [234]. An issue which is also widely discussed nowadays is the design and production of environmentally friendly mortars, aiming towards sustainability [235]. The use of traditional materials is in accordance with this tendency, as they are non-toxic, and have lower firing temperatures and a more sustainable life cycle, especially concerning CO_2 emissions.

Thus, fragility curves can serve as a tool to evaluate the contribution of restoration mortars on the response of the monument under dynamic stresses, which, coupled with a compatibility assessment and the fulfillment of the above principles, can lead to the selection and application of the optimum material, preserving masonry historic structures for centuries to come.

Table 7. Range of acceptability limits for different types of restoration mortars through thermal analysis results (TG/DTA) (physicochemical compatibility) and tensile strength measurements (mechanical compatibility) [233].

Mortar Type	Hygroscopic Water (%)	Hydraulic Water (%) Bound in Hydraulic Compounds	CO_2 (%) Bound in Calcareous Compounds	$CO_2/H_2O_{hydraulic}$ *	Tensile Strength (MPa)
Lime	<1	2–4	>30	>8.5	<0.35
Crushed brick–lime	1.5–4.5	2.3–5.3	<20	3.2–6.5	0.5–1.2
Hot lime	0.7–1.5	2–4.6	>25	6–15	0.85–1.5
Hydraulic	1–2.5	4–7.2	<25	1.8–6.1	-
Lime–Pozzolan	2–4	3.3–5.4	<22	1.3–5.1	-
Rubble masonry	-	5.6–5.9	<30	3.36–5.13	-

* CO_2/H_2O: Inverse hydraulicity ratio, representative of a mortar's hydraulicity. It is calculated as the ratio of CO_2 (%) loss during thermal analysis and attributed to calcareous compounds and the $H_2O_{hydraulic}$ (%) loss, attributed to water bound to hydraulic compounds (CSH, CASH, etc.). Low values (<10) are representative of mortars with hydraulicity, such as lime–poszzolan, natural hydraulic lime and lime–crushed brick mortars, while high values (>10) are representative of mortars with no hydraulicity, such as aerial lime mortars.

Table 8. Range of acceptability limits for different types of restoration mortars through mercury intrusion porosimetry results (MIP)—microstructural compatibility [233].

Mortar Type	Cumulative Volume (mm^3/g)	Apparent Density (g/cm^3)	Average pore Radius (μm)	Specific surface Area (m^2/g)	Total Porosity (%)
Lime	170–320	1.5–1.8	0.8–3.3	1.3–3.3	30–45
Crushed brick–lime	170–290	1.5–1.9	0.1–0.8	3.5–15	32–43
Hot lime	110–180	1.7–1.9	0.3–0.8	2.5–4.7	20–30
Hydraulic	90–230	1.7–2.1	0.1–3.5	2.5–13.5	18–40
Lime–Pozzolan	160–265	1.6–1.9	0.1–1.5	3–14	30–42
Rubble masonry	117–220	1.8–2.1	0.2–20.6	1.2–4.7	25–39

7. Case Studies

Aiming to assess the proposed methodology, its implementation is presented in this section both on theoretical, as well as on actual masonry structures.

7.1. 2D Masonry Walls

The behavior of four 2D masonry walls, with square openings, as presented in Figure 36, was studied. The values of the percentage of the openings (surface of the opening/wall surface) were 0%, 16%, 36% and 64%. The mechanical characteristics of the masonry material are presented in Table 9. It should be noted that the data used were considered as typical and are stated in the experimental study of Page, conducted in 1981 [236], the results of which have been widely utilized by the majority of researchers investigating the behavior of masonries, on both experimental and numerical levels.

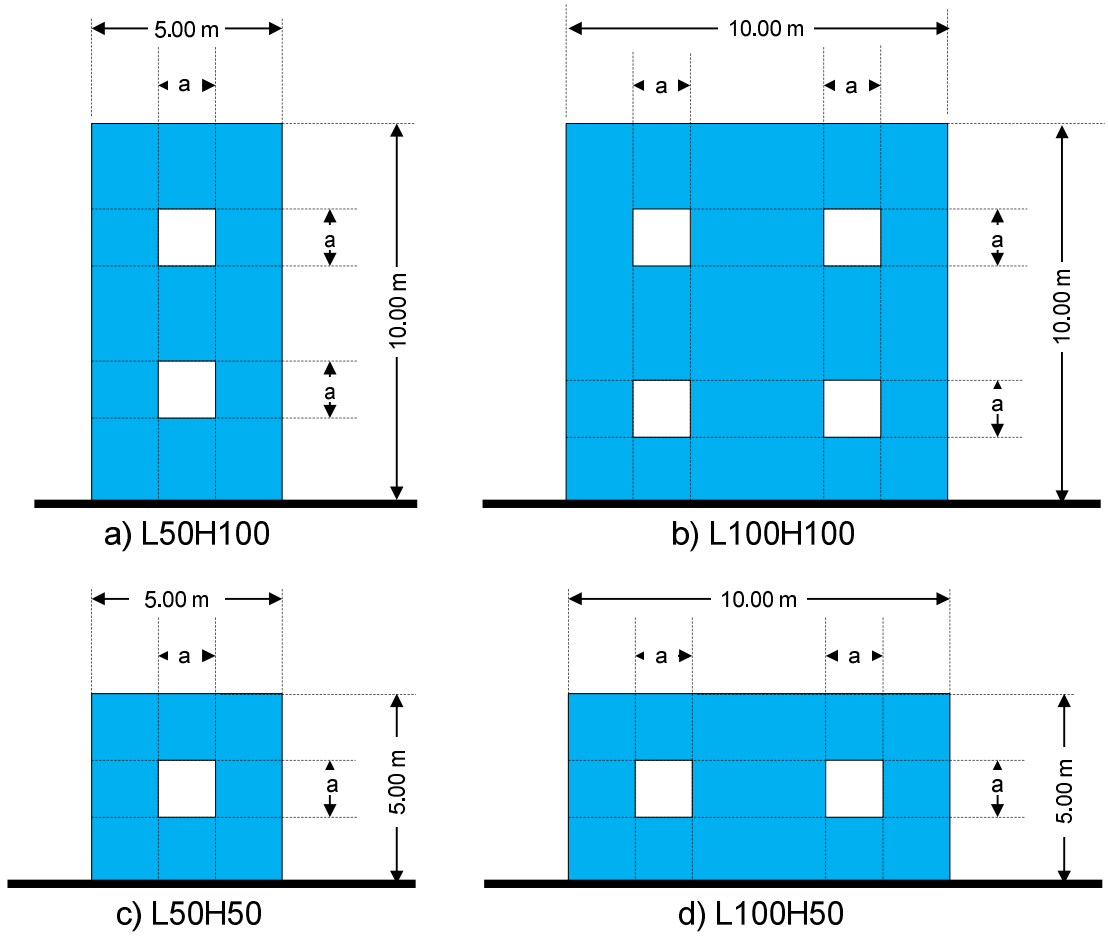

Figure 36. Cases of 2D masonry walls examined.

Table 9. Mechanical characteristics of masonry (Page 1981) [236].

Parameter	Value
Elasticity modulus in x direction (GPa)	4.3625
Elasticity modulus in y direction (GPa)	7.5550
Compressive strength in the x direction (MPa)	4.3625
Compressive strength in the y direction (MPa)	7.5550
Tensile strength in the x direction (MPa)	0.40
Tensile strength in the y direction (MPa)	0.10
Poisson ratio in the xy plane	0.20
Poisson ratio in the yx plane	0.20
Specific weight (kN/m^3)	20

In Figure 37, the failure areas of 2D masonry wall L50H100 are presented. This wall has two openings reaching a total opening percentage of 16% and two different failure criteria are utilized, with three different values of Peak Ground Acceleration (0.24, 0.32 and 0.40 g). These diagrams are especially useful for the determination of failing areas of the structure, as well as for the selection of the optimum repair measures aiming to their repair. More specifically, the failure areas are marked with different colors highlighting in distinct ways the kind of stress underpinning the failure. As can be easily perceived, different repair measures are demanded when failure occurs under biaxial compression, biaxial tension and heterosemous biaxial stress state (tension/compression). In Figure 38, the failure areas of 2D masonry wall L100H100 are presented for three different opening percentages (0%, 16% and 36%) using two different failure criteria and for a PGA = 0.32 g.

In Figures 39 and 40, the damage indices of 2D masonry walls L50H100 (Figure 36a) and L100H100 (Figure 36b), both without any opening (total opening percentage of 0%), are presented.

These diagrams are especially useful for the assessment of the seismic vulnerability in a preliminary stage. Namely, we can see that for both masonry walls the determined damage indices are under the lower limit of heavy damage of 25% for values of peak ground acceleration up to 0.24 g. Furthermore, a comparison between these two 2D masonry walls depicts that damage indices of the "shear" wall L100H100 are much less than the damage indices of the "cantilever" wall L50H100 something that is expected. Such diagrams are of great interest and extremely useful for the assessment of more complicated structures.

In Figure 41, the development process of fragility curves is presented. Namely, having determined the damage indices for the case of the 2D masonry wall L50H100 (Figure 36a) with opening percentage of 16% for a set of masonry tensile strengths ranging from 0.0650 to 0.4350 MPa using a step of 0.0465 MPa (response parameter) and for values of Peak Ground Acceleration (intensity measure (IM)) from 0.00 to 0.80 g using a step of 0.08 g, the probability of exceeding a damage limit state is determined. Based on these probabilities, the results for values of PGA equal to 0.00, 0.24, 0.48 and 0.72 g are presented in the four smaller images and the fragility curves are derived and presented in the larger image of Figure 41.

In Figure 42, the fragility curves of the current condition of wall L50H100 are presented, using the failure Von Mises modified failure criterion and for an opening percentage of 16% for normal and lognormal distribution. In Figure 43, the fragility curves of the current condition of wall L50H100 are presented, using the Kupfer and Girstle failure criterion [160], four different opening percentages (0%, 16%, 36% and 64%), lognormal distribution and moderate damage performance level.

In Figure 44, the fragility curves of the current condition of three different walls with percentage openings of 16% are presented, using the Syrmakezis et al. (1995) failure criterion [8,25], lognormal distribution and heavy damage performance level. This particular figure is indicative of the potential of fragility curves in quantifying the vulnerability of structures and especially in classifying structures according to their vulnerability.

In Figure 45, the fragility curves for the case of wall L50H100 are presented, using the Syrmakezis et al. (1995) failure criterion [8,25], regarding the current state of the wall, as well as the repaired states in the cases of using three different repair mortars M5, M10 and M15, of compressive strength 5, 10 and 15 MPa, respectively, using lognormal distribution and moderate damage performance level. These three types of restoration mortars were evaluated to cover the whole range of mechanical properties presented by restoration mortars, which have been assessed to be compatible for use in monuments and historical buildings (Moropoulou et al., 2005 [61]). In Table 10, the values of the tensile strengths (response parameter) for existing structures as well for the repaired ones used for the development of fragility curves are presented.

Table 10. Values of tensile strength (response parameter) of 2D masonry walls examined.

Structure	Tensile Strengths in MPa
Existing 2D masonry walls	0.065 to 0.435 by step 0.0465
Repaired 2D masonry walls with mortar M5	0.117 to 0.467 by step 0.0438
Repaired 2D masonry walls with mortar M10	0.142 to 0.566 by step 0.0530
Repaired 2D masonry walls with mortar M15	0.158 to 0.634 by step 0.0595

Based on Figures 44 and 45, it is obvious that the proposed approach offers a classification method which can assist authorities to optimize their decisions in relation to the selection, among a variety of structures, of the structure in the most need of repair, as well as in relation to the selection of the optimum repair scenario.

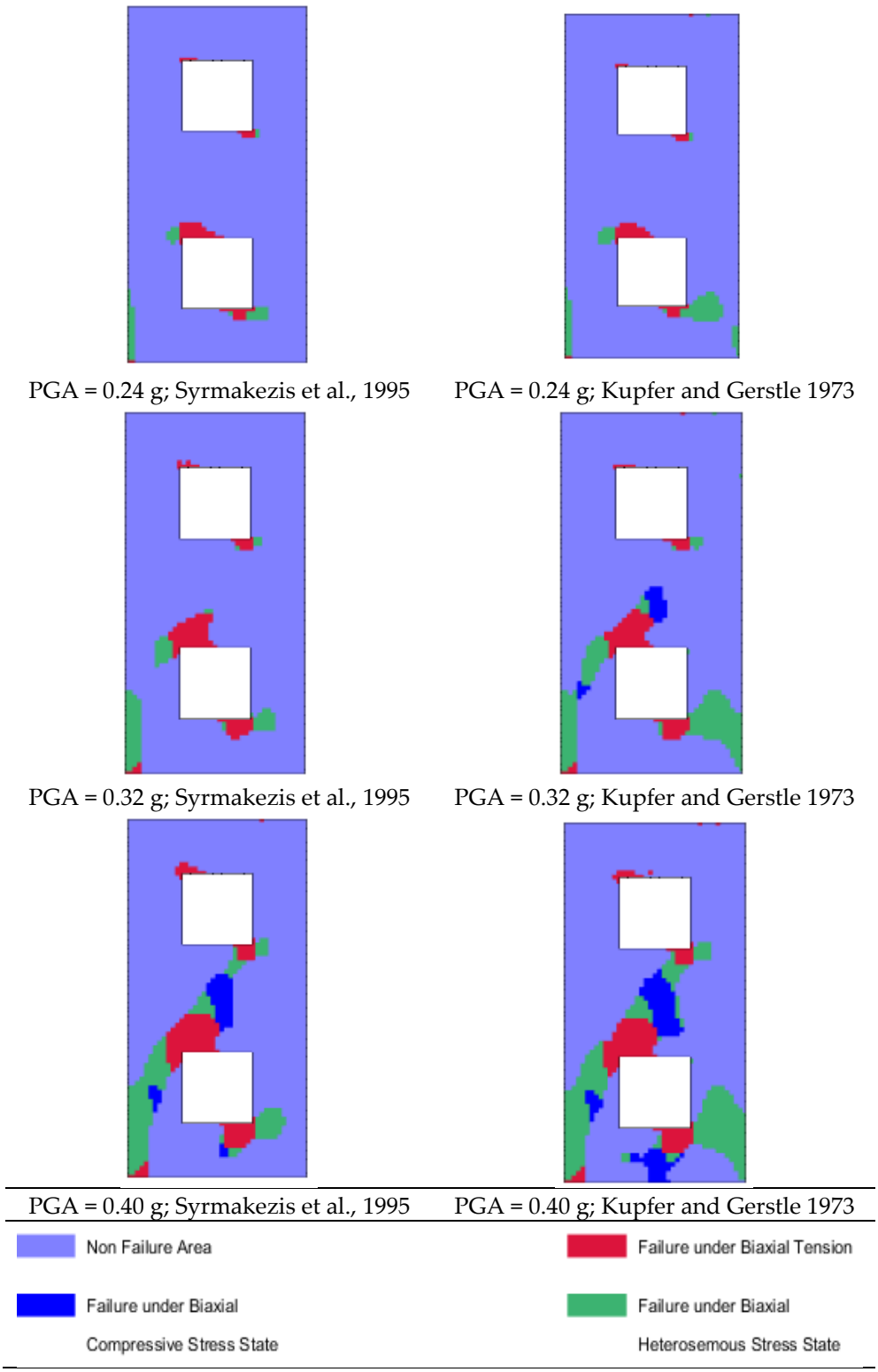

Figure 37. Failure of 2D masonry wall L50H100 (Figure 11a) with two openings, two different failure criteria and three different values of PGA.

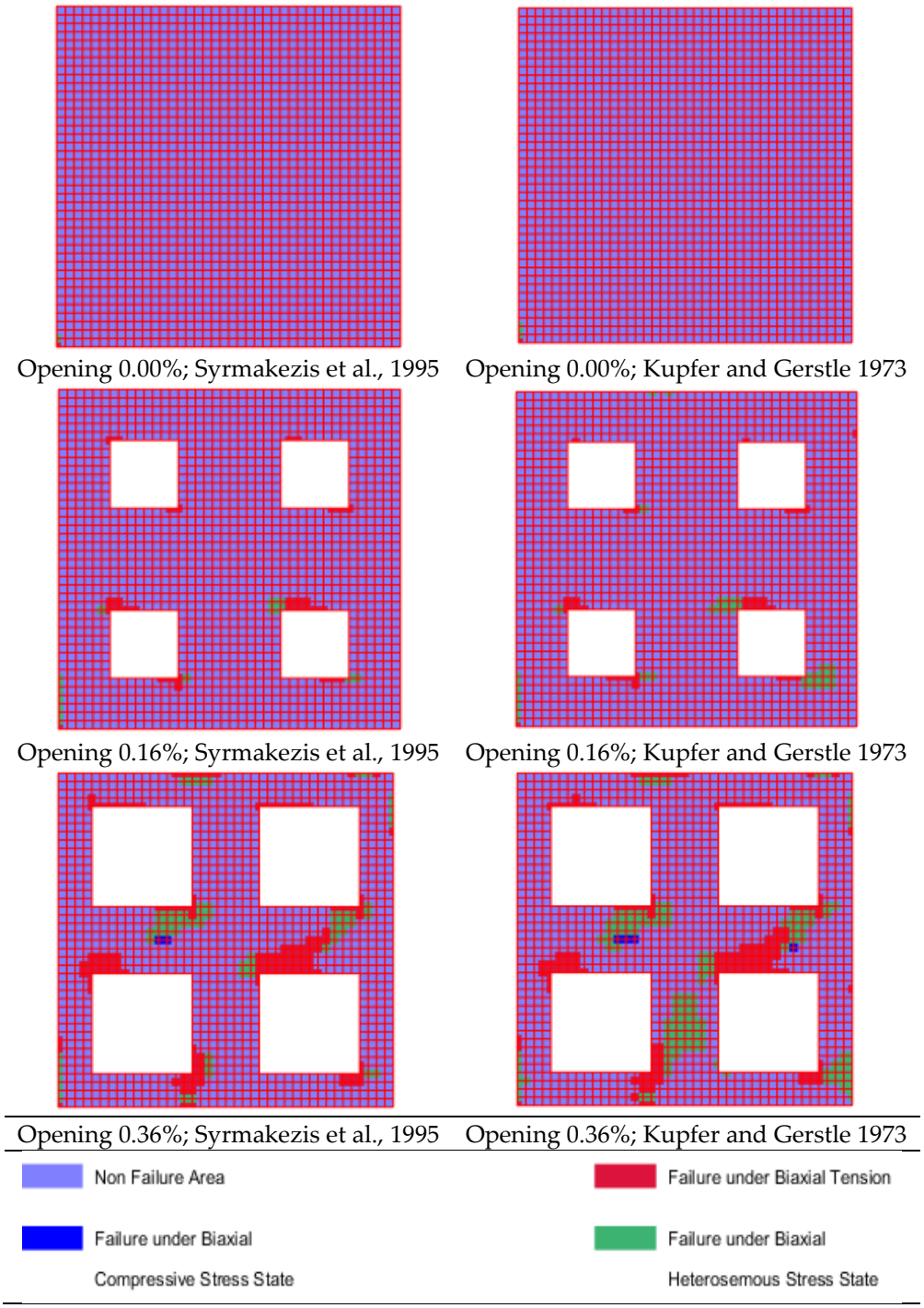

Figure 38. Failure of 2D masonry wall L100H100 (Figure 36b) for three different opening percentages, two different failure criteria and maximum ground acceleration value PGA = 0.32 g.

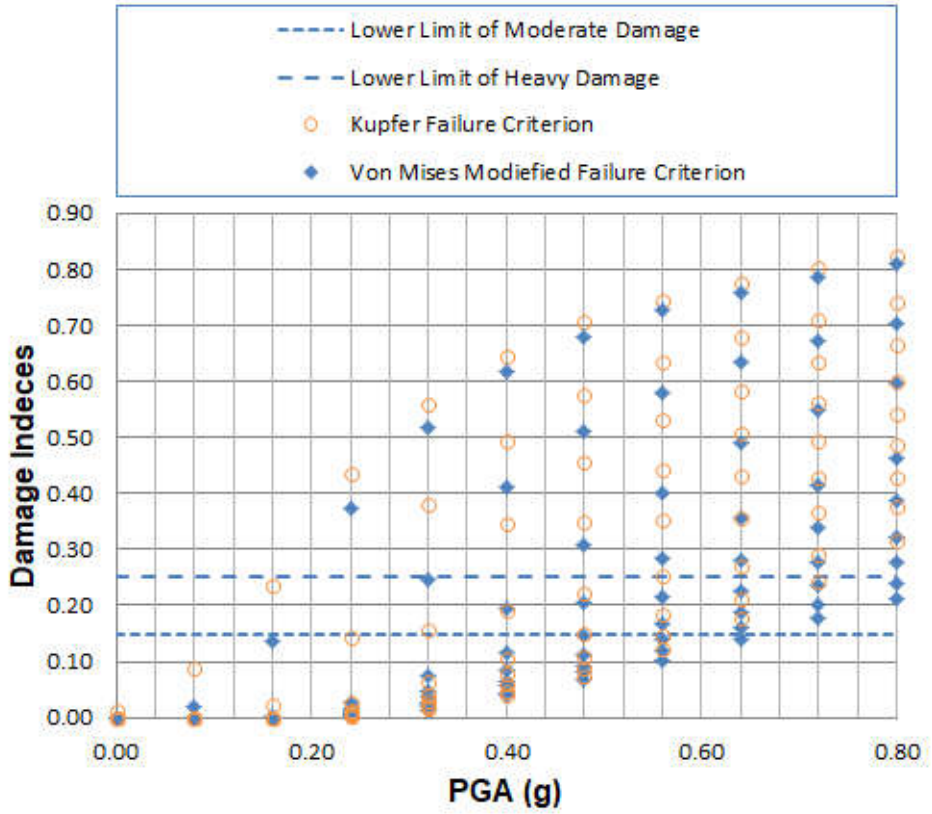

Figure 39. Damage Indices of 2D masonry wall L50H100 (Figure 36a) for opening percentages 0% and two different failure criteria (existing structure).

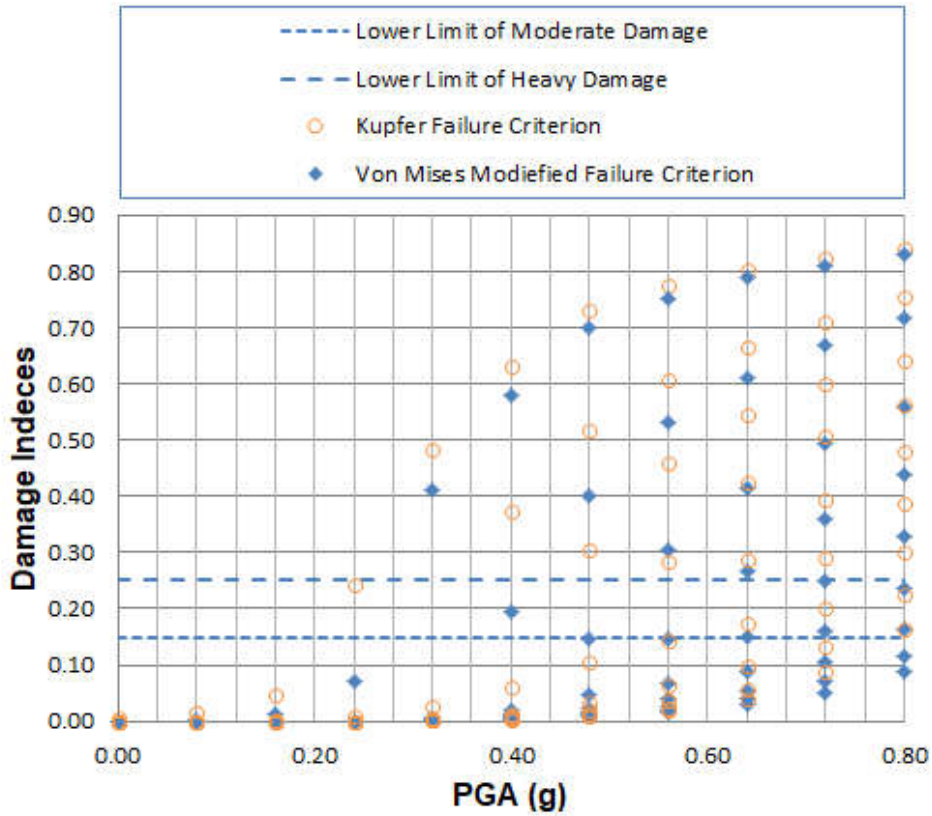

Figure 40. Damage Indices of 2D masonry wall L100H100 (Figure 36b) for opening percentages 0% and, two different failure criteria.

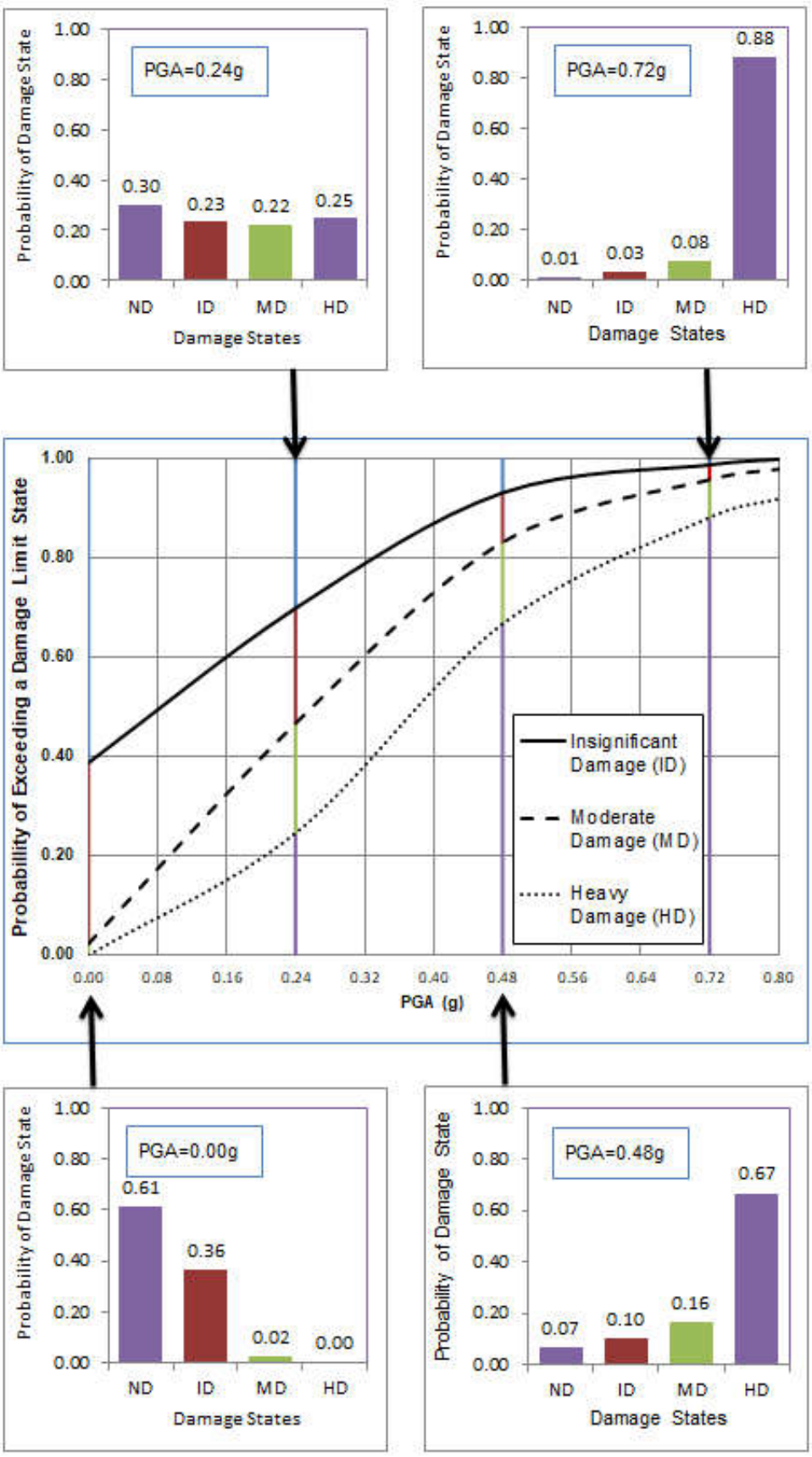

Figure 41. Derivation of fragility curves of the 2D masonry wall L50H100 (Figure 36a) with opening percentage of 16% using normal distribution and Von Mises modified failure criterion (ND, No Damage; ID, Insignificant Damage; MD, Moderate Damage; HD, Heavy Damage).

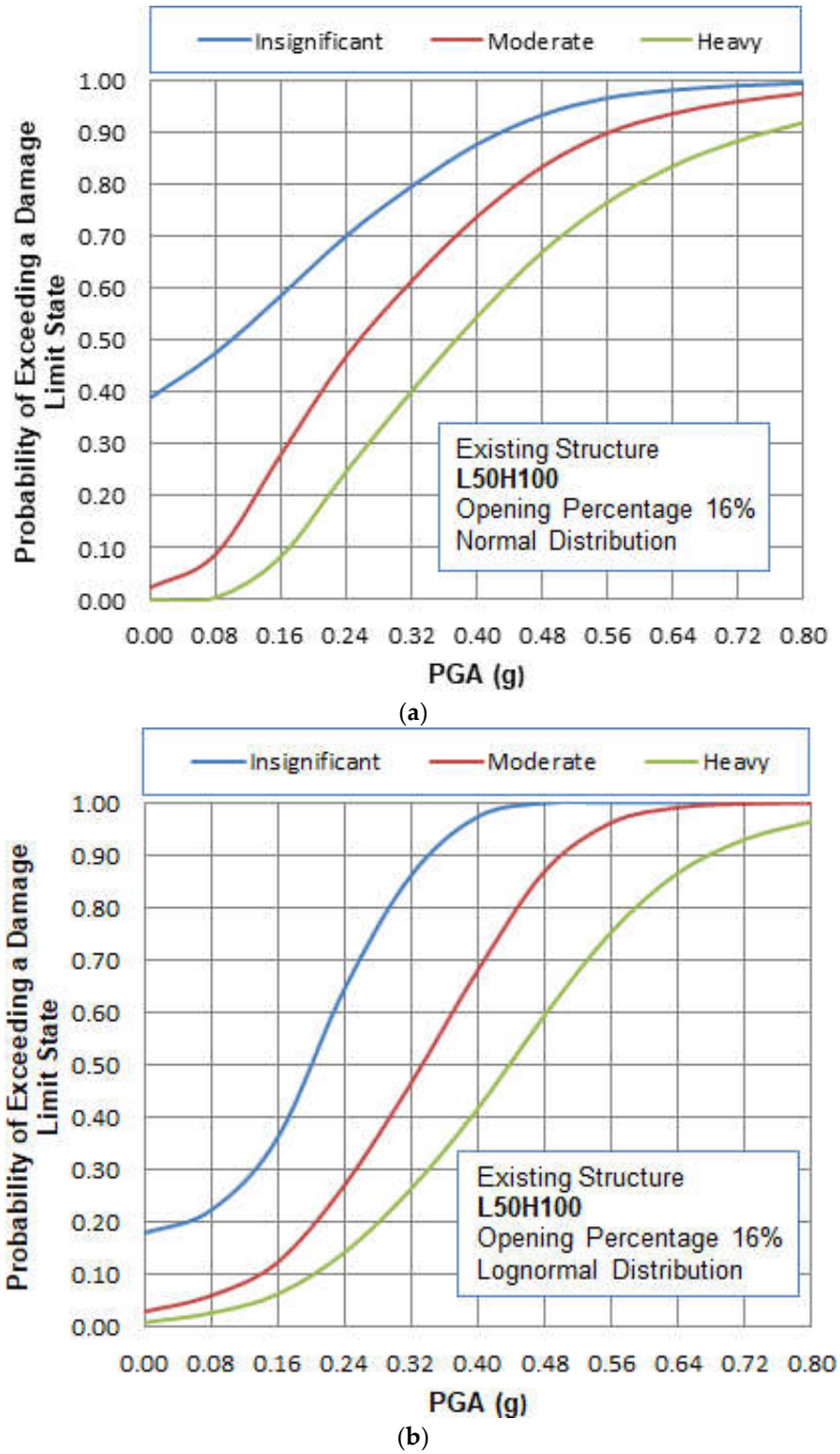

Figure 42. Fragility curves of wall L50H100 in its current condition, considering the Syrmakezis et al. (1995) failure criterion [8,25] and for an opening percentage of 16%: (**a**) normal distribution; and (**b**) lognormal distribution.

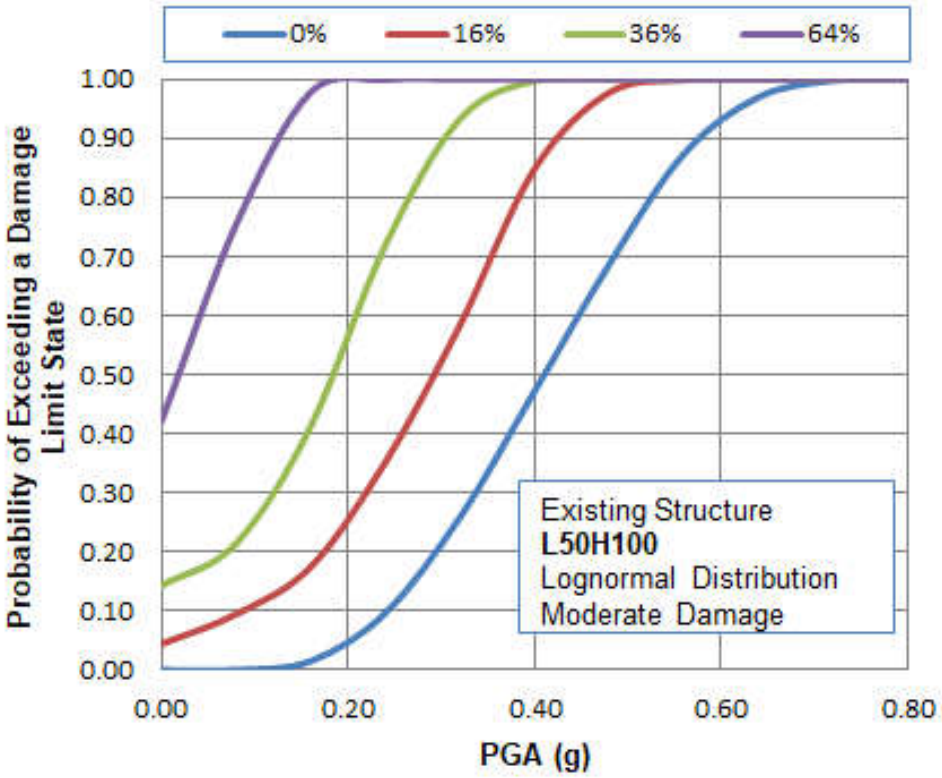

Figure 43. Fragility curves of wall L50H100 in its current condition, considering the Kupfer and Girstle (1973) failure criterion [160], four different opening percentages (0%, 16%, 36% and 64%), lognormal distribution and moderate damage performance level.

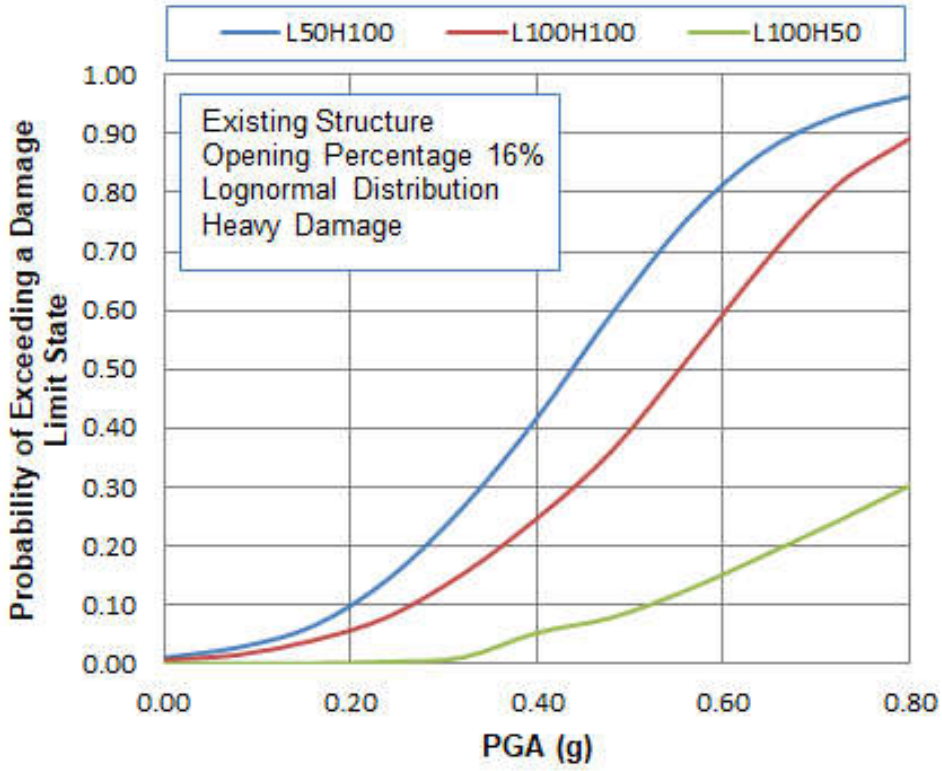

Figure 44. Fragility curves of wall L50H100 in its current condition, for three different walls with an opening percentage of 16%, considering the Syrmakezis et al. (1995) failure criterion [8,25], lognormal distribution and heavy damage performance level.

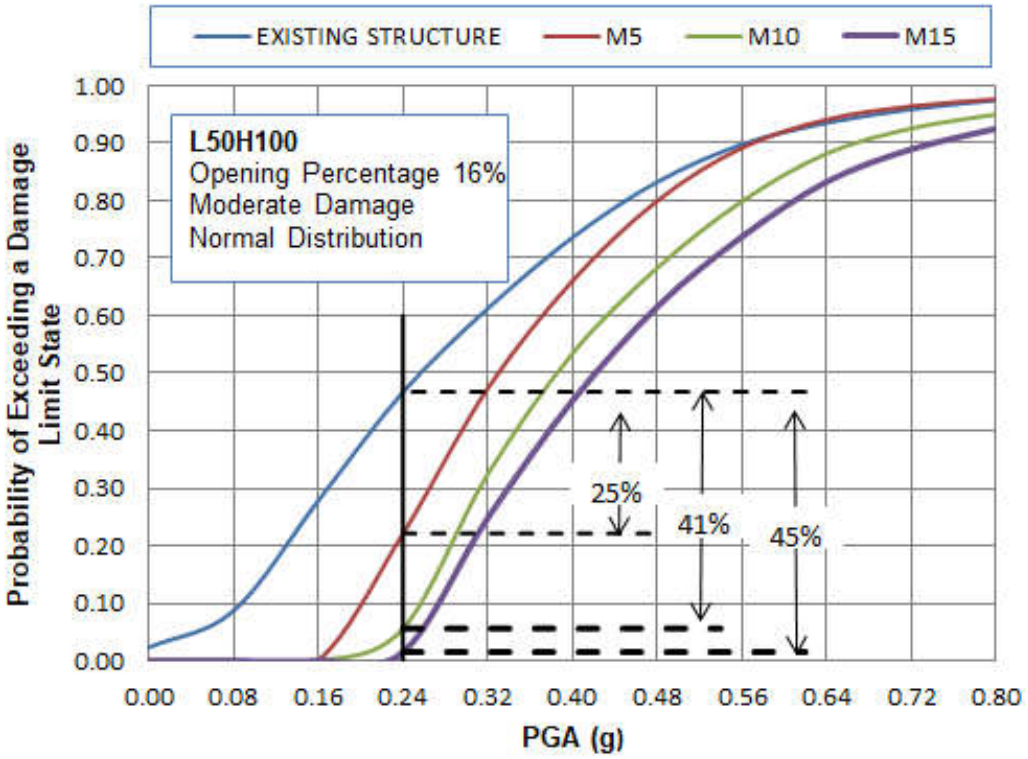

Figure 45. Fragility curves of wall L50H100, considering the Syrmakezis et al. (1995) failure criterion [8,25], for its current condition, as well as its behavior with the use of three different repair mortars of 5, 10 and 15 MPa compressive strength (M5, M10, M15), for lognormal distribution and moderate damage performance level.

7.2. Monumental Masonry Structures

In this section, the reliability of the proposed methodology is presented, through its application on two real case monumental masonry structures. Specifically, the presented methodology was employed to investigate the vulnerability of two different real case monumental masonry structures. The first structure is the Catholicon of Kaisariani Monastery (Figure 46), which was built in Athens in the late 11th–early 12th century AD, while the second case study structure is the Palace of Chania, Crete (Figure 47), which was built in the Chalepa area of Crete in 1882. In 1898, when Crete became autonomous, and acquired a ruler and a constitution, Prince George arrived in Crete as high commissioner of Crete. The mansion in question, the Palace, was selected as the most appropriate structure to serve as his dwelling.

In Figure 48, the fragility curves for the current situation for both monumental structures are presented, in lognormal distribution and heavy damage performance level. This figure is indicative of the potential of fragility curves to quantify the vulnerability of structures and furthermore to classify them, sorting them by descending degree of vulnerability. Based on this figure, it is obvious that for ground acceleration values lower than 0.20 g the Catholicon of Kaisariani Monastery presents lower vulnerability than the Palace, while the reverse is true for values above 0.20 g.

Figure 46. Front view of Kaisariani Monastery.

Figure 47. Front view of the Palace.

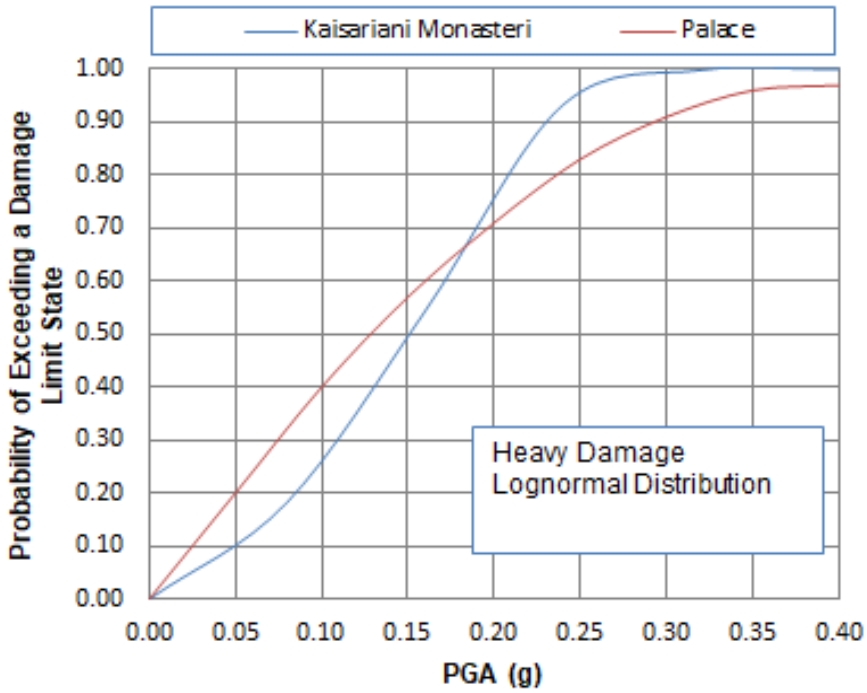

Figure 48. Fragility Curves of the current condition for two real case monumental structures using lognormal distribution.

The results for these two monumental structures, regarding the evaluation of their seismic vulnerability and the selection of the optimum repair scenarios, are presented in detail in the Masters' theses of Douvika (2017) [194] and Skentou (2018) [195], and in the research papers of Asteris et al., (2014, 2016, 2017) [38,42,237], Moropoulou et al. (2015) [238], Douvika et al. (2016) [239], Apostolopoulou et al. (2017) [45] and Maniatakis et al. (2018) [240].

8. Conclusions

The modeling and assessment of masonry structures, as well as any restoration actions applied, demand a holistic multi-disciplinary approach. In this paper, a methodology is presented for the evaluation of the seismic vulnerability of masonry structures, taking into account the probabilistic nature of the parameters involved in the simulation of the structure as well as in the mechanical characteristics of the materials and seismic forces. The evaluation of the vulnerability of the structures, as well as the evaluation of different repair scenarios and the selection of the optimum scenario are amongst the main conclusions of this paper. Furthermore, the proposed approach can act as a valuable tool for authorities involved in monument protection, as it offers a classification methodology, which can contribute in a decisive manner to decision making, not only in relation to the selection of the monument in the most need of protection, among several monuments, but also to the selection of the optimum repair scenario for each monument.

In the holistic framework, which the authors have attempted to provide in relation to masonry structures and their materials, a new finite element model has been proposed and a new failure criterion through neural networks has been developed.

Author Contributions: P.G.A. conceived and designed the research; A.D.S. and M.A. performed the computational implementation of the mathematical models; and all authors reviewed and revised the manuscript.

Funding: This research received no external funding.

Acknowledgments: The research was performed within the framework of the Master's Program in Applied Computational Structural Engineering (ACSE), which was partially financed by the Research Committee of the School of Pedagogical and Technological Education, Athens, Greece. The authors would like to thank the anonymous reviewers for their valuable comments and suggestions, which improved the quality of the paper.

They are also grateful to MSc student Maria G. Douvika for her assistance on computational implementation of the mathematical models.

Conflicts of Interest: The authors confirm that this article content has no conflict of interest.

Appendix A

The analytical form of the anisotropic finite element 8 × 8 stiffness matrix is defined by integration over the area of the element by the following, symmetric to the principal diagonal $\left(K_{ij} = K_{ji}\right)$ coefficients:

Appendix A.1. Stiffness Matrix Coefficients K_{1j} *(j = 1)*

$$K_{11} = \frac{E_x E_y G_{xy} t}{1-\nu_{xy}\nu_{yx}}\left[\frac{\beta}{3E_y G_{xy}} + \frac{\left(1-\nu_{xy}\nu_{yx}\right)}{3\beta E_x E_y}\right] \tag{A1}$$

Appendix A.2. Stiffness Matrix Coefficients K_{2j} *(j = 1, 2)*

$$K_{21} = \frac{E_x E_y G_{xy} t}{1-\nu_{xy}\nu_{yx}}\left[\frac{\lambda}{4} + \frac{\left(1-\nu_{xy}\nu_{yx}\right)}{4E_x E_y}\right] \tag{A2}$$

$$K_{22} = \frac{E_x E_y G_{xy} t}{1-\nu_{xy}\nu_{yx}}\left[\frac{1}{3\beta E_x G_{xy}} + \frac{\beta\left(1-\nu_{xy}\nu_{yx}\right)}{3E_x E_y}\right] \tag{A3}$$

Appendix A.3. Stiffness Matrix Coefficients K_{3j} *(j = 1, 2, 3)*

$$K_{31} = \frac{E_x E_y G_{xy} t}{1-\nu_{xy}\nu_{yx}}\left[\frac{-\beta}{3E_y G_{xy}} + \frac{\left(1-\nu_{xy}\nu_{yx}\right)}{6\beta E_x E_y}\right] \tag{A4}$$

$$K_{32} = \frac{E_x E_y G_{xy} t}{1-\nu_{xy}\nu_{yx}}\left[\frac{-\lambda}{4} + \frac{\left(1-\nu_{xy}\nu_{yx}\right)}{4E_x E_y}\right] \tag{A5}$$

$$K_{33} = K_{11} \tag{A6}$$

Appendix A.4. Stiffness Matrix Coefficients K_{4j} *(j = 1, 2, …, 4)*

$$K_{41} = \frac{E_x E_y G_{xy} t}{1-\nu_{xy}\nu_{yx}}\left[\frac{\lambda}{4} - \frac{\left(1-\nu_{xy}\nu_{yx}\right)}{4E_x E_y}\right] \tag{A7}$$

$$K_{42} = \frac{E_x E_y G_{xy} t}{1-\nu_{xy}\nu_{yx}}\left[\frac{1}{6\beta E_x G_{xy}} - \frac{\beta\left(1-\nu_{xy}\nu_{yx}\right)}{3E_x E_y}\right] \tag{A8}$$

$$K_{43} = \frac{E_x E_y G_{xy} t}{1-\nu_{xy}\nu_{yx}} \left[\frac{-\lambda}{4} - \frac{\left(1-\nu_{xy}\nu_{yx}\right)}{4E_x E_y} \right] \tag{A9}$$

$$K_{44} = K_{22} \tag{A10}$$

Appendix A.5. Stiffness Matrix Coefficients K_{5j} *(j = 1, 2, …, 5)*

$$K_{51} = -\frac{1}{2} K_{11} \tag{A11}$$

$$K_{52} = -K_{21} \tag{A12}$$

$$K_{53} = \frac{E_x E_y G_{xy} t}{1-\nu_{xy}\nu_{yx}} \left[\frac{\beta}{6E_y G_{xy}} - \frac{\left(1-\nu_{xy}\nu_{yx}\right)}{3\beta E_x E_y} \right] \tag{A13}$$

$$K_{54} = K_{32} \tag{A14}$$

$$K_{55} = K_{11} \tag{A15}$$

Appendix A.6. Stiffness Matrix Coefficients K_{6j} *(j = 1, 2, …, 6)*

$$K_{61} = K_{43} \tag{A16}$$

$$K_{62} = -\frac{1}{2} K_{22} \tag{A17}$$

$$K_{63} = -K_{32} \tag{A18}$$

$$K_{64} = \frac{E_x E_y G_{xy} t}{1-\nu_{xy}\nu_{yx}} \left[\frac{-1}{3\beta E_x G_{xy}} + \frac{\beta\left(1-\nu_{xy}\nu_{yx}\right)}{6E_x E_y} \right] \tag{A19}$$

$$K_{65} = K_{21} \tag{A20}$$

$$K_{66} = K_{22} \tag{A21}$$

Appendix A.7. Stiffness Matrix Coefficients K_{7j} *(j = 1, 2, …, 7)*

$$K_{71} = K_{53} \tag{A22}$$

$$K_{72} = K_{41} \tag{A23}$$

$$K_{73} = -\frac{1}{2} K_{11} \tag{A24}$$

$$K_{74} = K_{21} \tag{A25}$$

$$K_{75} = K_{31} \tag{A26}$$

$$K_{76} = K_{32} \tag{A27}$$

$$K_{77} = K_{11} \tag{A28}$$

Appendix A.8. Stiffness Matrix Coefficients K_{8j} *(j = 1, 2, …, 8)*

$$K_{81} = K_{32} \tag{A29}$$

$$K_{82} = K_{64} \tag{A30}$$

$$K_{83} = K_{21} \tag{A31}$$

$$K_{84} = -\frac{1}{2}K_{22} \tag{A32}$$

$$K_{85} = K_{41} \tag{A33}$$

$$K_{86} = K_{42} \tag{A34}$$

$$K_{87} = K_{43} \tag{A35}$$

$$K_{88} = K_{22} \tag{A36}$$

where t is the thickness of the element, $\beta = \frac{b}{a}$ (see Figure 6), and $\lambda = \frac{\nu_{yx}}{E_y G_{xy}} = \frac{\nu_{xy}}{E_x G_{xy}}$ according to Equation (9).

Abbreviations

ANNs	Artificial Neural Networks
BPNNs	Back-Propagation Neural Networks
CDF	Cumulative Distribution Function
DI	Damage Index
DOF	Degrees of Freedom
DS	Damage State
EC2	Eurocode 2
EC8	Eurocode 8
FE	Finite element
FEM	Finite Element Method
HD	Heavy Damage
ID	Insignificant Damage
IM	Intensity Measure
IML	Intensity Measure Level
logsig	Log-sigmoid transfer function
LN	Lognormal
LS	Limit state
MAFEA	MAsonry Finite Element Analysis
MD	Moderate Damage
ND	No Damage
PGA	Peak Ground Acceleration
PDF	Probability Density Function
purelin	Linear transfer function

RC	Reinforced Concrete
tansig	Hyperbolic Tangent Sigmoid transfer function
URM	UnReinforced Masonry

List of Symbols

Latin letters (Capital)

A_{fail}	Damaged surface area of the structure
A_{tot}	Total surface area of the structure
E	Modulus of elasticity
Ex	Modulus of Elasticity across x-axis
Ey	Modulus of Elasticity across y-axis
Gxy	Shear modulus in the xy plane
P(·)	Probability
Sa	Spectral acceleration
Sa(T)	Spectral acceleration at period T
Sd(T)	Spectral displacement at period T
SI	Spectrum Intensity

Latin letters (Small)

f_{wc}	Masonry compressive strength
f_{bc}	Brick compressive strength
f_{mc}	Mortar compressive strength
h	Height of masonry wall
t	Thickness of masonry wall
t_b	Height of brick
t_m	Thickness of mortar joint
v_u	Relative volume of unit
v_m	Relative volume of mortar

Greek letters

β	Ratio of finite element dimensions
ν	Poisson's ratio
ν_{xy}	Poisson's ratio in the xy plane
ν_{yx}	Poisson's ratio in the yx plane
σ_I	Principal stress across I-axis
σ_{II}	Principal stress across II-axis.
σ_x	Normal stress across x-axis
σ_y	Normal stress across y-axis
τ	Shear stress measured in the x-y plane

References

1. Ramos, L.; Lourenço, P.B. Modeling and vulnerability of historical city centers in seismic areas: A case study in Lisbon. *Eng. Struct.* **2004**, *26*, 1295–1310.
2. Lourenço, P.B.; Roque, J.A. Simplified indexes for the seismic vulnerability of ancient masonry buildings. *Constr. Build. Mater.* **2006**, *20*, 200–208.
3. Lagomarsino, S.; Resemini, S. The assessment of damage limitation state in the seismic analysis of monumental buildings. *Earthq. Spectra* **2009**, *25*, 323–346.
4. Milani, G.; Venturini, G. Automatic fragility curve evaluation of masonry churches accounting for partial collapses by means of 3D FE homogenized limit analysis. *Comput. Struct.* **2011**, *89*, 1628–1648.
5. ICOMOS1931. The Athens Charter for the Restoration of Historic Monuments. In Proceedings of the First International Congress of Architects and Technicians of Historic Monuments, Athens, Greece, 1931. Available online: http://www.icomos.org/athens_charter.html (accessed on 10 December 2018).

6. ICOMOS1964. The Venice Charter for the Restoration of Historic Monuments. In Proceedings of the Second International Congress of Architects and Technicians of Historic Monuments, Venice, Italy, 1964. Available online: http://www.international.icomos.org/charters/venice_e.htm (accessed on 10 December 2018).
7. Morton, B.; Hume, G.L. *The Secretary of the Interior's Standards for Historic Preservation Projects with Guidelines for Applying the Standards*; United States Department of the Interior, Heritage Conservation and Recreation Service: Washington, DC, USA, 1979.
8. Syrmakezis, C.A.; Chronopoulos, M.P.; Sophocleous, A.A.; Asteris, P.G. Structural analysis methodology for historical buildings. *Archit. Stud. Mater. Anal.* **1995**, *1*, 373–382.
9. Asteris, P.G., Giannopoulos, I.P. Vulnerability and Restoration Assessment of Masonry Structural Systems. *Electron. J. Struct. Eng.* **2012**, *12*, 82–93.
10. D'Ayala, D.; Speranza, E. An integrated procedure for the assessment of the seismic vulnerability of historic buildings. In Proceedings of the 12th European Conference on Earthquake Engineering, London, UK, 9–13 September 2002.
11. D'Ayala, D.; Speranza, E. Definition of collapse mechanisms and seismic vulnerability of masonry structures. *Earthq. Spectra* **2003**, *19*, 479–509.
12. D'Ayala, D.F.; Paganoni, S. Assessment and analysis of damage in L'Aquila historic city centre after 6th April 2009. *Bull. Earthq. Eng.* **2011**, *9*, 81–104.
13. D'Ayala, D. Force and Displacement Based Vulnerability Assessment for Traditional Buildings. *Bull. Earthq. Eng.* **2005**, *3*, 235–265.
14. Erberik, M.A. Generation of fragility curves for Turkish masonry buildings considering in-plane failure modes. *Earthq. Eng. Struct. Dyn.* **2008**, *37*, 387–405.
15. Erberik, M.A.; Seismic Risk Assessment of Masonry Buildings in Istanbul for Effective Risk Mitigation. *Earthq. Spectra* **2010**, *26*, 967–982.
16. Bartoli, G.; Betti, M.; Vignoli, A. A numerical study on seismic risk assessment of historic masonry towers: A case study in San Gimignano. *Bull. Earthq. Eng.* **2016**, *14*, 1475–1518.
17. Betti, M.; Drosopoulos, G.A.; Stavroulakis, G.E. Two non-linear finite element models developed for the assessment of failure of masonry arches. *Comptes Rendus Mec.* **2008**, *336*, 42–53.
18. Castori, G.; Borri, A.; De Maria, A.; Corradi, M.; Sisti, R. Seismic vulnerability assessment of a monumental masonry building. *Eng. Struct.* **2017**, *136*, 454–465.
19. Corradi, M.; Borri, A.; Castori, G.; Coventry, K. Experimental analysis of dynamic effects of FRP reinforced masonry vaults. *Materials* **2015**, *8*, 8059–8071.
20. Bartoli, G.; Betti, M.; Giordano, S. In situ static and dynamic investigations on the "Torre Grossa" masonry tower. *Eng. Struct.* **2013**, *52*, 718–733.
21. Lourenço, P.B.; Karanikoloudis, G.; Greco, F. In situ testing and modeling of cultural heritage buildings in Peru, Structural Analysis of Historical Constructions: Anamnesis, diagnosis, therapy, controls. In Proceedings of the 10th International Conference on Structural Analysis of Historical Constructions, SAHC, Leuven, Belgium, 13–15 September 2016, pp. 850–857.
22. Lourenço, P.B. Technologies for seismic retrofitting and strengthening of earthen and masonry structures: Assessment and application. *Geotech. Geol. Earthq. Eng.* **2018**, *46*, 501–518.
23. Karanikoloudis, G.; Lourenço, P.B. Structural assessment and seismic vulnerability of earthen historic structures. Application of sophisticated numerical and simple analytical models. *Eng. Struct.* **2018**, *160*, 488–509.
24. Tiedeman, H. A statistical evaluation of the importance of nonstructural damage to buildings. In Proceedings of the 7th World Conference on Earthquake Engineering, International Association of Earthquake Engineering (IAEE), Tokyo, Japan, September 8–13, 1980; Volume 6, pp. 617–624.
25. Syrmakezis, C.A.; Asteris, P.G.; Sophocleous, A.A. Earthquake resistant design of masonry tower structures. In Proceedings of Fifth International Conference on Structural Studies of Historical Buildings, San Sebastian, Spain, 25–27 June, 1997; Vol. 3, pp. 377–386.
26. Binda, L.; Saisi, A.; Tiraboschi, C. Investigation procedures for the diagnosis of historic masonries. *Constr. Build. Mater.* **2000**, *14*, 199–233.
27. Lourenço, P.B. Recommendations for restoration of ancient buildings and the survival of a masonry chimney. *Constr. Build. Mater.* **2006**, *20*, 239–251. doi: 10.1016/j.conbuildmat.2005.08.026.

28. Fang, D.L.; Napolitano, R.K.; Michiels, T.L.; Adriaenssens, S.M. Assessing the stability of unreinforced masonry arches and vaults: Acomparison of analytical and numerical strategies. *Int. J. Archit. Herit.* **2018**, doi:10.1080/15583058.2018.1463413.
29. Asteris, P.G. On the structural analysis and seismic protection of historical masonry structures. *Open Constr. Build. Technol. J.* **2008**, *2*, 124–133.
30. Onaka, T. A study of the documentation process for conservation of architectural heritage sites: Illustrated by examples from Egypt and Belgium. In Proceedings of the 22nd CIPA symposium, Kyoto, Japan, 11–15 October 2009.
31. Syrmakezis, C., Sophocleous, A., Asteris, P., Liolios, A. Earthquake resistant design of masonry structural systems. In Proceedings of the Earthquake Resistant Engineering Structures, ERES96, Thessaloniki, Greece, 30 October–1 November 1996.; Vol. 2, pp. 717–726,
32. Chronopoulos, P.M., Zigouris, N., Asteris, P.G. Investigation/Documentation and Aspects of Seismic Assesment and Redesign of Traditional Masonry Buildings in Greece. In Proceedings of the 5th European Conference on Structural Control (EACS 2012), Genoa, Italy, 18–20 June 2012.
33. Tassios, T.P. Seismic engineering of monuments. *Bull. Earthq. Eng.* **2010**, *8*, 1231–1265.
34. Chrysostomou, C.Z., Kyriakides, N., Roussis, P.C., Asteris, P.G. (2015). Emerging technologies and materials for the seismic protection of cultural heritage. *In Handbook of Research on Seismic Assessment and Rehabilitation of Historic Structures;* Asteris, P.G., Plevris, V., Eds.; IGI Global: Hershey, PA, USA, 2015.
35. Asteris, P.G.; Tzamtzis, A.D.; Vouthouni, P.P.; Sophianopoulos, D.S. Earthquake Resistant Design and Rehabilitation of Masonry Historical Structures. *Pract. Period. Struct. Des. Constr.* **2005**, *10*, 49–55.
36. Blasi, C.; Coïsson, E. The importance of historical documents for the study of stability of the, ancient buildings: The French Panthéon case study. *Asian J. Civ. Eng.* **2006**, *7*, 359–368.
37. Blasi, C.; Coïsson, E.; Iori, I. The fractures of the French Panthéon: Survey and structural analysis. *Eng. Fract. Mech.* **2008**, *75*, 379–388.
38. Asteris, P.G.; Chronopoulos, M.P.; Chrysostomou, C.Z.; Varum, H.; Plevris, V.; Kyriakides, N.; Silva, V. Seismic vulnerability assessment of historical masonry structural systems. *Eng. Struct.* **2014**, *62–63*, 118–134. doi: 10.1016/j.engstruct.2014.01.031.
39. Bartoli, G.; Betti, M.; Blasi, C.; Ottoni, F.; Coli, M.; Marchetti, E.; Ripepe, M. Synergistic and Interdisciplinary Approaches for the Conservation of Monumental Heritage: Cupola of Santa Maria del Fiore in Florence, Italy. *J. Perform. Constr. Facil.* **2016**, *30*, 04015091.
40. Asteris, P.G.; Sarhosis, V.; Mohebkhah, A.; Plevris, V.; Papaloizou, L.; Komodromos, P.; Lemos, J.V. Numerical Modeling of Historic Masonry Structures. In *Handbook of Research on Seismic Assessment and Rehabilitation of Historic Structures*; Asteris, P.G., Plevris, V., Eds.; IGI Global: Hershey, PA, USA, 2015.
41. Triantafillou, T.C.; Fardis, M.N. Strengthening of historic masonry structures with composite materials. *Mater. Struct. Mater. Et Constr.* **1997**, *30*, 486–496.
42. Asteris, P.G.; Douvika, M.; Karakitsios, P.; Moundoulas, P.; Apostolopoulou, M.; Moropoulou, A. A Stochastic Computational Framework for the Seismic Assessment of Monumental Masonry Structures. In Proceedings of the 5th International Conference on Integrity, Reliability and Failure, Faculty of Engineering, Porto, Portugal, 24–28 July 2016.
43. Mistler, M.; Butenweg, C.; Meskouris, K. Modelling methods of historic masonry buildings under seismic excitation. *J. Seismol.* **2006**, *10*, 497–510.
44. Asteris, P.G.; Plevris, V. *Handbook of Research on Seismic Assessment and Rehabilitation of Historic Structures*; IGI Global: Hershey, PA, USA, 2015; pp. 1–867, doi:10.4018/978-1-4666-8286-3.
45. Apostolopoulou, M.; Aggelakopoulou, E.; Siouta, L.; Bakolas, A.; Douvika, M.; Asteris, P.G.; Moropoulou, A. A methodological approach for the selection of compatible and performable restoration mortars in seismic hazard areas. *Constr. Build. Mater.* **2017**, *155*, 1–14.
46. Skentou, A.; Douvika, M.G.; Argyropoulos, I.; Apostolopoulou, M.; Moropoulou, A.; Asteris, P.G. Assessment of Masonry Structures Based on Analytical Damage Indices. In Proceedings of the 1st International Conference TMM_CH, Transdisciplinary Multispectral Modelling and Cooperation for the Preservation of Cultural Heritage, Athens, Greece, 10–13 October 2018.
47. RILEM Technical Committee. Rilem TC 203-RHM: Repair mortars for historic masonry. Testing of hardened mortars, a process of questioning and interpreting. *Mater. Struct.* **2009**, *42*, 853–865.

48. Barluenga, G.; Estirado, F.; Undurraga, R.; Conde, J.F.; Agua, F.; Villegas, M.Á.; García-Heras, M. Brick masonry identification in a complex historic building, the Main College of the University of Alcalá, Madrid (Spain). *Constr. Build. Mater.* **2014**, *54*, 39–46.
49. Moropoulou, A.; Zacharias, N.; Delegou, E.T.; Apostolopoulou, M.; Palamara, E.; Kolaiti, A. OSL mortar dating to elucidate the construction history of the tomb chamber of the Holy Aedicule of the Holy Sepulchre in Jerusalem. *J. Archaeol. Sci. Rep.* **2018**, *19*, 80–91.
50. Georgopoulos, A. CIPA's perspectives on cultural heritage. *Commun. Comput. Inf. Sci.* **2018**, *817*, 215–245.
51. Hatzopoulos, J.N.; Stefanakis, D.; Georgopoulos, A.; Tapinaki, S.; Pantelis, V.; Liritzis, I. Use of various surveying technologies to 3D digital mapping and modelling of cultural heritage structures for maintenance and restoration purposes: The Tholos in Delphi, Greece. *Mediterr. Archaeol. Archaeom.* **2017**, *17*, 311–336.
52. Labropoulos, K.; Moropoulou, A. Ground penetrating radar investigation of the bell tower of the church of the Holy Sepulchre. *Constr. Build. Mater.* **2013**, *47*, 689–700.
53. Agrafiotis, P.; Lampropoulos, K.; Georgopoulos, A.; Moropoulou, A. 3D modelling the invisible using ground penetrating radar, International Archives of the Photogrammetry. *Remote Sens. Spat. Inf. Sci. ISPRS Arch.* **2017**, *42*, 33–37.
54. Moropoulou, A.; Bakolas, A.; Bisbikou, K. Physico-chemical adhesion and cohesion bonds in joint mortars imparting durability to the historic structures. *Constr. Build. Mater.* **2000**, *14*, 35–46.
55. Bruno, P.; Calabrese, D.; Di Pierro, M.; Genga, A.; Laganara, C.; Manigrassi, D.A.P.; Traini, A.; Ubbrìaco, P. Chemical–physical and mineralogical investigation on ancient mortars from the archaeological site of Monte Sannace (Bari—Southern Italy). *Thermochim. Acta* **2004**, *418*, 131–141.
56. Moropoulou, A.; Bakolas, A.; Bisbikou, K. Investigation of the technology of historic mortars. *J. Cult. Herit.* **2000**, *1*, 45–58.
57. de Lorenzi Pezzolo, A.; Colombi, M.; Mazzocchin, G.A. Where did Roman masons get their material from? A preliminary DRIFTS/PCA investigation on mortar aggregates from X Regio buildings in the Veneto area (NE Italy) and their potential sources. *Environ. Sci. Pollut. Res.* **2018**, doi:10.1007/s11356-018-2202-0.
58. Middendorf, B.; Hughes, J.J.; Callebaut, K.; Baronio, G.; Papayianni, I. Investigative methods for the characterisation of historic mortars—Part 1: Mineralogical characterization. *Mater. Struct. Mater. Et Constr.* **2005**, *38*, 761–769.
59. Middendorf, B.; Hughes, J.J.; Callebaut, K.; Baronio, G.; Papayianni, I. Investigative methods for the characterisation of historic mortars—Part 2: Chemical characterization. *Mater. Struct. Mater. Et Constr.* **2005**, *38*, 771–780.
60. Moropoulou, A.; Bakolas, A.; Bisbikou, K. Characterization of ancient, byzantine and later historic mortars by thermal and X-ray diffraction techniques. *Thermochim. Acta* **1995**, *269–270*, 779–795.
61. Moropoulou, A.; Bakolas, A.; Anagnostopoulou, S. Composite materials in ancient structures. *Cem. Concr. Compos.* **2005**, *27*, 295–300.
62. Ingo, G.M.; Fragalà, I.; Bultrini, G.; De Caro, T.; Riccucci, C.; Chiozzini, G. Thermal and microchemical investigation of Phoenician–Punic mortars used for lining cisterns at Tharros (western Sardinia, Italy). *Thermochim. Acta* **2004**, *418*, 53–60.
63. Maravelaki-Kalaitzaki, P.; Bakolas, A.; Moropoulou, A. Physico-chemical study of Cretan ancient mortars. *Cem. Concr. Res.* **2003**, *33*, 651–661.
64. Palomo, A.; Blanco-Varela, M.T.; Martinez-Ramirez, S.; Puertas, F.; Fortes, C. *Historic Mortars: Characterization and Durability, New Tendencies for Research*; Eduardo Torroja Institute (CSIC): Madrid, Spain, 2002.
65. Hughes, J.J.; Groot, C.; van Balen, K.; Simsir, B.B.; Luigia, B.; Elsen, J.; van Hees, R.; von Konow, T.; Lindqvist, J.E.; Maurenbrecher, P.; et al. RILEM TC 203-RHM: Repair mortars for historic masonry. The role of mortar in Masonry: An introduction to requirement for the design of repair mortars. *Mater. Struct.* **2012**, *45*, 1287–1294, doi:10.1617/s11527-012-9847-9.
66. Moropoulou, A.; Bakolas, A.; Moundoulas, P.; Aggelakopoulou, E. Reverse engineering: A proper methodology for compatible restoration mortars. In *Proceedings of the Workshop Repair Mortars for Historic Masonry, TC RMH*; RILEM: Delft, The Netherlands, 2005.
67. Moropoulou, A.; Labropoulos, K.; Moundoulas, P.; Bakolas, A. The contribution of historic mortars on the earthquake resistance of Byzantine monuments. In *Measuring, Monitoring and Modeling Concrete Properties*; Springer: Dordrecht, The Netherlands, 2006; pp. 643–652.

68. Moropoulou, A.; Bakolas, A.; Moundoulas, P.; Aggelakopoulou, E.; Anagnostopoulou, S. Optimization of compatible restoration mortars for the earthquake protection of Hagia Sophia. *J. Cult. Herit.* **2013**, *14*, e147–e152.
69. Apostolopoulou, M.; Aggelakopoulou, E.; Bakolas, A.; Moropoulou, A. Compatible Mortars for the Sustainable Conservation of Stone in Masonries. In *Advanced Materials for the Conservation of Stone*; Springer: Cham, Switzerland, 2018; pp. 97–123.
70. Apostolopoulou, M.; Delegou, E.T.; Alexakis, E.; Kalofonou, M.; Lampropoulos, K.C.; Aggelakopoulou, E.; Bakolas, A.; Moropoulou, A. Study of the historical mortars of the Holy Aedicule as a basis for the design, application and assessment of repair mortars: A multispectral approach applied on the Holy Aedicule. *Constr. Build. Mater.* **2018**, *181*, 618–637.
71. Tassios, T.P.; Chronopoulos, M.P. A seismic dimensioning of interventions (repairs/strengthening) on low-strength masonry building. In Proceedings of the Middle East and Mediterranean Regional Conference on Earthen and Low-Strength Masonry Buildings in Seismic Areas, Ankara, Turkey, 31 August–6 September 1986.
72. Sarhat, S.R.; Sherwood, E.G. The prediction of compressive strength of ungrouted hollow concrete block masonry. *Constr. Build. Mater.* **2014**, *58*, 111–121.
73. Thaickavil, N.N.; Thomas, J. Behaviour and strength assessment of masonry prisms. *Case Stud. Constr. Mater.* **2018**, *8*, 23–38.
74. Tassios, T.P. *Meccanicadelle Murature*; Liguori Editore: Napoli, Italy, 1988.
75. Garzón-Roca, J.; Adam, J.M.; Sandoval, C.; Roca, P. Estimation of the axial behaviour of masonry walls based on Artificial Neural Networks. *Comput. Struct.* **2013**, *125*, 145–152.
76. Engesser, F. Über weitgespannte wölbbrücken. *Zeitschrift für Architekturs und Ingenieurwesen* **1907**, *53*, 403–440.
77. Bröcker, O. Die auswertung von tragfähigkeitsversuchen an gemauerten wänden. *Betonstein-Zeitung* **1963**, *10*, 19–21.
78. Mann, W. Statistical evaluation of tests on masonry by potential functions. In Proceedings of the Sixth International Brick Masonry Conference, Rome, Italy, 16–19 May 1982; pp. 86–98.
79. Hendry, A.W.; Malek, M.H. Characteristic compressive strength of brickwork walls from collected test results. *Mason. Int.* **1986**, *7*, 15–24.
80. Dayaratnam, P. *Brick and Reinforced Brick Structures*; Oxford & IBH: Delhi, India, 1987.
81. Apolo, G.L.; Matinez-Luengas, A.L. *Curso Técnicas de Intervención en El Patrimonio Arquitectonico*; Consultores Tecnicos de Contstruccion: *Zaragoza, Spain*, 1995.
82. Bennett, R.; Boyd, K.; Flanagan, R. Compressive properties of structural clay tile prisms. *J. Struct. Eng.* **1997**, *123*, 920–926.
83. AS Committee 3700-2001. *Masonry Structures*; Australian Standard Association: Sydney, Australia, 2001; 197p.
84. Dymiotis, C.; Gutlederer, B.M. Allowing for uncertainties in the modelling of masonry compressive strength. *Constr. Build. Mater.* **2002**, *16*, 443–452.
85. EN 1996-1-1. *Eurocode 6: Design of Masonry Structures-Part 1-1: General Rules for Reinforced and Unreinforced Masonry Structures*; European Committee for Standardization: Brussels, Belgium, 2005.
86. Kaushik, H.B.; Rai, D.C.; Jain, S.K. Stress-strain characteristics of clay brick masonry under uniaxial compression. *J. Mater. Civ. Eng.* **2007**, *19*, 728–739.
87. Gumaste, K.S.; Rao, K.S.N.; Reddy, B.V.V.; Jagadish, K.S. Strength and elasticity of brick masonry prisms and wallettes under compression. *Mater. Struct.* **2007**, *40*, 241–253.
88. Christy, C.F.; Tensing, D.; Shanthi, R. Experimental study on axial compressive strength and elastic modulus of the clay and fly ash brick masonry. *J. Civ. Eng. Constr. Technol.* **2013**, *4*, 134–141.
89. Garzón-Roca, J.; Marco, C.O.; Adam, J.M. Compressive strength of masonry made of clay bricks and cement mortar: Estimation based on neural networks and fuzzy logic. *Eng. Struct.* **2013**, *48*, 21–27.
90. Lumantarna, R.; Biggs, D.T.; Ingham, J.M. Uniaxialcompressive strength andstiffness of field-extracted andlaboratory-constructed masonry prisms. *J. Mater. Civ. Eng.* **2014**, *26*, 567–575.
91. Kumavat, H.R. An experimental investigation of mechanical properties in clay brick masonry by partial replacement of fine aggregate with clay brick waste. *J. Inst. Eng. India Ser. A* **2016**, *97*, 199–204.
92. British Standards Institution (BSI). *BS EN 1996 (Eurocode 6): Design of Masonry Structures*; British Standards Institution: London, UK, 2005; p. 128.

93. Asteris, P.G.; Argyropoulos, I.; Cavaleri, L.; Rodrigues, H.; Varum, H.; Thomas, J.; Paulo, B.; Lourenço, P.B. Masonry Compressive Strength Prediction using Artificial Neural Networks. In Proceedings of the 1st International Conference TMM_CH, Transdisciplinary Multispectral Modelling and Cooperation for the Preservation of Cultural Heritage, Athens, Greece, 10–13 October 2018.
94. FEMA 356. Federal Emergency Management Agency (FEMA). *Prestandard and Commentary for the Seismic Rehabilitation of Buildings*; Report No. FEMA 356; FEMA: Washington, DC, USA, 2000.
95. Lourenço, P.B.; Pina-Henriques, J. Validation of numerical and continuum numerical methodsfor estimating the compressive strength of masonry. *Comput. Struct.* **2006**, *84*, 1977–1989. doi:10.1016/j.compstruc.2006.08.009.
96. Papa, E. Damage and failure modes. In *Computational Modelling of Masonry, Brickwork and Blockwork Structures*; Bull, J.W., Ed.; Saxe-Coburg Publications: Stirling, UK, 2001; pp. 1–26, doi:10.4203/csets.6.1.
97. Rots, J.G. Numerical simulation of cracking in masonry. *HERON* **1991**, *36*, 49–63.
98. Tzamtzis, A.D., Asteris, P.G. (2003). Finite Element Analysis Masonry Structures: Part II-Proposed 3-D Nonlinear Microscopic Model. Proceedings of the Ninth North American Masonry Conference (9thNAMC), June 1-4, 2003, Clemson, South Carolina, USA, pp. 146-155.
99. Zucchini, A.; Lourenço, P.B. Mechanics of masonry in compression: Results from a homogenization approach. *Comput. Struct.* **2006**, *85*, 193–204.
100. Lourenço, P.B. Computational Strategies for Masonry Structures. Ph.D. Thesis, Delft University of Technology, Delft, The Netherlands, 1996.
101. Sarhosis, V.; Lemos, J.V. A detailed micro-modelling approach for the structural analysis of masonry assemblages. *Comput. Struct.* **2018**, *206*, 66–81.
102. Schlegel, R.; Rautenstrauch, K. Failure analyses of masonry shear walls. In *Numerical Modelling of Discrete Materials in Geotechnical Engineering, Civil Engineering and Earth Sciences*; Konietzky, H., Ed.; Taylor and Francis Group: London, UK, 2004; pp. 15–20.
103. Asteris, P.G.; Tzamtzis, A.D. Nonlinear Seismic Response Analysis of Realistic Gravity Dam-Reservoir Systems. *Int. J. Nonlinear Sci. Numer. Simul.* **2003**, *4*, 329–338.
104. Lourenço, P.B.; Rots, J.G. Multisurface interface model for analysis of masonry structures. *J. Eng. Mech.* **1997**, *123*, 660–668.
105. Mohebkhah, A.; Tasnimi, A.A.; Moghadam, H.A. Nonlinear analysis of masonry-infilled steel frames with openings using discrete element method. *J. Constr. Steel Res.* **2008**, *64*, 1463–1472.
106. Dialer, C. A distinct element approach for the deformation behaviour of shear stressed masonry panels. In Proceedings of the 6th Canadian Masonry Symposium, Saskatoon, SK, Canada, 15–17 June 1992; pp. 765–776.
107. Dialer, C. Typical masonry failures and repairs. a German Engineer's view. *Prog. Struct. Eng. Mater.* **2002**, *4*, 332–339.
108. Zhuge, Y. Micro-modelling of masonry shear panels with distinct element approach. In *Advances in Mechanics of Structures and Materials*; Chowdhury, L., Fragomeni, Eds.; Swets & Zeitinger: Lisse, The Netherlands, 2002; pp. 131–136.
109. Churilovand, S.; Dumova-Jovanoska, E. Calibration of a numerical model for masonry with applications to experimental results. *J. Arch. Civ. Eng. Environ. Sil. Univ. Technol.* **2008**, *3*, 41–48.
110. Alexandris, A.; Protopapa, E.; Psycharis, I. Collapse mechanisms of masonry buildings derived by the distinct element method. In Proceedings of the 13th World Conference on Earthquake Engineering, Paper No. 548, Vancouver, BC, Canada, 1–6 August 2004.
111. Mohebkhah, A.; Sarv-cheraghi, A.A. Nonlinear analysis of unreinforced masonry buildings using distinct element method. *Modares Civ. Eng. J.* **2015**, *15*, 85–92.
112. Giordano, A.; Mele, E.; Luca, A. Modelling of historical masonry structures.Comparison of different approaches through a case study. *Eng. Struct.* **2002**, 24, 1057–1069.
113. Roberti, G.M. Discrete element analysis on the Sardinian "Nuraghe". In *Historical Constructions*; Lourenço, P.B., Roca, P., Eds.; University of Minho: Guimarães, Portugal, 2001; pp. 719–727.
114. Sarhosis, V.; Asteris, P.G.; Mohebkhah, A.; Xiao, J.; Wang, T. Three dimensional modelling of ancient colonnade structural systems subjected to harmonic and seismic loading. *Struct. Eng. Mech.* **2016**, *60*, 633–653.

115. Sarhosis, V.; Lignola, G.P.; Asteris, P.G. Seismic vulnerability of ancient colonnade: Two story colonnade of the forum in Pompeii. In *Handbook of Research on Seismic Assessment and Rehabilitation of Historic Structures*; IGI Global: Hershey, PA, USA, 2015; pp. 331–358.
116. Sarhosis, V.; Asteris, P.; Wang, T.; Hu, W.; Han, Y. On the stability of colonnade structural systems under static and dynamic loading conditions. *Bull. Earthq. Eng.* **2016**, *14*, 1131–1152.
117. Azevedo, J.; Sincraian, G.; Lemos, J.V. Seismic behavior of blocky masonry structures. *Earthq. Spectra* **2000**, *16*, 337–365.
118. Lemos, J.V. Assessment of the ultimate load of a masonry arch using discrete elements. In *Computer Methods in Structural Masonry—3*; Middleton, J., Pande, G.N., Eds.; Books and Journals International: Swansea, UK, 1995; pp. 294–302.
119. Lemos, J.V. Discrete element modelling of the seismic behaviour of stone masonry arches. In *Computer Methods in Structural Masonry—4*; Pande, G.N., Middleton, J., Kralj, B., Eds.; E & FN Spon: London, UK, 1997; pp. 220–227.
120. Roberti, M.G.; Calvetti, F. Distinct element analysis of stone arches. In *Proceedings of the Second International Conference on Arch Bridges*; Sinopolo: Italy, Venice, 1998; pp. 181–186.
121. Toth, A.R.; Orban, Z.; Bagi, K. Discrete element analysis of a masonry arch. *Mech. Res. Commun.* **2009**, *36*, 469–480.
122. Sincraian, G.E.; Lemos, J.V. Seismic analysis of a stone masonry aqueduct using Discrete Elements. In Proceedings of the 8th Canadian Conference on Earthquake Engineering, Vancouver, BC, Canada, 13–16 June 1999; pp. 131–136.
123. Sarhosis, V.; Oliveira, D.V.; Lemos, J.V.; Lourenco, P.B. The effect of skew angle on the mechanical behaviour of masonry arches. *Mech. Res. Commun.* **2014**, *61*, 53–59.
124. Mohebkhah, A.; Sarhosis, V.; Tavafi, E.; Asteris, P.G. Seismic behaviour of an ancient stone masonry tower using the distinct element method. In Proceedings of the 16th European Conference on Earthquake Engineering (16ECEE), Thessaloniki, Greece, 18–21 June 2018.
125. ITASCA. *3DEC-Universal Distinct Element Code Manual. Theory and Background*; Itasca Consulting Group: Minneapolis, MN, USA, 2004.
126. Papantonopoulos, C.; Psycharis, I.N.; Papastamatiou, D.Y.; Lemos, J.V.; Mouzakis, H.P. Numerical prediction of the earthquake response of classical columns using the distinct element method. *Earthq. Eng. Struct. Dyn.* **2002**, *31*, 1699–1717.
127. Lourenço, P.B.; Rots, J.G.; Blaauwendraad, J. Continuum model for masonry: Parameter estimation and validation. *J. Struct. Eng.* **1998**, *124*, 642–652.
128. Papa, E.; Taliercio, A.; Mirabella-Roberti, G. A damage model to predict the behaviour of masonry under sustained load. In Proceedings of the International Brick/Block Masonry Conference, Madrid, Spain, 25–28 June 2000; pp. 1777–1790.
129. Syrmakezis, C.A.; Asteris, P.G. Masonry Failure Criterion Under Biaxial Stress State. *J. Mater. Civ. Eng. Am. Soc. Civ. Eng.* **2001**, *13*, 58–64.
130. Asteris, P.G.; Tzamtzis, A.D. On the Use of a Regular Yield Surface for the Analysis of Unreinforced Masonry Walls, Electronic. *J. Struct. Eng.* **2003**, *3*, 23–42.
131. Asteris, P.G. Lateral stiffness of brick masonry infilled plane frames. *J. Struct. Eng.* **2003**, *129*, 1071–1079.
132. El-Dakhakhni, W.W.; Drysdale, R.G.; Khattab, M.M. Multilaminate macromodel for concrete masonry: Formulation and verification. *J. Struct. Eng.* **2006**, *132*, 1984–1996.
133. Magenes, G.; Della Fontana, A. Simplified Non-linear Seismic Analysis of Masonry Buildings. In Proceedings of the 5th International Masonry Conference, London, UK, 13–15 October 1998.
134. Tomazevic, M.; Weiss, P. A rational, experimentally based method for the verification of earthquake resistance of masonry buildings. In Proceedings of the 4th U.S. National Conference on Earthquake Engineering, Paper No. 2, Palm Springs, CA, USA, 20–24 May 1990; pp. 349–359.
135. Magenes, G. A Method for Pushover Analysis in Seismic Assessment of Masonry Buildings. In Proceedings of the 12th World Conference on Earthquake Engineering, Paper No. 1866, Auckland, New Zealand, 30 January–4 February 2000.
136. Kappos, A.J.; Penelis, G.G.; Drakopoulos, C.G. Evaluation of simplified models for lateral load analysis of unreinforced masonry buildings. *J. Struct. Eng.* **2002**, *128*, 890–897.
137. Penelis, G.G. An efficient approach for pushover analysis of unreinforced masonry (URM) structures. *J. Earthq. Eng.* **2006**, *10*, 359–379.

138. Pasticier, L.; Amadio, C.; Fragiacomo, M.; Nonlinear seismic analysis and vulnerability evaluation of masonry buildings by means of SAP2000 V.10 code. *Earthq. Eng. Struct. Eng.* **2008**, *37*, 467–485.
139. Belmouden, Y.; Lestuzzi, P. An equivalent frame model for seismic analysis of masonry and reinforced concrete buildings. *Constr. Build. Mater.* **2009**, *23*, 40–53.
140. Milani, G.; Beyer, K.; Dazio, A. Upper bound limit analysis of meso-mechanical spandrel models for the pushover analysis of 2D masonry frames. *Eng. Struct.* **2009**, *31*, 2696–2710.
141. Roca, P.; Molins, C.; Marí, A.R. Strength capacity of masonry wall structures by the equivalent frame method. *J. Struct. Eng.* **2005**, *131*, 1601–1610.
142. Caliò, I.; Marletta, M.; Pantò, B. A new discrete element model for the evaluation of the seismic behaviour of unreinforced masonry buildings. *Eng. Struct.* **2012**, *40*, 327–338.
143. Lagomarsino, S.; Penna, A.; Galasco, A.; Cattari, S. TREMURI program: An equivalent frame model for the nonlinear seismic analysis of masonry buildings. *Eng. Struct.* **2013**, *56*, 1787–1799.
144. Moaveni, B.; Stavridis, A.; Lombaert, G.; Conte, J.P.; Shing, P.B. Finite-element model updating for assessment of progressive damage in a 3-story infilled RC Frame. *J. Struct. Eng.* **2013**, *139*, 1665–1674.
145. Beyer, K.; Mangalathu, S. Review of strength models for masonry spandrels. *Bull. Earthq. Eng.* **2013**, *11*, 521–542.
146. Penna, A.; Lagomarsino, S.; Galasco, A. A nonlinear macroelement model for the seismic analysis of masonry buildings. *Earthq. Eng. Struct. Dyn.* **2014**, *43*, 159–179.
147. Clementi, F.; Mezzapelle, P.A.; Cocchi, G.; Lenci, S. Global analyses of historical masonry buildings: Equivalent frame vs. 3D solid models. *AIP Conf. Proc.* **2017**, *1863*, 450006, doi:10.1063/1.4992615.
148. Berti, M., Salvatori, L., Orlando, M., Spinelli, P. Unreinforced masonry walls with irregular opening layouts: Reliability of equivalent-frame modelling for seismic vulnerability assessment. *Bull. Earthq. Eng.* **2017**, *15*, 1213–1239.
149. Casapulla, C.; Maione, A.; Argiento, L.U. Seismic analysis of an existing masonry building according to the multi-level approach of the italian guidelines on cultural heritage. *Ing. Sismica* **2017**, *34*, 40–59.
150. Ayouby, H.; Tirca, L.; Bagchi, A. Seismic assessment of stone masonry building using the equivalent frame model. In Proceedings of the Annual Conference—Canadian Society for Civil Engineering, Vancouver, Canada, 31 May–3 June 2017; pp. 472–481.
151. Clementi, F.; Gazzani, V.; Poiani, M.; Lenci, S. Assessment of seismic behaviour of heritage masonry buildings using numerical modelling. *J. Build. Eng.* **2016**, *8*, 29–47.
152. Quagliarini, E.; Maracchini, G.; Clementi, F. Uses and limits of the Equivalent Frame Model on existing unreinforced masonry buildings for assessing their seismic risk: A review. *J. Build. Eng.* **2017**, *10*, 166–182.
153. Milani, G.; Bruggi, M. Simple Homogenization-Topology Optimization Approach for the Pushover Analysis of Masonry Walls. *Int. J. Archit. Herit.* **2018**, *12*, 395–408.
154. Siano, R.; Roca, P.; Camata, G.; Pelà, L.; Sepe, V.; Spacone, E.; Petracca, M. Numerical investigation of non-linear equivalent-frame models for regular masonry walls. *Eng. Struct.* **2018**, *173*, 512–529.
155. Giamundo, V.; Sarhosis, V.; Lignola, G.P.; Sheng, Y.; Manfredi, G. Evaluation of different computational modelling strategies for the analysis of low strength masonry structures. *Eng. Struct.* **2014**, *73*, 160–169.
156. D'Ambra, C.; Lignola, G.P.; Prota, A. Multi-Scale Analysis of In-plane Behaviour of Tuff Masonry. *Open Constr. Build. Technol. J.* **2016**, *10*, 312–328.
157. Samarasinghe, W. The In-Plane Failure of Brickwork. Ph.D. Thesis, University of Edinburgh, Edinburgh, UK, 1980.
158. Asteris, P.G. Analysis of Anisotropic Nonlinear Masonry. Ph.D. Thesis, National Technical Univ. of Athens, Athens, Greece, 2000.
159. Asteris, P.G. Finite element micro-modeling of infilled frames. *Electron. J. Struct. Eng.* **2008**, *8*, 1–11.
160. Kupfer, H.B.; Gerstle, K.H. Behavior of concrete under biaxial stress. *J. Eng. Mech. Div. ASCE* **1973**, *99*, 853–866.
161. Kupfer, H.; Hilsdorf, H.K.; Rusch, H. Behavior of concrete under biaxial stresses. *J. Am. Concr. Inst.* **1969**, 66.
162. Ignatakis, C.E.; Stavrakakis, E.J.; Penelis, G.G. Parametric analysis of reinforced concrete columns under axial and shear loading using the finite element method. *ACI Struct. J.* **1989**, *86*, 4.
163. Triantafillou, T.; Fardis, M. Advanced composites for strengthening historic structures. In Proceedings of the IABSE Symposium, Structural Preservation of the Architectural Heritage, Rome, Italy, September 13–17, 1993; Volume 70, pp. 541–548.

164. Cerioni, R.; Donida, G. A finite-element model for the nonlinear-analysis of reinforced nad prestressed masonry walls. *Comput. Struct.* **1994**, *53*, 1291–1306.
165. Yi, T.; Moon, F.L.; Leon, R.T.; Kahn, L.F. Analyses of a two-story unreinforced masonry building. *J. Struct. Eng.* **2006**, *132*, 653–662.
166. El-Borgi, S.; Smaoui, H.; Casciati, F.; Jerbi, K.; Kanoun, F. Seismic evaluation and innovative retrofit of a historical building in Tunisia. *Struct. Control Health Monit.* **2006**, *12*, 179–195.
167. El-Borgi, S.; Choura, S.; Neifar, M.; Smaoui, H.; Majdoub, M.S.; Cherif, D. Seismic vulnerability assessment of a historical building in Tunisia. *Smart Struct. Syst.* **2008**, *4*, 209–220.
168. El-Borgi, S.; Neifar, M.; Jabeur, M.B.; Cherif, D.; Smaoui, H. Use of copper shape memory alloys in retrofitting historical monuments. *Smart Struct. Syst.* **2008**, *4*, 247–259.
169. Karatzetzou, A.; Pitilakis, D.; Kržan, M.; Bosiljkov, V. Soil–foundation–structure interaction and vulnerability assessment of the Neoclassical School in Rhodes. Greece. *Bull. Earthq. Eng.* **2015**, *13*, 411–428.
170. Korkmaz, K.A.; Nuhoglu, A.; Arisoy, B.; Carhoglu, A.I. Investigation of structural safety of existing masonry healthcare facilities in Turkey. *J. Vib. Control* **2012**, *18*, 867–877.
171. Asteris, P.G. A simple heuristic algorithm to determine the set of closed surfaces of the cubic tensor polynomial. *Open Appl. Math. J.* **2010**, *4*, 1–5.
172. Asteris, P.G. Unified Yield Surface for the Nonlinear Analysis of Brittle Anisotropic Materials. *Nonlinear Sci. Lett. A* **2013**, *4*, 46–56.
173. Dhanasekar, M.; Page, A.W.; Kleeman, P.W. The failure of brick masonry under biaxial stresses. *Instn. Civ. Engrs* **1985**, *79*, 295–313.
174. Scarpas, A. *Non-Local Plasticity Softening Model for Brittle Materials/Experimental Evidence/Analytical Modelling/Preliminary Results*; Lab. of Reinforced Concrete, National Technical University of Athens: Athens, Greece, 1991.
175. Andreaus, U. Failure criteria for masonry panels under in-planeloading. *J. Struct. Eng.* **1996**, *122*, 37–46.
176. Syrmakezis, C.A.; Asteris, P.G. Design recommendations for masonry walls under vertical concentrated loads. In Proceedings of the 8th Norm American Masonry Conference, Paper No. 86, Austin, TX, USA, 6–9 June 1999.
177. Apostolopoulour, M.; Douvika, M.G.; Kanellopoulos, I.N.; Moropoulou, A.; Asteris, P.G. Prediction of Compressive Strength of Mortars using Artificial Neural Networks. In Proceedings of the 1st International Conference TMM_CH, Transdisciplinary Multispectral Modelling and Cooperation for the Preservation of Cultural Heritage, Athens, Greece, 10–13 October 2018.
178. Plevris, V.; Asteris, P.G. Modeling of masonry failure surface under biaxial compressive stress using Neural Networks. *Constr. Build. Mater.* **2014**, *55*, 447–461.
179. Asteris, P.G.; Plevris, V. Anisotropic masonry failure criterion using artificial neural networks. *Neural Comput. Appl.* **2017**, *28*, 2207–2229.
180. Asteris, P.G.; Nozhati, S.; Nikoo, M.; Cavaleri, L.; Nikoo, M. Krill herd algorithm-based neural network in structural seismic reliability evaluation. *Mech. Adv. Mater. Struct.* **2018**, doi:10.1080/15376494.2018.1430874.
181. Asteris, P.G.; Kolovos, K.G.; Douvika, M.G.; Roinos, K. Prediction of self-compacting concrete strength using artificial neural networks. *Eur. J. Environ. Civ. Eng.* **2016**, 20, s102–s122.
182. Asteris, P.G.; Kolovos, K.G. Self-compacting concrete strength prediction using surrogate models. *Neural Comput. Appl.* **2018**, doi:10.1007/s00521-017-3007-7.
183. Asteris, P.G.; Roussis, P.C.; Douvika, M.G. Feed-forward neural network prediction of the mechanical properties of sandcrete materials. *Sensors* **2017**, *17*, 1344.
184. Cavaleri, L.; Chatzarakis, G.E.; Di Trapani, F.D.; Douvika, M.G.; Roinos, K.; Vaxevanidis, N.M.; Asteris, P.G. Modeling of surface roughness in electro-discharge machining using artificial neural networks. *Adv. Mater. Res.* **2017**, *6*, 169–184.
185. Asteris, P.G.; Tsaris, A.K.; Cavaleri, L.; Repapis, C.C.; Papalou, A.; Di Trapani, F.; Karypidis, D.F. Prediction of the fundamental period of infilled rc frame structures using artificial neural networks. *Comput. Intell. Neurosci.* **2016**, *2016*, 5104907.
186. Asteris, P.G.; Nikoo, M. Artificial Bee Colony-Based Neural Network for the Prediction of the Fundamental Period of Infilled Frame Structures. *Neural Comput. Appl.* **2019**, doi:10.1007/s00521-018-03965-1.
187. Park, Y.J.; Ang, H.; Wen, Y.K. Damage-limiting a seismic design of buildings. *Earthq. Spectra* **1987**, *3*, 1–26.

188. D'Ayala, D. Assessing the seismic vulnerability of masonry buildings. In *Handbook of Seismic Risk Analysis and Management of Civil Infrastructure Systems*; Tesfamariam, S.; Goda, K.; Eds.; Woodhead Publishing: Cambridge, UK, 2013; pp. 334–365, doi:10.1533/978057098986.3.334.
189. Stephenson, V.; D'Ayala, D. A new approach to flood vulnerability assessment for historic buildings in England. *Nat. Hazards Earth Syst. Sci.* **2014**, *14*, 1035–1048.
190. Yepes-Estrada, C.; Silva, V.; Rossetto, T.; D'Ayala, D.; Ioannou, I.; Meslem, A.; Crowley, H. The global earthquake model physical vulnerability database. *Earthq. Spectra* **2016**, *32*, 2567–2585.
191. Bosiljkov, V.; D'Ayala, D.; Novelli, V. Evaluation of uncertainties in determining the seismic vulnerability of historic masonry buildings in Slovenia: Use of macro-element and structural element modelling. *Bull. Earthq. Eng*. **2015**, *13*, 311–329.
192. Rota, M. Advances in the Derivation of Fragility Curves for Masonry Buildings. Ph.D. Thesis, European School for Advanced Studies in Reduction of Seismic Risk (ROSE School), Pavia, Italy, 2007.
193. Zamora, J.E.M. Seismic Fragility Analysis of Reinforced Masonry Buildings. Ph.D. Thesis, Colorado State University, Fort Collins, CO, USA, 2013.
194. Douvika, M.G. Seismic Vulnerability Assessment of Monumental Masonry Structures. Master's Thesis, School of Pedagogical & Technological Education, Athens, Greece, 2017. Available online: https://www.researchgate.net/publication/318259801_Seismic_Vulnerability_Assessment_of_Monumental_Masonry_Structures (accessed on 10 December 2018).
195. Skentou, A.D. Seismic Vulnerability Assessment of Masonry Structures. Master's Thesis, School of Pedagogical & Technological Education, Athens, Greece, 2018. Available online: https://www.researchgate.net/publication/324684962_Seismic_Vulnerability_Assessment_of_Masonry_Structures (accessed on 10 December 2018).
196. FEMA-273. *NEHRP guidelines for the seismic rehabilitation of buildings*; Federal Emergency Management Agency: Washington, DC, USA, 1997.
197. CEN. *Eurocode 8: Design of Structures for Earthquake Resistance. Part 3: Assessment and Retrofitting of Buildings*; EN 1998-3; CEN: Brussels, Belgium, March 2005.
198. Kennedy, R.P.; Cornell, C.A.; Campbell, R.D.; Kaplan, S.; Perla, H.F. Probabilistic Seismic Safety of an Existing Nuclear Power Plant. *Nucl. Eng. Des.* **1980**, *59*, 315–338.
199. Kircher CA, Nasser AA, Kutsu, O., Holmes WT. Developing of building damage functions for earthquake loss estimation. *Earthq. Spectra* **1997**, *13*, *664–681.*
200. Porter, K.; Hamburger, R.; Kennedy, R. Practical Development and Application of Fragility Functions. In Proceedings of the SEI Structures Congress, Long Beach, CA, USA, 16–19 May 2007.
201. Porter, K.; Kennedy, R.; Bachman, R. Creating fragility functions for performance-based earthquake engineering. *Earthq. Spectra* **2007**, *23*, 471–489.
202. D'Ayala, D.F.; Jaiswal, K.S.; Wald, D.J.; Porter, K.; Greene, M. Collaborative effort to estimate collapse fragility for buildings worldwide: The WHE-PAGER project. In Proceedings of the 9th US National and 10th Canadian Conference on Earthquake Engineering, Including Papers from the 4th International Tsunami Symposium, Toronto, ON, USA, 25–29 July 2010; Volume 5, pp. 3709–3719.
203. Cattari, S.; Lagomarsino, S. Performance-based approach to earthquake protection of masonry cultural heritage. In Proceedings of Structural Analysis of Historical Constructions, DWE, Wrocław, Poland, 15–17 October 2012; Jasien´ko, J., Ed.; pp. 2914–2922, ISBN 978-83-7125-216-7.
204. Kazantzi, A.K.; Vamvatsikos, D.; Porter, K. Analytical seismic vulnerability assessment for a class of modern low-rise steel frames. In Proceedings of the 12th International Conference on Applications of Statistics and Probability in Civil Engineering, ICASP, Vancouver, BC, Canada, 12–15 July 2015.
205. HAZUS-MH. *Multi-Hazard Loss Estimation Methodology: Earthquake Model*; Department of Homeland Security, FEMA: Washington, DC, USA, 2003.
206. Azizi-Bondarabadi, H.; Mendes, N.; Lourenço, P.B.; Sadeghi, N.H. Empirical seismic vulnerability analysis for masonry buildings based on school buildings survey in Iran. *Bull. Earthq. Eng.* **2018**, doi:10.1007/s10518-016-9944-1.
207. Giovinazzi, S. The Vulnerability Assessment and the Damage Scenario in Seismic Risk Analysis. Ph.D. Thesis, University of Florence and Technical University Carolo-Wilhelmina, Braunschweig, Germany, 2005.
208. Petrini, V. *Rischio sismico di edifici pubblici, parte I, Aspetti metodologici*; Pubblicazione del GNDT-CNR: Roma, Italy, 1993.

209. Barron-Corverra, R. Spectral Evaluation of Seismic Fragility in Structures. Ph.D. Thesis, Department of Civil, Structural & Environmental Engineering, University at Buffalo, The State University of New York, Buffalo, NY, USA, 2000.
210. Reinhorn, A.M.; Barron-Corverra, R.; Ayala, A.G. Spectral evaluation of seismic fragility of structures. In Proceedings of the ICOSSAR 2001, Newport Beach, CA, USA, 17–21 June 2001.
211. Noh, H.Y.; Lallemant, D.; Kiremidjian, A.S. Development of empirical and analytical fragility functions using kernel smoothing methods. *Earthq. Eng. Struct. Dyn.* **2015**, *44*, 1163–1180.
212. Gazepidis, F.P. Aseismic Design and Reinforcement Recommendations of a Masonry Structure Using Fragility Curves. Master's Thesis, National Technical University, Athens, Greece, 2011.
213. M. Rota, M.; Penna, A.; Magenes, G. A methodology for deriving analytical fragility curves for masonry buildings based on stochastic nonlinear analyses. *Eng. Struct.* **2010**, *32*, 1312–1323.
214. Pinto, P.E.; Giannini, R.; Franchin, P. *Seismic Reliability Analysis of Structures*; IUSS Press: Pavia, Italy, 2004.
215. Singhal, A.; Kiremidjian, A. Method for probabilistic evaluation of seismic structural damage. *J. Struct. Eng.* **1996**, *122*, 1459–1467.
216. Silva, V.; Crowley, H.; Pinho, R.; Varum, H. Extending displacement-based earthquake loss assessment (DBELA) for the computation of fragility curves. *Eng. Struct.* **2013**, *56*, 343–356.
217. Crowley, H.; Polidoro, B.; Pinho, R.; Van Elk, J. Framework for developing fragility and consequence models for local personal risk. *Earthq. Spectra* **2017**, *33*, 1325–1345.
218. Silva, V.; Crowley, H.; Colombi, M. Fragility Function Manager Tool. *Geotech. Geol. Earthq. Eng.* **2014**, *27*, 385–402.
219. Sarchi, L.; Varum, H.; Monteiro, R.; Silveira, D. Seismic behavior of two Portuguese adobe buildings: Part II—Numerical modeling and fragility assessment. *Int. J. Arch. Herit.* **2018**, doi:10.1080/15583058.2017.1423132.
220. Tarque, N.; Crowley, H.; Pinho, R.; Varum, H. Displacement-based fragility curves for seismic assessment of adobe buildings in Cusco, Peru. *Earthq. Spectra* **2012**, *28*, 759–794.
221. Vicente, R.; Parodi, S.; Lagomarsino, S.; Varum, H.; Silva, J.A.R.M. Seismic vulnerability and risk assessment: Case study of the historic city centre of Coimbra, Portugal. *Bull. Earthq. Eng.* **2011**, *9*, 1067–1096.
222. Pagnini, L.C.; Vicente, R.; Lagomarsino, S.; Varum, H. A mechanical model for the seismic vulnerability assessment of old masonry buildings. *Earthq. Struct.* **2011**, *2*, 25–42.
223. European Charter of the Architectural Heritage. 1975. Available online: http://www.icomos.org/en/charters-and-texts/179-articles-en-francais/ressources/charters-and-standards/170-european-charter-of-the-architectural-heritage (accessed on 10 December 2018).
224. The Declaration of Amsterdam, 1975 Declaration of Amsterdam. 1975. Available online: http://www.international.icomos.org/en/charters-and-texts/179-articles-en-francais/ressources/charters-and-standards/169-the-declaration-of-amsterdam (accessed on 10 December 2018).
225. Moropoulou, A.; Korres, E.; Georgopoulos, A.; Spyrakos, C.; Mouzakis, C.; Lampropoulos, K.C.; Apostolopoulou, M.; Delegou, E.T.; Alexakis, E. The rehabilitation of the Holy Aedicule. In Proceedings of the XXXIII Convegno Internazionale Scienza e Beni Culturali, Le Nuove Frontiere del Restauro: Trasferimenti, Contaminazioni, Ibridazioni, Bressanone, 27–30 July 2017; pp. 1–16.
226. Philokyprou, M. The Earliest Use of Lime and Gypsum Mortars in Cyprus. In *Historic Mortars*; Válek, J., Hughes, J., Groot, C., Eds.; RILEM Bookseries; Springer, Dordrecht, The Netherlands, 2012; Volume 7.
227. Moropoulou, A.; Polikreti, K.; Bakolas, A.; Michailidis, P. Correlation of physicochemical and mechanical properties of historical mortars and classification by multivariate statistics. *Cem. Concr. Res.* **2003**, *33*, 891–898.
228. Klrca, Ö. Ancient binding materials, mortars and concrete technology: History and durability aspects. In Proceedings of the 4th International Seminar on Structural Analysis of Historical Constructions, Padova, Italy, 10–13 November 2004; pp. 87–94.
229. Freire, T.; Santos Silva, A.; Veiga, M.R.; Brito, J.D. Characterization of Portuguese historical gypsum mortars. In Proceedings of the HMC08—1st Historical Mortars Conference, Lisbon, Portugal, 24–26 September 2008; pp. 24–26.
230. Böke, H.; Akkurt, S. Ettringite formation in historic bath brick–lime plasters. *Cem. Concr. Res.* **2003**, *33*, 1457–1464.

231. Moropoulou, A.; Bakolas, A.; Moundoulas, P.; Anagnostopoulou, S.; Aggelakopoulou, E. Compatible restoration mortars for the earthquake protection of Hagia Sophia. PACT. *J. Eur. Study Group Phys. Chem. Biol. Math. Tech. Appl. Archaeol.* **2000**, *59*, 29–51.
232. Aggelakopoulou, E.; Bakolas, A.; Moropoulou, A. Properties of lime–metakolin mortars for the restoration of historic masonries. *Appl. Clay Sci.* **2011**, *53*, 15–19.
233. Moropoulou, A.; Bakolas, A. Range of acceptability limits of physical, chemical and mechanical characteristics deriving from the evaluation of historic mortars, PACT. *J. Eur. Study Group Phys. Chem. Biol. Math. Tech. Appl. Archaeol.* **1998**, *56*, 165–178.
234. Schueremans, L.; Cizer, O.; Janssens, E.; Serré, G.; Balen, K.V. Characterization of repair mortars for the assessment of their compatibility in restoration projects: Research and practice. *Constr. Build. Mater.* **2011**, *25*, 4338–4350.
235. Corinaldesi, V. Environmentally-friendly bedding mortars for repair of historical buildings. *Constr. Build. Mater.* **2012**, *35*, 778–784.
236. Page, A.W. The biaxial compressive strength of brick masonry. *Proc. Inst. Civ. Eng.* **1981**, *71*, 893–906.
237. Asteris, P.G.; Douvika, M.G.; Apostolopoulou, M.; Moropoulou, A. Seismic and restoration assessment of monumental masonry structures. *Materials* **2017**, *10*, 895, doi:10.3390/ma10080895.
238. Moropoulou, A.; Apostolopoulou M.; Moundoulas, P.; Karoglou, M.; Delegou, E.; Lampropoulos, K.; Gritsopoulou, M.; Bakolas, A. The combination of NDTS for the diagnostic study of historical buildings: The case study of Kaisariani Monastery, COMPDYN 2015. In Proceedings of the 5th ECCOMAS Thematic Conference on Computational Methods in Structural Dynamics and Earthquake Engineering, Crete Island, Greece, 25–27 May 2015; pp. 2321–2336.
239. Douvika, M.G.; Apostolopoulou, M.; Moropoulou, A.; Asteris, P.G. Seismic Vulnerability Assessment of Monumental Masonry Structures (in greek). In Proceedings of the 17th Panhellenic Concrete Conference, Thessaloniki, Greece, 19–21 September 2016.
240. Maniatakis, C.A.; Spyrakos, C.C.; Kiriakopoulos, P.D.; Tsellos, K.-P. Seismic response of a historic church considering pounding phenomena. *Bull. Earthq. Eng.* **2018**, *16*, 2913–2941.